WIND FIELD ESTIMATION AND ITS UTILIZATION IN TRAJECTORY AND INPUT PREDICTION

by

JANE-WIT KAMPOON

Presented to the Faculty of the Graduate School of
The University of Texas at Arlington in Partial Fulfillment
of the Requirements
for the Degree of

DOCTOR OF PHILOSOPHY

THE UNIVERSITY OF TEXAS AT ARLINGTON

December 2014

Copyright © by JANE-WIT KAMPOON 2014

All Rights Reserved

To Pornpimol, Charoongchai, Siravee, Ussanee, Pongkun, Palika and Palin.

Acknowledgements

I would like to thank the University of Texas at Arlington, Mechanical and Aerospace Engineering Department as well as the Royal Thai Air Force, which have financially supported me throughout my graduate studies.

I am highly grateful for my supervising professor, Dr. Atilla Dogan for the relentless guidance and encouragement he provided during the course of my study and research. I wish to thank my academic advisors Dr. Kent L. Lawrence, Dr. Donald R. Wilson, Dr. Brian Huff and Dr. Kamesh Subbarao for their time spent and interest presented in my research as they reviewed this dissertation and participated in my defense committee.

I would also like to thank all the colleagues at the Aeronautical and Aviation Engineering Department, Royal Thai Air Force Academy for their support and encouragement.

Finally, I would like to express my extreme gratitude to my parents, my sister and my wife for their relentless encouragement and the patience to my achievement.

November 19, 2014

Abstract

WIND FIELD ESTIMATION AND ITS UTILIZATION IN TRAJECTORY AND INPUT PREDICTION

JANE-WIT KAMPOON, Ph.D.

The University of Texas at Arlington, 2014

Supervising Professor: Atilla Dogan

This dissertation work develops a method for onboard estimation of wind field with spatial and temporal variation based on local wind vector estimation and/or measurements from multiple aircraft flying in the same airspace. Aircraft flying in the same airspace of operation are considered airborne wind sensors scattered over the airspace because of the fact that aircraft carry along with them wind information inherent in their dynamics and kinematics. The onboard wind field estimation is formulated in the framework of parameter estimation based on various wind field models, which are different function of position and time.

The online wind field estimation is utilized in trajectory prediction of aircraft flying in spatially and temporally varying wind. Various simulation cases are presented to demonstrate the feasibility of wind field estimation and the benefit of using such information in trajectory prediction. Further this dissertation presents a method of input prediction for an aircraft flying in spatially and temporally varying wind field. Input prediction is done using inverse simulation to compute the required control variables (control surface deflections and thrust level) for an aircraft to fly

through a prescribed trajectory. Estimated wind field is also used in inverse simulation for input prediction as in the trajectory prediction case. Various simulation cases are presented to demonstrate the feasibility of input prediction method and the importance of including wind field information in inverse simulations.

Table of Contents

List of Illustrations

List of Tables

Chapter 1

INTRODUCTION

1.1 Motivation

Atmospheric wind plays an important role in aircraft operations. The effect of wind on aircraft can be detrimental or beneficial. Detrimental effects include performance degradation, aircraft incidents and accidents. Weather, mostly wind, is reported to be a contributing factor in about 30% of all aviation accidents [3]. Wind can also be used to aircraft advantage. For example, wind can be utilized to fly through optimal trajectories to save time or/and fuel [4]. Wind is also used for soaring by extracting energy in the form of airspeed or altitude gain [5]. Thus, whether detrimental or beneficial, information about the wind aircraft is and will be exposed to is important to know. This will help avoid or reduce risk associated with wind exposure or increase the benefit obtained from wind exposure.

Rapid growth in air transportation along with plans for integration UAS into civilian airspace requires better situational awareness for both air traffic controllers and onboard pilots in terms of flight trajectories of aircraft relative to each other. Information about aircraft current positions and intended trajectories can help mitigate the risk of conflict and collision between aircraft operating in the same airspace. In the case of an emergency such as engine failure or loss of control surface effectiveness, it becomes imperative to compute feasible trajectories in order to determine alternative landing fields. Accuracy and reliability of trajectory prediction enhanced by the information of wind variation will improve the performance of various tasks such as conflict detection and avoidance, and planning of emergency landing.

In some cases, instead of computing the trajectory of an aircraft, a predefined trajectory is given to the aircraft to fly. For example, when a conflict with another aircraft is detected, conflict avoidance algorithms compute new trajectories for the aircraft to follow to avoid the conflict. Another example is the emergency landing situation mentioned above. Once an emergency occurs and emergency landing is required, a trajectory is prescribed for the aircraft to follow to the emergency landing site. There are cases where military aircraft required to follow a prescribed trajectory, for example, in combat maneuvers or in rendezvous with other aircraft such as in aerial refueling. The feasibility of such prescribed trajectories requires the control surface deflections and engine thrust to be within their saturation and rate limits. This leads to the problem of "input prediction" which is to compute the required control surface deflections and engine thrust for the aircraft to fly through the prescribed trajectory. The feasibility of a given trajectory depends on atmospheric wind conditions as much as the capabilities of the aircraft. Thus, in this problem, too, the information of wind field will improve the prediction of required input variation.

1.2 Problem Statement

This research effort aims at estimating wind field with spatial and temporal variation based on local wind vector estimations or measurements from multiple aircraft flying in the vicinity. The implementation of new technologies like ADS-B (Automatic Dependent Surveillance-Broadcast) system will enable the required communication among aircraft in the same airspace for sharing local wind information. This research further aims to develop trajectory prediction and input prediction methods that utilize the estimated wind field information to improve prediction accuracy.

The wind field estimation problem will be formulated in the framework of parameter estimation based on various wind field models, which are different functions

of position and time. The trajectory prediction will be based on a set of equations of motion that include the effect of wind. The trajectory prediction will utilize the wind field information and flight intent as well as the control input data.

Input prediction will be based on the inverse simulation of equations of motion including wind terms. The goal of input prediction is to determine the required control surface deflections and thrust for aircraft to fly through a given trajectory in the wind field that is concurrently estimated.

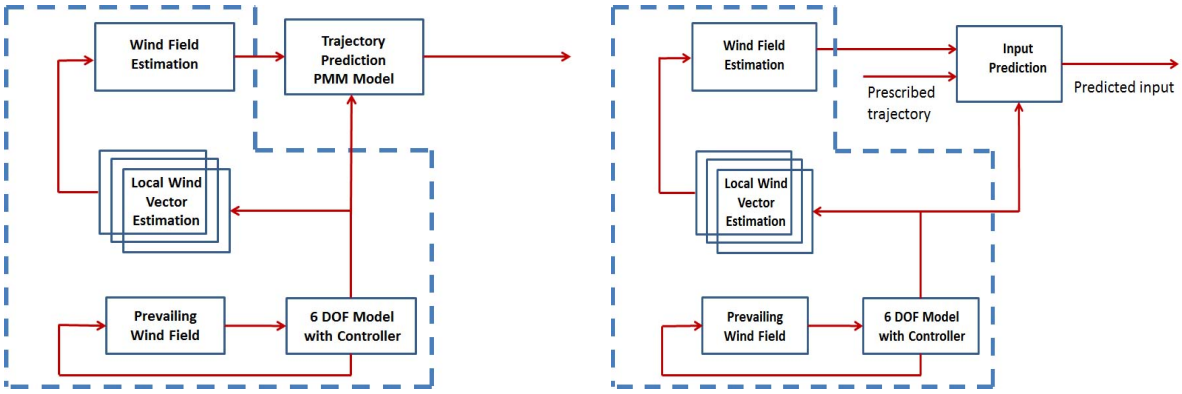

(a) Trajectory prediction (b) Input prediction

Figure 1.1. Research problems' work flow diagrams.

Flow diagrams of the research tasks are shown in Fig. 1.1. The common tasks between the trajectory prediction and input prediction, as a comparison of Fig. 1.1-(a) and Fig. 1.1-(b) shows, are (i) 6-DOF Model with Controller, (ii) Prevailing Wind Field, (iii) Local Wind Vector Estimation, and (iv) Wind Field Estimation. The 6-DOF Model with Controller includes the aircraft dynamic and kinematic equations as well as a controller to fly the aircraft with commanded airspeed, altitude and turn rate. Prevailing Wind Field module is the model of the spatially and temporally varying wind field that generates the local wind vector that the aircraft experiences.

Local Wind Vector Estimation module estimates the local wind vector the aircraft is exposed to based on the response of the aircraft to wind exposure. Note that there are multiple boxes for this module to indicate that multiple aircraft flying in the same airspace estimate their own wind exposure and share that information with the aircraft that does the wind field estimation. The local wind vector data obtained from multiple aircraft are used in Wind Field Estimation module to approximate the wind velocity vector field, which is used in both trajectory prediction and input prediction modules.

1.3 Literature Review

1.3.1 Local Wind Vector Estimation

Dynamics and kinematics of aircraft are affected by the local wind it is exposed to. Various methods have been developed to estimate the local wind vector or some properties of it.

The most common methods for local wind vector estimation are based on Kalman Filter frameworks as reported in Ref. [6, 7, 8, 9]. Ref. [6] uses a two state Extended Kalman Filter (EKF) to estimate wind speed assuming that the wind components are quasi-constant and have minimal impact onto the UAV dynamics. This method can estimate both 2D and 3D wind components. Ref. [7] develops a technique based on Unscented Kalman Filter (UKF) to estimate the horizontal local wind velocity by utilizing the state-estimation techniques that have the ability to reconstruct exogenous disturbance signals that are not directly measured. Ref. [8] uses both linear and nonlinear Kalman Filter techniques to estimate the horizontal local wind components assuming that the local wind around the aircraft are constant. The measurement signals are the position, airspeed and heading of each aircraft. These

signals are obtained by radar track data. Ref. [9] proposes a method of using an aircraft with a single-antenna GPS receiver and Pitot tube to estimate wind speed and direction and to calibrate the airspeed. An EKF is implemented to estimate wind parameters. Other studies reported in the literature [10, 11] use numerical integration based on Forward Euler integration for computing wind velocity from aircraft response. This approach relies on an accurate dynamic model and accurate state estimates. Assuming horizontal constant wind, Ref. [10] presents an algorithm for wind estimation onboard a small kite-like delta wing UAV, named Kiteplane, based on measurements of angular velocity components and translational accelerations. Ref. [11] estimates wind velocity by comparison of measurements of aircraft motion with respect to the earth with the predictions of aircraft motion obtained from a dynamic model. Ref. [12] and [1, 2], use an onboard airdata sensor along with GPS/INS unit to estimate wind speed and direction based on aircraft kinematics. Refs. [13, 14, 15] use the Square-Root Unscented Kalman Filter to estimate aircraft states as well as local wind vector that includes prevailing wind, turbulence and additional wind induced by other aircraft flying in proximity.

1.3.2 Wind Field Estimation

The previous section discusses methods reported in the literature for estimating local wind that aircraft flies in. However, many applications may further benefit from the knowledge of spacial and temporal variation of wind within the airspace of operation. This information is referred to as "wind field", which consists of wind velocity vector representation as a function of position and time. Such a mathematical representation can be used, for example, in trajectory prediction of aircraft. Ref. [16] presents a method for wind field estimation that uses a known structure to simplify estimation. A polynomial parameterization of the wind field is used, allowing im-

plementation of linear Kalman Filter for parameter estimation. Ref. [8, 17, 18] use aircraft data to improve their weather models. Basically, aircraft flying in the traffic are considered as airborne wind sensors scattered over the airspace because of the fact that aircraft carry along with them wind information inherent in theirs dynamics and kinematics. The idea of using aircraft data to improve meteorological data is not new. The Aircraft Meteorological Data Relay (AMDAR) program was first proposed by the World Meteorology Organization in the 1970s and has been using aircraft data to improve their weather models since the late 1990s [18]. Ref. [8] generates the global wind map by using vector spline interpolation and Finite Element Method in solving the 2D Shallow Water Equation (SWE) as the wind field model. Ref. [17] uses the linear interpolation to compute wind information from spatially and temporally varying wind field model, which is represented by joint Gaussian random variables at specified nodes. Ref. [18] uses linear interpolation to estimate the vertical wind profile. The wind field is represented by statistical models and logarithmic profile, which is the mathematical model of wind variation with altitude in the neutral boundary layer over the lowest 100 m from surface. A logarithmic profile estimate based on power law is used as an initial estimate when data are insufficiently available.

Modeling of wind field is also important for aircraft simulation. Wind is in general modeled as a combination of deterministic and stochastic components. The deterministic component is usually the nominal or mean wind while the stochastic component represents the uncertainty or error in wind information and is modeled as a random process with known statistical properties. Most research studies reported in the literature considering only deterministic wind component assume constant wind [6, 8, 9, 12]. Others model deterministic wind component as a time-varying function such as triangular wave form [7] or a polynomial function [11]. In applications where trajectory of aircraft is in question or the wind exposure may vary based on position,

wind model as function of time is not adequate. Ref. [19] and [20] model wind as spatially varying functions. There are other papers that consider prevailing wind only as random variables [17, 21, 22].

1.3.3 Trajectory Prediction

The aircraft trajectory prediction has been defined as the method to estimate/predict the future position of the aircraft in flight, given the aircraft current conditions, a nominal path to be followed by the aircraft, environmental information, and aircraft-specific data [23]. The aircraft trajectory in flight can be obtained by numerically integrating the aircraft equations of motion, which is the set of nonlinear ordinary differential equation. In general, the solutions will provide the variables (position, altitude, velocity and fuel consumption), which describe a time history of the aircraft trajectory.

Various research studies in trajectory prediction have been conducted for decades. In the literature, mathematical models for describing the aircraft trajectory can be categorized as follow [24]. (i) Point-Mass Models (PMM), which consider an aircraft as a moving point such that the rotational motions is not considered, as in Ref. [25, 26, 27]. (ii) Kinematic Models, which deal only with position, heading, and speed data of aircraft, as in Ref. [28]. (iii) Kinetic Models, which are the full nonlinear 6 DOF equations of motion of aircraft, as in Ref. [29], and (iv) Other models, which include all models that do not fall into the previously defined models, e.g. energy model and holding pattern model as in Ref. [30, 31], respectively. Many papers in the area of trajectory prediction model aircraft motion by using PMM. Although these mathematical models have different level of fidelity, it does not mean that one approach outperforms the others. As a matter of fact, the trajectory prediction ac-

curacy depends upon both the modeling and the quality of the input data used to drive the model [23].

Three different trajectory prediction methods are reported in the literature: (i) Nominal method, which projects the current states into the future without taking uncertainties into account. This results in a single trajectory. (ii) Worst-case method, which projects the current states into the future based on assumption that an aircraft will perform any range of maneuvers. (iii) Probabilistic method, which models uncertainties to describe potential variations in the future trajectory of the aircraft.

Most prior research studies employing nominal trajectory/state propagation methods do not consider wind effect [32, 33, 34, 35, 36]. Many studies considering air traffic environments [37, 38, 39, 40, 41, 42] address wind effect by adding safety buffer zone around aircraft. References [37, 38, 39] assume all aircraft are exposed to the same wind vector, i.e., flying in uniform wind field. Others [40, 41, 42] include wind effect in trajectory prediction error.

Worst-case trajectory/state propagation is used only in a small number of prior research efforts [43, 44, 45] mainly because of high false alarm rate. Most such research studies do not account for wind effect in trajectory propagation. For example, Ref. [44, 45] ignore wind effect while studying close parallel approaches of commercial airplanes into airports.

There are numerous research efforts that use probabilistic approaches for trajectory/state propagation [46, 47, 48, 49, 50, 51, 52, 53, 54, 55, 22]. Some [46, 47] neglect wind effect in trajectory prediction. Others [48, 49, 50] assume wind effect as part of prediction uncertainty or error from nominal trajectory. Ref. [51] expresses wind effect in along-track and cross-track uncertainties. Ref. [52, 53] include wind effect in position errors as normal distribution with zero mean. Ref. [55] categorizes probabilistic approaches in terms of how spatial and/or temporal correlations of wind

components are modeled such as i) uncorrelated, ii) correlated in space but not time, iii) correlated both space and time and iv) uncorrelated between different aircraft flying in the same airspace. Ref. [55] models the uncertainties in deviations of wind predictions, obtained from the Rapid Update Cycle-1 (RUC-1) forecast, which is an operational weather prediction system developed by the National Oceanic and Atmospheric Administration (NOAA) for users needing frequently updated short-range weather forecasts, as both spatially and temporally correlated. Ref. [22], on the other hand, only considers spatial correlation in wind prediction errors.

Inaccuracies in trajectory prediction are attributed to two main sources of errors: (i) modeling errors in governing equations, and (ii) errors in data driving the model such as initial conditions, aircraft data, environmental information and intent information [23]. One aspect of weather information that greatly affects aircraft trajectory is the wind [21]. Timely and accurate knowledge of the wind and its spatial and temporal variation in the airspace of operation, either from ground-based radar or on-board measurements, can significantly improve the accuracy of aircraft trajectory prediction.

Generally, the aircraft navigation through the controlled airspace is required to strictly follow the submitted flight plan, which describes where to go from one way-point to the other and how to maneuver in between those way-points, for example, from way-point A to B, maintain constant speed, altitude and heading. Thus, this indicates that the intent information inherently exists in the flight plan. The aircraft intent is the aircraft's operation plan and defines in detail how the aircraft intends to meet its objectives within the constraints defined in the operation plan [56]. Intent information is one of the important factors to improve accuracy of trajectory prediction. Several studies in [56, 57, 58, 59, 60, 61] show that intent information sharing either via existing data-link (Flight Management System (FMS)) or future

technology data-link (Automatic Dependent Surveillance-Broadcast (ADS-B)) among aircraft or between aircraft and ground-based trajectory prediction system, results in greatly improved the accuracy of the predicted trajectory. Ref. [57] uses intent information in a probabilistic trajectory prediction method to analyze the probabilistic conflict between aircraft. Ref. [58] develops a real-time intent based trajectory prediction algorithm for air traffic control application. This study focuses on nominal trajectory prediction method. Refs. [60, 61] develop the Aircraft Intent Description Language (AIDL), which is a formal language for the unambiguous definition of aircraft trajectories, in order to interchange aircraft intent information for the Air Traffic Management Systems (ATM). They show great improvement in accuracy of ground-based trajectory prediction by communication of aircraft intent. The references cited above assume prior knowledge of intent information and conformance of aircraft to the intent. Others such as Ref. [59] consider cases when intent information is not accurately present, or does not exist and develop intent inference algorithms to infer the pilot's intent in real time and apply to weather cell avoidance and constraint region avoidance. Ref. [56] shows that an inferred aircraft intent can be extracted by using existing data-link technology (FMS and ATM) for ground-based trajectory prediction. This study focuses on descent phase of flight.

It is obvious that the predictability of aircraft trajectory or the accuracy of the predicted trajectory from trajectory prediction algorithms will provide effective trajectory based operations, and reduce fuel consumption and emissions [62]. However, the prediction is never perfect due to several sources of error as presented in [23]. Inaccurate wind information is the major source of aircraft trajectory prediction error. Additionally, the lack of flight and aircraft intent information will result in aircraft trajectory prediction error as well.

1.3.4 Input Prediction

The preceding section discusses trajectory prediction, which can be considered as an application of conventional (forward) simulation techniques. In that case, the equations of motion, generally linear or nonlinear differential equations, are solved starting with initial conditions for prescribed time variations of input variables, or forcing terms. In the problem of trajectory prediction, for prescribed future variation of the input variables, the forward simulation techniques determine how the aircraft states will propagate in the immediate future by solving the differential equations starting from the current aircraft states. In other problems, the inverse is desired. Namely, the trajectory of the aircraft is prescribed and the question is to determine the required input variation for the aircraft to follow the prescribed trajectory. Such methods are referred to as "inverse simulation" or "input prediction" [63].

By using the concept of inverse simulation, the feasibility of a desired trajectory can be determined in terms of whether the variations of control variables will be within their saturation and rate limits. This analysis can be made more precise by taking into account the effect of wind on aircraft trajectory, which will benefit from knowledge of the wind variation, i.e., the wind field, in the airspace of operation.

The development of various inverse simulation algorithms have been presented and explained along with their advantages and disadvantages comprehensively in Ref. [63, 64]. Inverse simulation techniques have been found in the literature, particularly in area of aircraft flight control applications as in Ref. [65, 66] and in area of aircraft handling qualities investigation as in Ref. [67, 68].

Only a few papers in the literature consider wind field effect in aircraft dynamics to be analyzed by inverse simulation techniques. Ref. [69] investigates the control input histories that ensure safe turbulence penetration and preserve prescribed flight path in the presence of atmospheric disturbances by using an inverse simulation tech-

nique. A simple local wind shear atmospheric disturbance is modeled by the superposition of (i) a full period sinusoidal wind, parallel to the ground, in the plane of flight path, changing from a head to a tail wind and (ii) a downflow consisting of a half-period sinusoid over the same length, so that the peak downflow corresponds to the change form head to tailwind. This paper focuses on vertical maneuvering flight of a fighter aircraft. Ref. [70] applies a based inverse simulation to analyzing fighter flight accidents and verifying flight tracks generated by using general optimization method, which defined a constrained performance index as a function of state variables. A simple wind field as a function of altitude is used; the wind velocity vector always points to the same horizontal direction but its magnitude varies with altitude. Ref. [71] utilizes inverse simulation to help identify safe regions on a ship's flight deck for landing a rotorcraft in various atmospheric conditions. The wind conditions around a ship deck and superstructure were obtained from wind tunnel tests.

1.4 Original Contributions

The novel contributions of this research can be listed in three groups.

(i) A new method is developed that determines the "best" approximation for spatially and temporally varying wind fields from multiple candidate models in terms of the smallest approximation error. The approximation models are multivariable polynomials with various orders. Their coefficients and the approximation errors (residuals) are determined using WLSE (Weighted Least Squares Estimation) based on local wind vector "measurements" obtained from multiple aircraft flying in the same airspace. The best approximation models is defined as the one with the smallest residual. The local wind velocity vectors that each aircraft is exposed to are computed using various local wind estimation methods and are shared among the aircraft through a common communication protocol like the ADS-B system. This will enable

each aircraft to have access to local wind information from other aircraft as well as its own for onboard wind field estimation. The weighting of the measurements in the WLSE is done based on the predicted or intended position of each aircraft. That is, measurements coming from other aircraft flying in the area of interest may have more weighting than the measurements from its own aircraft.

(ii) An aircraft trajectory prediction method is developed that processes the estimated wind field as well as the current aircraft states and aircraft intent through an aircraft PMM that includes the effect of wind exposure. This enables the prediction of aircraft trajectory in the presence of spatially and temporally varying wind. The accuracy of the prediction will depend on the past trajectory of other aircraft flying in the area since the wind field estimation depends on the local wind information from other aircraft.

(iii) An inverse simulation method is developed for input prediction of aircraft flying through a prescribed trajectory in the presence of spatially and/or temporally varying wind. The inverse simulation is based on a set of equations of motion including wind effects and will process the estimated wind field as in the case of trajectory prediction discussed above.

1.5 Organization of the Dissertation

The remainder of the dissertation is composed of five chapters. Chapter 2 introduces models for prevailing wind field which are considered to be spatially and temporally varying vector fields defined relative to the inertial reference frame. Chapter 3 presents several set of equation of motions with different degrees of freedom that will be implemented in simulation, trajectory prediction and input prediction. Chapter 4 presents the wind field estimation. The wind field estimation problem is posed as to determine, from a list of candidate models, the best model to represent the vari-

ation of wind vector over an airspace of interest. The LSE (Least Square Estimation) method is selected as it suits well with the problem formulation. The wind field estimation algorithms and simulation results are also presented in this chapter. Chapter 5 presents the utilization of wind field estimation in the trajectory prediction application. The trajectory prediction algorithms and simulation results are also included in this chapter. Chapter 6 presents the utilization of wind field estimation in the input prediction application for investigation of feasibility of specified trajectories in the spatially and temporally varying wind fields. The input prediction algorithms and simulation results are also presented. Conclusions and suggestions for future work are presented in Chapter 7.

Chapter 2

PREVAILING WIND FIELD MODELS

Motion of the air within the atmosphere wrapping around Earth shows highly nonlinear and even chaotic behavior. It is still an open problem to develop equations of atmospheric motion that can include all dynamic factors. There are, however, models developed under various assumptions for specific cases. For example, considering atmosphere as fluid governed by fundamental physical laws, a set of partial differential equations are derived in terms of standard state variables as dependent variables and space and time as independent variables [72]. Meteorologists traditionally consider vertical and horizontal motion of atmosphere separately. Vertical motion of atmosphere is termed as "updraft" or "downdraft" and horizontal one as "wind" [73, 74]. However, the term "wind" in this research includes all components of atmospheric motion.

For the simulation of aircraft flying in spatially and temporally varying wind, there should be a model that captures the variation of wind over position and time. The spatial and temporal extent of the model should be large enough to enable analysis of aircraft flying for a long time as well as multiple aircraft flying in an airspace. Several research studies have developed wind field models specific to different types of wind such as wind over ocean surface [75] or mountainous terrain [76, 77, 78, 79], wind in urban area [80], tornadoes [81] and microburst [19, 82].

This chapter introduces the mathematical models used to represent prevailing wind velocity vector fields with spatially and/or temporal variations. This research limits the wind to horizontal wind only and thus vertical wind component is not

included in the models. However, the variation of the horizontal wind components with altitude is included. The wind velocity vector generated by these models are relative to the inertial frame and the components are also expressed in the inertial frame. The wind field models are used in simulation to generate local wind velocity vectors that each aircraft is exposed to while flying along a trajectory.

The representation of the wind vector in the inertial frame is written as

$$\mathbf{W}(x,y,z,t) = \begin{bmatrix} W_x(x,y,z,t) \\ W_y(x,y,z,t) \\ W_z(x,y,z,t) \end{bmatrix} \tag{2.1}$$

where W_x, W_y, W_z are the wind components along x-axis, y-axis, and z-axis, respectively. The time rate of change of the wind velocity experienced by the aircraft is formulated in terms of the partial derivatives and the components of the aircraft velocity in the inertial frame $(\dot{x}, \dot{y}, \dot{z})$ as

$$\frac{d}{dt}\mathbf{W}(x,y,z,t) = \begin{bmatrix} \frac{\partial W_x}{\partial t} \\ \frac{\partial W_y}{\partial t} \\ \frac{\partial W_z}{\partial t} \end{bmatrix} + \begin{bmatrix} \frac{\partial W_x}{\partial x} & \frac{\partial W_y}{\partial y} & \frac{\partial W_z}{\partial z} \\ \frac{\partial W_x}{\partial x} & \frac{\partial W_y}{\partial y} & \frac{\partial W_z}{\partial z} \\ \frac{\partial W_x}{\partial x} & \frac{\partial W_y}{\partial y} & \frac{\partial W_z}{\partial z} \end{bmatrix} \begin{bmatrix} \dot{x} \\ \dot{y} \\ \dot{z} \end{bmatrix} \tag{2.2}$$

where the first term is due to the temporal variation of the wind and the second term is because of the spatial variation represented in terms of the wind gradients. The temporal variation term is ignored when the velocity of the aircraft in a spatially varying wind field is very large relative to the time rate of change in wind at the current location (x, y, z) of the aircraft.

There are five wind models considered in this research. They are simplified solutions to more complicated physics-based models in terms of partial differential equations. These models will be used for two different purposes. (1) A wind model with specified parameters will be used in simulation of aircraft flying in spatially and

temporally varying wind field. (2) Wind field estimation will be done by estimating the parameters of the wind models based on computed or provided local wind vector data. The wind models are only for the horizontal components of the wind as the focus in this research is on multiple aircraft flight at the same altitude and the vertical wind component is assumed to be negligible.

2.1 Wind Model-1

This model represents the basic kinematics of the horizontal atmospheric wind [72].

$$\begin{aligned} W_x(x,y,z,t) &= W_{x0}(z,t) + \frac{1}{2}\Big\{\Big[D(z,t) + F_1(z,t)\Big](x-x_0) \\ &\quad + \Big[-\zeta(z,t) + F_2(z,t)\Big](y-y_0)\Big\} \qquad (2.3) \\ W_y(x,y,z,t) &= W_{y0}(z,t) + \frac{1}{2}\Big\{\Big[\zeta(z,t) + F_2(z,t)\Big](x-x_0) \\ &\quad + \Big[D(z,t) - F_1(z,t)\Big](y-y_0)\Big\} \qquad (2.4) \end{aligned}$$

where W_{x0}, W_{y0} are mean wind components along x- and y-axis, respectively; x_0, y_0 are the arbitrary fixed position in the inertial reference frame. D is referred to as "*divergence*" and related to $\frac{\partial W_x}{\partial x} + \frac{\partial W_y}{\partial y}$; F_1 is referred to as "*stretching deformation*" and related to $\frac{\partial W_x}{\partial x} - \frac{\partial W_y}{\partial y}$; F_2 is "*shearing deformation*" and related to $\frac{\partial W_y}{\partial x} + \frac{\partial W_x}{\partial y}$; ζ is called "*vorticity*" and related to $\frac{\partial W_y}{\partial x} - \frac{\partial W_x}{\partial y}$ [72]. While this model includes only horizontal components, the variations of the horizontal components with altitude is model through the dependency of its parameters on altitude, z. The model can be further simplified as

$$\begin{aligned} W_x(x,y,z,t) &= W_{x0}(z,t) + A(z,t)(x-x_0) + B(z,t)(y-y_0) \qquad (2.5) \\ W_y(x,y,z,t) &= W_{y0}(z,t) + C(z,t)(x-x_0) + E(z,t)(y-y_0) \qquad (2.6) \end{aligned}$$

where $A(z,t) = [D(z,t) + F_1(z,t)]$, $B(z,t) = [-\zeta(z,t) + F_2(z,t)]$, $C(z,t) = [\zeta(z,t) + F_2(z,t)]$, and $E(z,t) = [D(z,t) - F_1(z,t)]$, respectively.

As the arguments of the coefficients indicate, the temporal variation of wind components are modeled through the dependency of the coefficients on time. The temporal variations are assumed linear and formulated as

$$W_{x0}(z,t) = w_{x0} \tag{2.7}$$

$$W_{y0}(z,t) = w_{y0} \tag{2.8}$$

$$A(z,t) = a_0 + a_1 t \tag{2.9}$$

$$B(z,t) = b_0 + b_1 t \tag{2.10}$$

$$C(z,t) = c_0 + c_1 t \tag{2.11}$$

$$E(z,t) = e_0 + e_1 t \tag{2.12}$$

where the variation along altitude is not considered since the cases studied in this research are limited to constant altitude flight. In Eqs. (2.7) and (2.8), the mean wind components W_{x0} and W_{y0} are modeled constant to ensure that the magnitude of the wind throughout the simulation stays reasonable and do not increase too much that the aircraft control variable requirements would be more than the feasible limits.

2.2 Wind Model-2

This model represents uniform wind field, i.e., no spacial variation in x- and y-axis. Thus, this model is a simplified version of Wind Model-1 as

$$W_x(x,y,z,t) = W_{x0}(z,t) \tag{2.13}$$

$$W_y(x,y,z,t) = W_{y0}(z,t) \tag{2.14}$$

2.3 Wind Model-3

Another simplified version of Wind Model-1 is obtained when the mean wind components are zero.

$$W_x(x,y,z,t) = A(z,t)(x-x_0) + B(z,t)(y-y_0) \tag{2.15}$$

$$W_y(x,y,z,t) = C(z,t)(x-x_0) + D(z,t)(y-y_0) \tag{2.16}$$

2.4 Wind Model-4

This model represents logarithmic variation of x-component of wind as

$$W_x(x,y,z,t) = W_{x0}(z,t) \tag{2.17}$$

$$+ \; A(z,t)[\log(B(z,t) + C(z,t)(x-x_0)^2 \tag{2.18}$$

$$+ \; D(z,t)(y-y_0)^2)] \tag{2.19}$$

$$W_y(x,y,z,t) = W_{y0}(z,t) + E(z,t)(x-x_0) \tag{2.20}$$

Temporal variation of the wind components are modeled by some of the coefficients formulated as linear functions of time as

$$W_{x0}(z,t) = w_{x0} \tag{2.21}$$

$$W_{y0}(z,t) = w_{y0} + w_{y1}t \tag{2.22}$$

$$A(z,t) = a_0 \tag{2.23}$$

$$B(z,t) = b_1 t \tag{2.24}$$

$$C(z,t) = c_0 \tag{2.25}$$

$$D(z,t) = d_0 \tag{2.26}$$

$$E(z,t) = e_0 \tag{2.27}$$

2.5 Wind Model-5

This model represents a horizontal sinusoidal wave, which show the variation of wind field along x-axis and y-axis as [20]

$$W_x(x,y,z,t) = -W_{wave}(z,t)\Big\{ \cos\Big[\frac{\pi t}{6}\cos\big(\frac{2\pi(x-x_0)}{\lambda}\big)\Big] \tag{2.28}$$

$$+ \sin\Big[\frac{\pi}{3}\sin\big(\frac{2\pi(y-y_0)}{\lambda}\big)\Big]\Big\} \tag{2.29}$$

$$W_y(x,y,z,t) = -W_{wave}(z,t)\Big\{ \cos\Big[\frac{\pi}{3}\cos\big(\frac{2\pi(x-x_0)}{\lambda}\big)\Big] \tag{2.30}$$

$$+ \sin\Big[\frac{\pi}{3}\cos\big(\frac{2\pi(y-y_0)}{\lambda}\big)\Big]\Big\} \tag{2.31}$$

where λ is the wave length and $W_{wave}(z,t)$ is the magnitude of the wave speed, which varies with time as

$$W_{wave}(z,t) = a_0 + a_1 e^{-a_2 t} + a_3 t \tag{2.32}$$

2.6 Example Wind Fields generated by the Models

Figure 2.1 shows examples of spatially varying horizontal wind vector fields over 300×300 km area generated by each of the first four wind models when $z = 7010$ m, $x_0 = 0$ and $y_0 = 0$. In all figures, the blue arrows indicate the direction and the magnitude of the wind vector at a given point while the contour lines show some isolines in terms of the wind speed. Fig. 2.1-(a) shows a wind vector field by Wind Model - 1 when $D(z,t) = 4 \times 10^{-5}, \zeta(z,t) = 5 \times 10^{-8}, F_1(z,t) = 3 \times 10^{-5}, F_2(z,t) = 5 \times 10^{-5}$. In this wind vector field, the wind speed variation ranges from 1 to 6 m/s. Fig. 2.1-(b) shows a wind vector field by Wind Model-2 when $W_{x0}(z,t) = -10, W_{y0}(z,t) = 15$ that results in uniform wind speed about 18 m/s over the entire area.

Fig. 2.1-(c) shows a wind vector field by Wind Model-3 where $A(z,t) = -2 \times 10^{-5}, B(z,t) = -2 \times 10^{-5}, C(z,t) = 2 \times 10^{-5}, E(z,t) = -2 \times 10^{-5}$ with wind speed

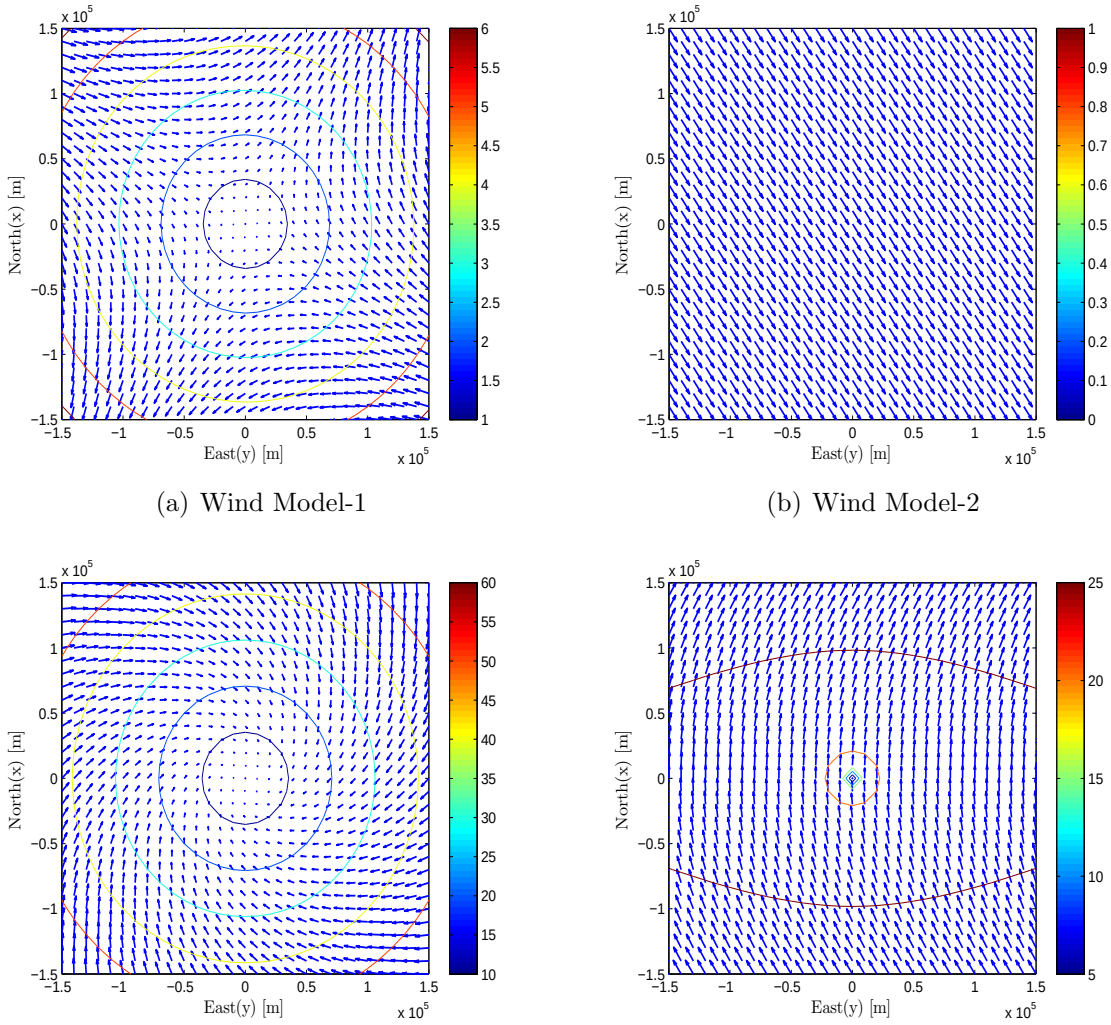

(a) Wind Model-1

(b) Wind Model-2

(c) Wind Model-3

(d) Wind Model-4

Figure 2.1. Example wind fields by Wind Models-1, -2, -3, and -4.

variation ranging from 10 to 60 m/s over the airspace. Fig. 2.1-(d) shows a wind vector field by Wind Model-4 where $W_{x0}(z,t) = 0, W_{y0}(z,t) = 0$ and $A(z,t) = B(z,t) = C(z,t) = D(z,t) = 1,\ E(z,t) = 1 \times 10^{-5}$ with wind speed variation ranging from 5 to 25 m/s over the airspace.

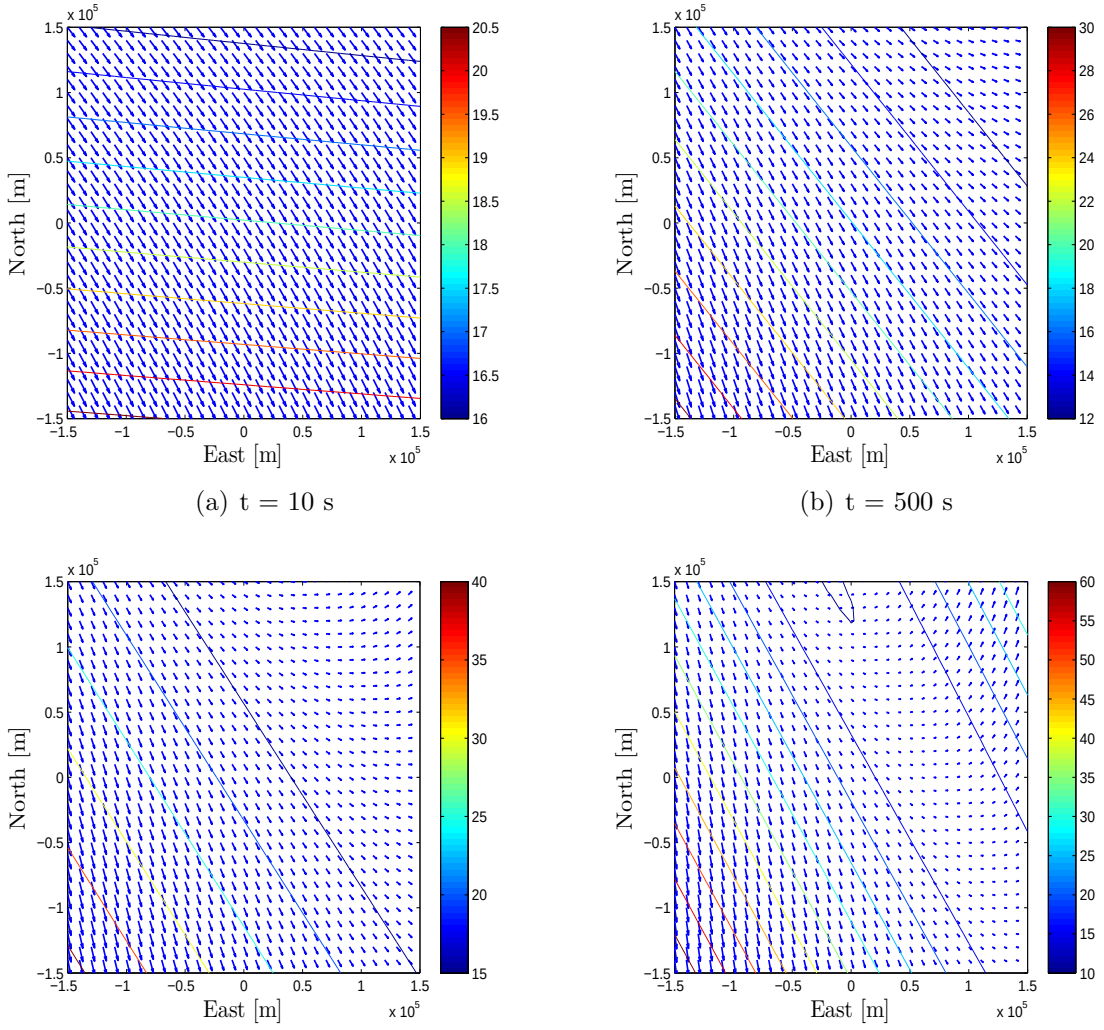

(a) t = 10 s

(b) t = 500 s

(c) t = 1000 s

(d) t = 2000 s

Figure 2.2. Spatially and temporally varying wind field by Model-1.

Figure 2.2 shows snapshots at different time instants of spatially and temporally varying horizontal wind vector fields generated by Wind Model-1 when $z = 7010$ m, $x_0 = 300$ and $y_0 = 300$. The mean wind components are $W_{x0}(z,t) = -10$ m/s and $W_{y0}(z,t) = 15$ m/s and $A(z,t) = 19 \times 10^{-6} + 5 \times 10^{-8}t, B(z,t) = -5 \times 10^{-7} + 1 \times 10^{-6}t, C(z,t) = 15 \times 10^{-7} + 1 \times 10^{-8}t, E(z,t) = -15 \times 10^{-7} + 5 \times 10^{-9}t$. Figs.

2.2-(a)-(d) show wind speed and direction variation over the 300 × 300 km area at four different times $t = 10, 500, 1000$ and 2000 sec, respectively. This Wind Model-1 generates wind speed variation ranging from 16 to 60 m/s over the airspace.

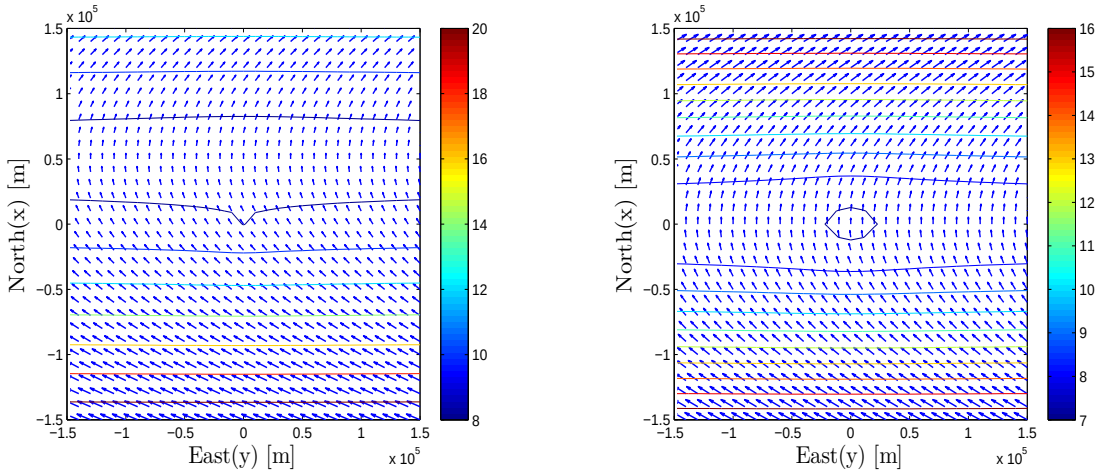

(a) t = 10 s

(b) t = 500 s

(c) t = 1000 s

(d) t = 2000 s

Figure 2.3. Spatially and temporally varying wind field by Model-4.

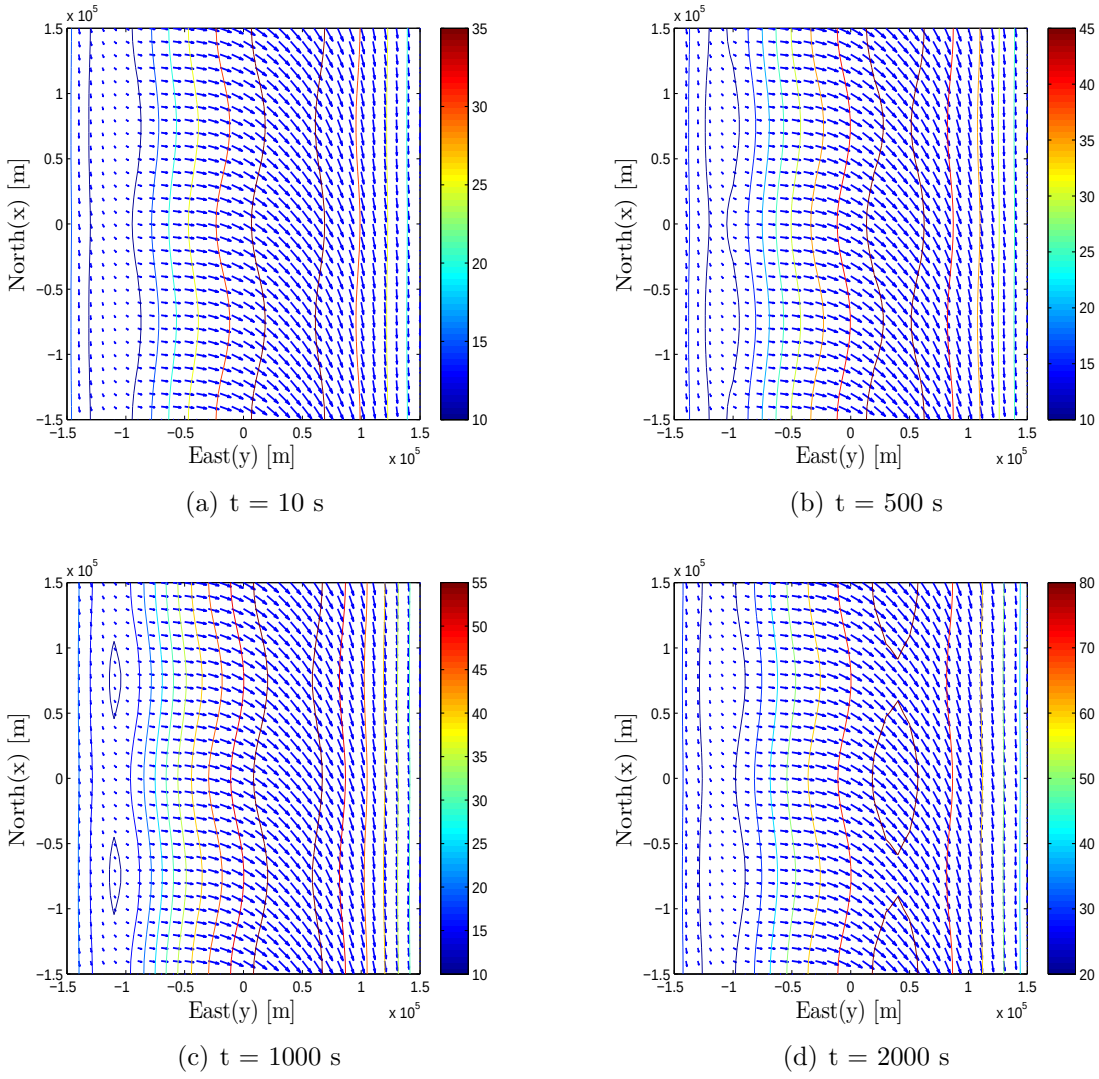

(a) t = 10 s

(b) t = 500 s

(c) t = 1000 s

(d) t = 2000 s

Figure 2.4. Spatially and temporally varying wind field by Model-5.

Figure 2.3 shows snapshots at different time instants of spatially and temporally varying horizontal wind vector fields generated by Wind Model-4 when $z = 7010$ m, $x_0 = 300$ and $y_0 = 300$. The mean wind components are $W_{x0}(z,t) = -10$ m/s and $W_{y0}(z,t) = 15 + 1 \times 10^{-2}t$ m/s and $A(z,t) = 1 \times 10^{-1}, B(z,t) = 1 \times 10^{-2}t, C(z,t) = D(z,t) = 1, E(z,t) = 1 \times 10^{-6}$. Figs. 2.3-(a)-(d) show wind speed and direction

variation over the 300×300 km area at four different times $t = 10, 500, 1000$ and 2000 sec, respectively. This Wind Model-4 captures the wind speed variation ranging from 8 to 30 m/s.

Figure. 2.4 shows snapshots at different time instants of horizontal spatially and temporally varying wind vector fields generated by Wind Model-5 when $z = 7010$ m. The wave length is $\lambda = 3 \times 10^5$. The wave speed $W_{wave}(z,t) = 15 + e^{\frac{1}{180}t} + 1 \times 10^{-2}t$ m/s. Figs. 2.4-(a)-(d) show wind speed and direction variation over the 300×300 km area at four different times $t = 10, 500, 1000$ and 2000 sec, respectively. This Wind Model-5 captures the wind speed variation ranging from 10 to 80 m/s.

Chapter 3

AIRCRAFT MODELS

This chapter presents several sets of equations of motion used in simulation, trajectory prediction and input prediction. First, the 6-DOF nonlinear equations of motion used in simulating flight in a spatially and temporally varying wind field are introduced. This is followed by the 3-DOF nonlinear equations utilized in trajectory prediction and another set of 6-DOF nonlinear equations used in input prediction. Note that the reference frames used for the derivation of equations of motion and for the description of variables are presented in Appendix A.

3.1 Model for Simulation

In order to simulate flight in spatially and temporally varying wind, the 6-DOF nonlinear equations of motion with explicit wind terms, which are developed in Ref. [1] are used. These equations are derived under the following assumptions: (i) the aircraft is a rigid body, (ii) the aircraft has a plane of symmetry, (iii) the earth rotation and surface curvature are neglected (i.e., flat-earth approximation), (iv) the Earth-fixed frame is considered as the inertial reference frame.

3.1.1 Translational Dynamics

The aircraft translational dynamics with respect to the inertial frame [$\hat{I}$] is written in matrix form as

$$\begin{aligned}\begin{bmatrix} \dot{V} \\ \dot{\beta} \\ \dot{\alpha} \end{bmatrix} &= \mathcal{E}^{-1}\mathbf{S}(\omega_{\mathbf{B}})\mathbf{R_{BW}}V_W - \mathcal{E}^{-1}\mathbf{R_{BI}}\dot{W} \\ &+ \frac{1}{m}\mathcal{E}^{-1}\Big(\mathbf{R_{BI}}M + \mathbf{R_{BW}}A + P\Big)\end{aligned} \tag{3.1}$$

where

$$\mathcal{E}^{-1} = \begin{bmatrix} \cos\alpha\cos\beta & \sin\beta & \cos\beta\sin\alpha \\ -\frac{1}{V}\cos\alpha\sin\beta & \frac{1}{V}\cos\beta & -\frac{1}{V}\sin\alpha\sin\beta \\ -\frac{1}{V}\sec\beta\sin\alpha & 0 & \frac{1}{V}\cos\alpha\sec\beta \end{bmatrix} \tag{3.2}$$

where (V, β, α) are the airspeed, side slip angle and angle-of-attack of the aircraft. V_W is the velocity of the aircraft relative to the surrounding air expressed in wind frame [$\hat{W}$]. $\mathbf{R_{BI}}$ is the rotation matrix from the inertial frame to the body frame of the aircraft, $\mathbf{R_{BW}}$ is the rotation matrix from the aircraft wind frame to body frame.

The external forces acting on the aircraft are the gravitational force M (expressed in the inertial frame [$\hat{I}$]), the aerodynamic force A (expressed in the wind frame [$\hat{W}$]) and propulsive force P (expressed in the body frame [$\hat{B}$]). In general, the representations of the forces are

$$M = \begin{bmatrix} 0 \\ 0 \\ m\ g \end{bmatrix} \quad A = \begin{bmatrix} -D \\ -S \\ -L \end{bmatrix} \quad P = \begin{bmatrix} T\cos\delta \\ 0 \\ -T\sin\delta \end{bmatrix} \tag{3.3}$$

where g is the gravitational acceleration, m is the mass of the aircraft, (D, S, L) are the drag, side force and lift on the aircraft, respectively, T is the thrust magnitude, and δ is the thrust inclination angle. Also, $\omega_{\mathbf{B}}$ is the representation of the angular velocity

vector of the aircraft relative to the inertial frame expressed in its own body frame and note that $\mathbf{S}(\cdot)$ is the skew-symmetric matrix operation on the representation of a vector and defined as

$$\mathbf{S}(\omega_B) = \begin{bmatrix} 0 & r & -q \\ -r & 0 & p \\ q & -p & 0 \end{bmatrix} \tag{3.4}$$

where

$$\omega_{\mathbf{B}} = \begin{bmatrix} p \\ q \\ r \end{bmatrix} \tag{3.5}$$

3.1.2 Rotational Dynamics

The aircraft rotational dynamics with respect to the inertial frame [$\hat{I}$] is written in matrix form as

$$\dot{\omega}_B = \underline{\underline{\mathbf{I}}}^{-\mathbf{1}} M_B + \underline{\underline{\mathbf{I}}}^{-\mathbf{1}} \mathbf{S}(\omega_{\mathbf{B}}) \underline{\underline{\mathbf{I}}} \omega_B \tag{3.6}$$

where $\underline{\underline{\mathbf{I}}}$ is the inertia matrix of the aircraft, M_B is the moment of the external forces around the origin of body frame and expressed in the aircraft body frame as

$$M_B = \begin{bmatrix} \mathcal{L} \\ \mathcal{M} \\ \mathcal{N} \end{bmatrix} \tag{3.7}$$

3.1.2.1 Translational Kinematics

The flight trajectory of aircraft with respect to the inertial reference frame [$\hat{I}$] is written in matrix form as

$$\dot{r}_B = \mathbf{R}_{\mathbf{BI}}^{\mathbf{T}} \mathbf{R}_{\mathbf{BW}} V_W + W_I \tag{3.8}$$

where r_B is the position of the aircraft relative to the inertial frame expressed in the inertial frame, $\mathbf{R_{BI}}$ is the rotation matrix from the inertial frame to the body frame of the aircraft, $\mathbf{R_{BW}}$ is the rotation matrix from the aircraft wind frame to body frame, V_W is the velocity of aircraft relative to the surrounding air expressed in aircraft wind frame.

3.1.3 Rotational Kinematics

The aircraft rotational kinematics with respect to the inertial frame [$\hat{I}$] is written in terms of the Euler angles as

$$\dot{\phi} = p + q\sin\phi\tan\theta + r\cos\phi\tan\theta \tag{3.9}$$

$$\dot{\theta} = q\cos\phi - r\sin\phi \tag{3.10}$$

$$\dot{\psi} = (q\sin\phi + r\cos\phi)\sec\theta \tag{3.11}$$

where both the orientation in terms of (ψ, θ, ϕ), and the angular velocity, (p, q, r), of the aircraft are relative to the inertial frame. By reversing the relations formulated in Eqs. (3.9)-(3.11), the angular velocity components can be written in terms of Euler angles and their derivatives as

$$p = \dot{\phi} - \dot{\psi}\sin\theta \tag{3.12}$$

$$q = \dot{\theta}\cos\phi + \dot{\psi}\sin\phi\cos\theta \tag{3.13}$$

$$r = \dot{\psi}\cos\theta\cos\phi - \dot{\theta}\sin\phi \tag{3.14}$$

3.1.4 Aerodynamics Forces and Moments

The aerodynamic forces are given by the following standard expressions as

$$D = \frac{1}{2}\rho V^2 \mathcal{S} C_D \tag{3.15}$$

$$S = \frac{1}{2}\rho V^2 \mathcal{S} C_S \tag{3.16}$$

$$L = \frac{1}{2}\rho V^2 \mathcal{S} C_L \tag{3.17}$$

where $\mathcal{S}$ is the reference area of the aircraft and ρ is the ambient air density. The aerodynamic coefficients are

$$C_D = C_{D0} + C_{D\alpha^2}\ \alpha^2 \tag{3.18}$$

$$C_S = C_{S0} + C_{S\beta}\beta + C_{S\delta_r}\delta_r \tag{3.19}$$

$$C_{L_{wing}} = C_{L0} + C_{L\alpha}\alpha + C_{L\alpha 2}\ (\alpha - \alpha_{ref})^2 + C_{Lq}\frac{c}{2V}q \tag{3.20}$$

$$C_{L_{tail}} = C_{L\delta_e}\delta_e \tag{3.21}$$

$$C_L = C_{L_{wing}} + C_{L_{tail}} \tag{3.22}$$

where (δ_a,δ_e,δ_r) are the deflections of the control surfaces (aileron, elevator, rudder, respectively) and c is the chord length for the aircraft.

The aerodynamic moments, which are the rolling, pitching and yawing moments, respectively, are given by the following standard expression as

$$\mathcal{L} = \frac{1}{2}\rho V^2 \mathcal{S} b C_{\mathcal{L}} \tag{3.23}$$

$$\mathcal{M} = \frac{1}{2}\rho V^2 \mathcal{S} c C_{\mathcal{M}} + \Delta_z T \tag{3.24}$$

$$\mathcal{N} = \frac{1}{2}\rho V^2 \mathcal{S} b C_{\mathcal{N}} \tag{3.25}$$

where b is the wingspan of the aircraft and Δ_z is the moment arms of the thrust in the aircraft's body frame. The aerodynamic moment coefficients are

$$C_{\mathcal{L}} = C_{\mathcal{L}0} + C_{\mathcal{L}\delta_a}\delta_a + C_{\mathcal{L}\delta_r}\delta_r + C_{\mathcal{L}\beta}\beta + C_{\mathcal{L}p}\frac{b}{2V}p + C_{\mathcal{L}r}\frac{b}{2V}r \tag{3.26}$$

$$C_{\mathcal{M}} = C_{\mathcal{L}\alpha}\alpha + C_{\mathcal{L}\delta_e}\delta_e + C_{\mathcal{M}q}\frac{c}{2V}q \tag{3.27}$$

$$C_{\mathcal{N}} = C_{\mathcal{N}0} + C_{\mathcal{N}\delta_a}\delta_a + C_{\mathcal{N}\delta_r}\delta_r + C_{\mathcal{N}\beta}\beta + C_{\mathcal{N}p}\frac{b}{2V}p + C_{\mathcal{N}r}\frac{b}{2V}r \tag{3.28}$$

3.1.5 Engine Dynamics

The thrust generated by the engine (T) is

$$T = \delta_T \, T_{max} \tag{3.29}$$

where δ_T denotes the instantaneous throttle setting and T_{max} is the maximum available thrust of the aircraft and assumed to be constant in this research. The engine dynamics is modeled as that of a first order system with time constant τ. Thus, we have

$$\dot{\delta}_T = \frac{\delta_T - \delta_{t_T}}{\tau} \ , \tag{3.30}$$

where δ_{t_T} is the commanded throttle setting ($0 \leq \delta_{t_T} \leq 1$).

3.1.6 Actuator Dynamics

For the present study, the actuator saturation and rate limit are considered. The deflection range attainable from each control surface deflection is (-20 deg, 20 deg). A rate limit of 50 deg/sec is applied on control surface deflections.

3.2 Model for Trajectory Prediction

When the focus is on predicting trajectory of aircraft, i.e., the change in the position of the CM of the aircraft over time, the rotational motion can be ignored. This leads to the concept of Point-Mass-Model (PMM), which is also referred to

as "Performance Model" [26]. Since the rotational motion is not considered, the equations of motion governs only the translational motion, i.e., 3-DOF motion is considered.

3.2.1 Translational Kinematics

The flight trajectory of aircraft with respect to the inertial reference frame [$\hat{I}$] is written in scalar form as

$$\dot{x} = V\cos\gamma\cos\mu + W_x(x,y,z,t) \tag{3.31}$$

$$\dot{y} = V\cos\gamma\sin\mu + W_y(x,y,z,t) \tag{3.32}$$

$$\dot{z} = V\sin\gamma + W_z(x,y,z,t) \tag{3.33}$$

where x, y, z is the aircraft position in the inertial frame, V is the airspeed, angles γ and μ specifies the direction of the airspeed vector (velocity vector relative to air) and W_x, W_y, W_z are the spatially and temporally varying wind components along inertial x, y, z axes.

3.2.2 Translational Dynamics

The aircraft translational dynamics with wind effects included are written in scalar form as

$$\dot{V} = \frac{T - D - mg\sin\gamma}{m} - \dot{W}_x \tag{3.34}$$

$$\dot{\gamma} = \frac{\frac{L}{m}\cos\zeta - g\cos\gamma + \dot{W}_z\cos\zeta + \dot{W}_y\sin\zeta}{V} \tag{3.35}$$

$$\dot{\mu} = \frac{\frac{L}{m}\sin\zeta - \dot{W}_y\cos\zeta + \dot{W}_z\sin\zeta}{V\cos\gamma} \tag{3.36}$$

where ζ is velocity-roll angle, which is the angular displacement of wind frame by rotating about $O_W X_W$ axis with respect to the inertial frame [$\hat{I}$], (L, D) are aerodynamic lift and drag, respectively, T is thrust, g is gravitational acceleration, m

is the mass and $\dot{W}_x, \dot{W}_y, \dot{W}_z$ are time rate of change of wind velocity components experienced by the aircraft.

3.2.3 Discretized PMM for Trajectory Prediction

For the online implementation of PMM equations for trajectory prediction, the differential equation given in previous section are discretized using the forward Euler's formula, which leads to the following difference equations:

$$x(n+1) = x(n) + V(n)\cos\gamma(n)\cos\mu(n)\Delta t + W_x\Delta t \tag{3.37}$$

$$y(n+1) = y(n) + V(n)\cos\gamma(n)\sin\mu(n)\Delta t + W_y\Delta t \tag{3.38}$$

$$z(n+1) = z(n) + V(n)\sin\gamma(n)\Delta t + W_z\Delta t \tag{3.39}$$

$$\begin{aligned} V(n+1) &= V(n) + \frac{T}{m}\Delta t - \frac{D}{m}\Delta t \\ &- g\sin\gamma(n)\Delta t - \dot{W}_x\Delta t \end{aligned} \tag{3.40}$$

$$\begin{aligned} \gamma(n+1) &= \gamma(n) + \frac{L}{mV(n)}\cos\zeta\Delta t - \frac{g}{V(n)}\cos\gamma(n)\Delta t \\ &+ \frac{\dot{W}_z}{V(n)}\cos\zeta\Delta t - \frac{\dot{W}_y}{V(n)}\sin\zeta\Delta t \end{aligned} \tag{3.41}$$

$$\begin{aligned} \mu(n+1) &= \mu(n) + \frac{L\sin\zeta\Delta t}{mV(n)\cos\gamma(n)} - \frac{\dot{W}_y\cos\zeta\Delta t}{V(n)\cos\gamma(n)} \\ &+ \frac{\dot{W}_z\sin\zeta\Delta t}{V(n)\cos\gamma(n)} \end{aligned} \tag{3.42}$$

where n is the discrete time and Δt is the sampling period. The trajectory prediction includes the time propagation of these difference equations into the future until a specified "look-ahead" time.

3.3 Model for Input Prediction

As stated earlier, input prediction requires the inverse simulation of the equations of motion. That is, given the trajectory of the aircraft, i.e., the locus of the

CM of the aircraft in 4-DOF space (time and 3-DOF space in the inertial frame), the equations of motion should be solved to determine the required input variables, i.e., aerodynamic control surface deflections and throttle setting. The 6-DOF nonlinear equations of motion, given in Section 3.1, especially the translational and rotational dynamics equations, will be employed for this purpose. Notice that, the scalar form of the dynamic equations is needed in order to explicitly show all the input variables.

3.3.1 Translational Dynamics

The translational dynamic equations represent the force-balance relations in the case of steady state (no acceleration) flight and required force and acceleration relations in case of flight through trajectory requiring translational acceleration. The

translational equations with the aerodynamic force expressions for a KC-135 aircraft are written in scalar form as follows.

$$\begin{aligned}
\dot{V} &= g\left[\cos\theta\sin\beta\sin\phi + \cos\beta\left(\cos\phi\cos\theta\sin\alpha - \cos\alpha\sin\theta\right)\right] \\
&\quad + \frac{1}{m}\left[-K_{1v}V^2 - K_{2v}\alpha^2V^2 + \delta_T T_{max}\cos\left(\alpha+\delta\right)\cos\beta\right] \\
&\quad + \left[er(1,1)\dot{W}_x + er(1,2)\dot{W}_y + er(1,3)\dot{W}_z\right] \qquad (3.43) \\
\dot{\beta} &= -r\cos\alpha + p\sin\alpha \\
&\quad + \frac{g}{V}\left[-\cos\phi\cos\theta\sin\alpha\sin\beta + \cos\beta\cos\theta\sin\phi + \cos\alpha\sin\beta\sin\theta\right] \\
&\quad - \frac{1}{m\,V}\left[K_{1b}V^2 + K_{2b}\beta V^2 + K_{3b}V^2\delta_r + \delta_T T_{max}\cos\left(\alpha+\delta\right)\sin\beta\right] \\
&\quad + \left[er(2,1)\dot{W}_x + er(2,2)\dot{W}_y + er(2,3)\dot{W}_z\right] \qquad (3.44) \\
\dot{\alpha} &= q - \left(p\cos\alpha + r\sin\alpha\right)\tan\beta \\
&\quad + \frac{g\ \sec\beta}{V}\left[\cos\alpha\cos\phi\cos\theta + \sin\alpha\sin\theta\right] \\
&\quad - \frac{\sec\beta}{m\,V}\left[K_{1a}V^2 + K_{2a}\alpha V^2 + K_{3a}V^2\left(\alpha-\alpha_{ref}\right)^2\right] \\
&\quad + \left[K_{4a}qV + K_{5a}V^2\delta_e + \delta_T T_{max}\sin\left(\alpha+\delta\right)\right] \\
&\quad + \left[er(3,1)\dot{W}_x + er(3,2)\dot{W}_y + er(3,3)\dot{W}_z\right] \qquad (3.45)
\end{aligned}$$

where V is the airspeed, α, β are angle of attack and side slip angle, which define the orientation of velocity vector relative to body frame [$\hat{B}$]. ψ, θ, ϕ are the Euler's angles, which define the orientation of body frame [$\hat{B}$] relative to inertial frame [$\hat{I}$]. $\delta_T, \delta_e, \delta_r$ are thrust setting, elevator and rudder deflection angles, respectively.

In Eq. (3.43)-(3.45), the "K-coefficients" are introduced in terms of the stability and control derivatives for brevity as follows. Note that these coefficients are not constant as the air density changes with altitude.

$$\begin{aligned}
K_{1v} &= \frac{1}{2}\rho SC_{D_0} \quad K_{2v} = \frac{1}{2}\rho SC_{D_{\alpha^2}} \\
K_{1b} &= \frac{1}{2}\rho SC_{S_0} \quad K_{2b} = \frac{1}{2}\rho SC_{S_\beta} \quad K_{3b} = \frac{1}{2}\rho SC_{S_{\delta_r}} \\
K_{1a} &= \frac{1}{2}\rho SC_{L_0} \quad K_{2a} = \frac{1}{2}\rho SC_{L_\alpha} \quad K_{3a} = \frac{1}{2}\rho SC_{L_{\alpha^2}} \\
K_{4a} &= \frac{1}{4}\rho ScC_{L_q} \quad K_{5a} = \frac{1}{2}\rho SC_{L_{\delta_e}}
\end{aligned}$$

Matrix er is calculated by

$$er = \mathcal{E}^{-1}\mathbf{R}(\psi, \theta, \phi) \tag{3.46}$$

and

$$\mathcal{E}^{-1} = \begin{bmatrix} \cos\alpha\cos\beta & \sin\beta & \cos\beta\sin\alpha \\ -\frac{1}{V}\cos\alpha\sin\beta & \frac{1}{V}\cos\beta & -\frac{1}{V}\sin\alpha\sin\beta \\ -\frac{1}{V}\sec\beta\sin\alpha & 0 & \frac{1}{V}\cos\alpha\sec\beta \end{bmatrix} \tag{3.47}$$

where the entities of matrix er are:

$$\begin{aligned}
er(1,1) &= \cos\beta\sin\alpha\,(\sin\phi\sin\psi + \cos\phi\cos\psi\sin\theta) \\
&\quad - \sin\beta\,(\cos\phi\sin\psi - \cos\psi\sin\phi\sin\theta) \\
&\quad + \cos\alpha\cos\beta\cos\psi\cos\theta \qquad (3.48) \\
er(1,2) &= \cos\beta\sin\alpha\,(-\sin\phi\cos\psi + \cos\phi\sin\psi\sin\theta) \\
&\quad + \sin\beta\,(\cos\phi\cos\psi + \sin\psi\sin\phi\sin\theta) \\
&\quad + \cos\alpha\cos\beta\sin\psi\cos\theta \qquad (3.49) \\
er(1,3) &= -\cos\alpha\cos\beta\sin\theta + \sin\beta\sin\phi\cos\theta \\
&\quad + \cos\beta\sin\alpha\cos\phi\cos\theta \qquad (3.50)
\end{aligned}$$

$$
\begin{aligned}
er(2,1) &= -\frac{1}{V}\left(\cos\alpha\sin\beta\cos\theta\cos\psi\right) \\
&\quad +\frac{1}{V}\left(-\cos\phi\sin\psi+\cos\psi\sin\phi\sin\theta\right)\cos\beta \\
&\quad -\frac{1}{V}\left(\sin\phi\sin\psi+\cos\phi\sin\theta\cos\psi\right)\sin\alpha\sin\beta \qquad (3.51)\\
er(2,2) &= -\frac{1}{V}\left(\cos\alpha\sin\beta\cos\theta\sin\psi\right) \\
&\quad +\frac{1}{V}\left(\cos\phi\cos\psi+\sin\psi\sin\phi\sin\theta\right)\cos\beta \\
&\quad -\frac{1}{V}\left(-\sin\phi\cos\psi+\cos\phi\sin\theta\sin\psi\right)\sin\alpha\sin\beta \qquad (3.52)\\
er(2,3) &= -\frac{1}{V}(\cos\alpha\sin\beta\sin\theta)+\frac{1}{V}(\sin\beta\sin\phi\cos\theta) \\
&\quad +\frac{1}{V}(\cos\beta\sin\alpha\cos\phi\cos\theta) \qquad (3.53)
\end{aligned}
$$

$$
\begin{aligned}
er(3,1) &= -\frac{1}{V}\left(\sec\beta\sin\alpha\cos\theta\cos\psi\right) \\
&\quad +\frac{1}{V}\left(\sin\phi\sin\psi+\cos\phi\sin\theta\cos\psi\right)\cos\alpha\sec\beta \qquad (3.54)\\
er(3,2) &= -\frac{1}{V}\left(\sec\beta\sin\alpha\cos\theta\sin\psi\right) \\
&\quad +\frac{1}{V}\left(-\sin\phi\cos\psi+\cos\phi\sin\theta\sin\psi\right)\cos\alpha\sec\beta \qquad (3.55)\\
er(3,3) &= -\frac{1}{V}(\sec\beta\sin\alpha\sin\theta) \\
&\quad +\frac{1}{V}(-\sec\beta\sin\alpha\cos\phi\cos\theta) \qquad (3.56)
\end{aligned}
$$

3.3.2 Rotational Dynamics

Rotational dynamic equations represent the moment-balance relation in case of steady-state (unaccelerated) flight and the required moment-angular acceleration relation when the aircraft follows a specified "angular trajectory", i.e, variation of the aircraft orientation relative to the inertial frame. The rotational dynamic equations

with the KC-135 aerodynamic moment expressions included are written in the scalar form as follows:

$$\begin{aligned}
\dot{p} &= K_{1p}\ p\ q + K_{2p}\ q\ r + K_{3p}\ V^2 \\
&\quad + K_{4p}\ \delta_a\ V^2 + K_{5p}\ \delta_r\ V^2 + K_{6p}\ \beta\ V^2 \\
&\quad + K_{7p}\ p\ V + K_{8p}\ r\ V \qquad (3.57) \\
\dot{q} &= K_{1q}\ p\ r + K_{2q}\ (r^2 - p^2) + K_{3q}\ V^2 \\
&\quad + K_{4q}\ \alpha\ V^2 + K_{5q}\ \delta_e\ V^2 + K_{6q}\ q\ V \qquad (3.58) \\
\dot{r} &= K_{1r}\ p\ q + K_{2r}\ q\ r + K_{3r}\ V^2 \\
&\quad + K_{4r}\ \delta_a\ V^2 + K_{5r}\ \delta_r\ V^2 + K_{6r}\ \beta\ V^2 \\
&\quad + K_{7r}\ p\ V + K_{8r}\ r\ V \qquad (3.59)
\end{aligned}$$

where p, q, r are angular velocity components in frame [$\hat{B}$] and δ_a is the aileron deflection angle. The "K-coefficients" in Eq. (3.57)-(3.59) are introduced in brevity in terms of aerodynamic stability and control derivatives. These coefficients, as in the

case of translational dynamics, may vary through air density when there is change in altitude.

$$
\begin{aligned}
K_{1p} &= \frac{(I_{xx}-I_{yy}+I_{zz})I_{xz}}{I_{xx}I_{zz}-I_{xz}^2} & K_{2p} &= \frac{I_{yy}-I_{zz}+I_{zz}^2-I_{xz}^2}{I_{xx}I_{zz}-I_{xz}^2} \\
K_{3p} &= \frac{\rho Sb(I_{zz}C_{L_0}+I_{xz}C_{N_0})}{2(I_{xx}I_{zz}-I_{xz}^2)} & K_{4p} &= \frac{\rho Sb(I_{zz}C_{L_{\delta_a}}+I_{xz}C_{N_{\delta_a}})}{2(I_{xx}I_{zz}-I_{xz}^2)} \\
K_{5p} &= \frac{\rho Sb(I_{zz}C_{L_{\delta_r}}+I_{xz}C_{N_{\delta_r}})}{2(I_{xx}I_{zz}-I_{xz}^2)} & K_{6p} &= \frac{\rho Sb(I_{zz}C_{L_\beta}+I_{xz}C_{N_\beta})}{2(I_{xx}I_{zz}-I_{xz}^2)} \\
K_{7p} &= \frac{\rho Sb^2(I_{zz}C_{L_p}+I_{xz}C_{N_p})}{4(I_{xx}I_{zz}-I_{xz}^2)} & K_{8p} &= \frac{\rho Sb^2(I_{zz}C_{L_r}+I_{xz}C_{N_r})}{4(I_{xx}I_{zz}-I_{xz}^2)} \\
K_{1q} &= \frac{I_{zz}-I_{xx}}{I_{yy}} & K_{2q} &= \frac{I_{xz}}{I_{yy}} & K_{3q} &= \frac{\rho ScC_{M_0}}{2I_{yy}} \\
K_{4q} &= \frac{\rho ScC_{M_\alpha}}{2I_{yy}} & K_{5q} &= \frac{\rho ScC_{M_{\delta_e}}}{2I_{yy}} & K_{6q} &= \frac{\rho Sc^2C_{M_q}}{4I_{yy}} \\
K_{1r} &= \frac{I_{xx}^2-I_{xx}I_{yy}+I_{xz}^2}{I_{xx}I_{zz}-I_{xz}^2} & K_{2r} &= \frac{(-I_{xx}+I_{yy}-I_{zz})I_{xz}}{I_{xx}I_{zz}-I_{xz}^2} \\
K_{3r} &= \frac{\rho Sb(I_{xz}C_{L_0}+I_{xx}C_{N_0})}{2(I_{xx}I_{zz}-I_{xz}^2)} & K_{4r} &= \frac{\rho Sb(I_{xz}C_{L_{\delta_a}}+I_{xx}C_{N_{\delta_a}})}{2(I_{xx}I_{zz}-I_{xz}^2)} \\
K_{5r} &= \frac{\rho Sb(I_{xz}C_{L_{\delta_r}}+I_{xx}C_{N_{\delta_r}})}{2(I_{xx}I_{zz}-I_{xz}^2)} & K_{6r} &= \frac{\rho Sb(I_{xz}C_{L_\beta}+I_{xx}C_{N_\beta})}{2(I_{xx}I_{zz}-I_{xz}^2)} \\
K_{7r} &= \frac{\rho Sb^2(I_{xz}C_{L_p}+I_{xx}C_{N_p})}{4(I_{xx}I_{zz}-I_{xz}^2)} & K_{8r} &= \frac{\rho Sb^2(I_{xz}C_{L_r}+I_{xx}C_{N_r})}{4(I_{xx}I_{zz}-I_{xz}^2)}
\end{aligned}
$$

3.3.3 Discretized Dynamics Model for Input Prediction

In order to implement these equations in the input prediction process, all the derivative terms are approximated by using backward difference scheme (BDS). Note that, BDS approximates time derivative of a variable using its value at the current discrete time and that at the previous time [83]. The time derivative of state x is, then, approximated as

$$\dot{\mathbf{x}} \cong \frac{\mathbf{x}-\mathbf{x}_{(n-1)}}{\Delta t} \tag{3.60}$$

where Δt is the time step. Note x in the above equation denotes the value of variable x at the current discrete time step and $x_{(n-1)}$ refers to the value of x at the previous discrete time, $n-1$.

Note that the equation of motion includes derivative of wind components. The wind derivatives are not approximated as they are assumed to be calculated by Eq. (2.2). Replacing all the other derivative terms with their approximations and rearranging the equations such that they are in the form of $\mathbf{f}(x) = 0$ yields the following algebraic equations. As state above, variables in the following equations without an index are at the current discrete time n while variables with index $n-1$ refers to the value of the corresponding variable at the previous discrete time $n-1$.

$$\begin{aligned}
0 &= g\left[\cos\theta\sin\beta\sin\phi + \cos\beta\left(\cos\phi\cos\theta\sin\alpha - \cos\alpha\sin\theta\right)\right] \\
&\quad + \frac{1}{m}\left[-K_{1v}V^2 - K_{2v}\alpha^2V^2 + \delta_T T_{max}\cos\left(\alpha+\delta\right)\cos\beta\right] \\
&\quad + \left[er(1,1)\dot{W}_x + er(1,2)\dot{W}_y + er(1,3)\dot{W}_z\right] - \left[\frac{V - V_{n-1}}{\Delta t}\right] \qquad (3.61) \\
0 &= -r\cos\alpha + p\sin\alpha \\
&\quad + \frac{g}{V}\left[-\cos\phi\cos\theta\sin\alpha\sin\beta + \cos\beta\cos\theta\sin\phi + \cos\alpha\sin\beta\sin\theta\right] \\
&\quad - \frac{1}{m\,V}\left[K_{1b}V^2 + K_{2b}\beta^2V^2 + K_{3b}V^2\delta_r + \delta_T T_{max}\cos\left(\alpha+\delta\right)\sin\beta\right] \\
&\quad + \left[er(2,1)\dot{W}_x + er(2,2)\dot{W}_y + er(2,3)\dot{W}_z\right] - \left[\frac{\beta - \beta_{n-1}}{\Delta t}\right] \qquad (3.62) \\
0 &= q - \left(p\cos\alpha + r\sin\alpha\right)\tan\beta \\
&\quad + \frac{g\ \sec\beta}{V}\left[\cos\alpha\cos\phi\cos\theta + \sin\alpha\sin\theta\right] \\
&\quad - \frac{\sec\beta}{m\,V}\left[K_{1a}V^2 + K_{2a}\alpha V^2 + K_{3a}V^2\left(\alpha - \alpha_{ref}\right)^2\right] \\
&\quad + \left[K_{4a}qV + K_{5a}V^2\delta_e + \delta_T T_{max}\sin\left(\alpha+\delta\right)\right] \\
&\quad + \left[er(3,1)\dot{W}_x + er(3,2)\dot{W}_y + er(3,3)\dot{W}_z\right] - \left[\frac{\alpha - \alpha_{n-1}}{\Delta t}\right] \qquad (3.63)
\end{aligned}$$

where (p, q, r) are expressed in terms of Euler's angles and their derivatives by Eqs. (3.12)-(3.14) as

$$p = [\frac{\phi - \phi_{n-1}}{\Delta t}] - [\frac{\psi - \psi_{n-1}}{\Delta t}] \sin\theta \tag{3.64}$$

$$q = [\frac{\theta - \theta_{n-1}}{\Delta t}] \cos\phi - [\frac{\psi - \psi_{n-1}}{\Delta t}] \sin\phi \cos\theta \tag{3.65}$$

$$r = [\frac{\psi - \psi_{n-1}}{\Delta t}] \cos\phi \cos\theta - [\frac{\theta - \theta_{n-1}}{\Delta t}] \sin\phi \tag{3.66}$$

$$\begin{aligned} 0 = {} & K_{1p}pq + K_{2p}qr + K_{3p}V^2 \\ & + K_{4p}\delta_a V^2 + K_{5p}\delta_r V^2 + K_{6p}\beta V^2 \\ & + K_{7p}pV + K_{8p}rV - [\frac{p - p_{n-1}}{\Delta t}] \end{aligned} \tag{3.67}$$

$$\begin{aligned} 0 = {} & K_{1q}pr + K_{2q}(r^2 - p^2) + K_{3q}V^2 \\ & + K_{4q}\alpha V^2 + K_{5q}\delta_e V^2 + K_{6q}qV - [\frac{q - q_{n-1}}{\Delta t}] \end{aligned} \tag{3.68}$$

$$\begin{aligned} 0 = {} & K_{1r}pq + K_{2r}qr + K_{3r}V^2 \\ & + K_{4r}\delta_a V^2 + K_{5r}\delta_r V^2 + K_{6r}\beta V^2 \\ & + K_{7r}pV + K_{8r}rV - [\frac{r - r_{n-1}}{\Delta t}] \end{aligned} \tag{3.69}$$

This set of nonlinear algebraic equations will be solved based on the differentiation method to compute the variation of aircraft control input variables over a specified time interval.

Chapter 4

WIND FIELD ESTIMATION

Multiple aircraft flying in the same airspace can be used as mobile sensors measuring local wind vectors, as stated in the previous section. This section discusses a method that estimates the wind field, i.e., the spatial and temporal variation of wind vector over a larger airspace. The estimation of the wind field is especially useful in areas that the aircraft are likely to fly to in the immediate future. Assuming that the wind field can be represented by smooth (continuous and differentiable) functions, the wind field estimation problem is posed as to determine, from a list of candidate models, the best functional approximation to represent the variation of wind vector over an airspace of interest. The candidate wind models can be any smooth function of position and time with unknown parameters. In this research, the wind models introduced in the following section are used as the candidate models. Then, the problem can be formulated with two steps: (i) parameter estimation for each model, and (ii) choosing the model with the minimum estimation error as the best model. For the solution of this problems, the LSE (Least Square Estimation) method is employed as it suits well with the problem formulation.

4.1 Wind Estimation Models

The spatially and temporally varying wind models introduced in Chapter 2 are used in simulations when the main goal is to study the dynamic response of aircraft flying in such a wind vector field. The second use of the wind models is in approximating the wind field in which multiple aircraft are flying by estimating the parameters of

wind models based on local wind vector measurements. The parameter estimation is carried out using LSE (Least Square Estimation) method, which approximates functions to be estimated as a linear combination of basis functions. Some of the wind models introduced in Chapter 2 can be rearranged such that the basis functions can be identified. This procedure applied to Wind model-1 as shown in Appendix B leads to a wind Estimation Model-2 (EM-2) with polynomial basis functions. Note that, the order of the following presentations of the wind EM depends on the number of coefficients in the model. This section describes various additional polynomial basis functions of time and position used in this research.

Wind Estimation Model-1 : This model has the same structure as Wind Model-1 but the temporal variation is neglected as

$$\widehat{W}_x(x,y,z,t) = \widehat{c}_{x1} + \widehat{c}_{x2}\ x + \widehat{c}_{x3}\ y \tag{4.1}$$

$$\widehat{W}_y(x,y,z,t) = \widehat{c}_{y1} + \widehat{c}_{y2}\ x + \widehat{c}_{y3}\ y \tag{4.2}$$

The basis functions to be used in LSE of this Estimation Model (EM) are

$$h_1(x,y,z,t) = 1 \tag{4.3}$$

$$h_2(x,y,z,t) = x \tag{4.4}$$

$$h_3(x,y,z,t) = y \tag{4.5}$$

Consider q number of aircraft gathering and sharing their local wind information. Each part of the basis function matrix is constructed based on the data from each aircraft. Consider aircraft-i has gathered p_i number of local wind vector infor-

mation at discrete times $\{t_{i1} \dots t_{ip_i}\}$. Then, **H**-matrix from aircraft-i at discrete time $k \geq t_{ip_i}$ is

$$\mathbf{H}_i(k) = \begin{bmatrix} 1 & x_{i1} & y_{i1} \\ 1 & x_{i2} & y_{i2} \\ \vdots & \vdots & \vdots \\ 1 & x_{ip_i} & y_{ip_i} \end{bmatrix} \in \mathbb{R}^{p_i \times 3} \tag{4.6}$$

Combining data from all the aircraft, the overall **H**-matrix is constructed as

$$\mathbf{H}(k) = \begin{bmatrix} H_1(k) \\ \vdots \\ H_q(k) \end{bmatrix} \in \mathbb{R}^{(p_i \times q) \times 3} \tag{4.7}$$

Wind Estimation Model-2 : As demonstrated in Appendix B, this wind estimation model is developed from Wind Model-1 defined in Section 2.1.

$$\widehat{W}_x(x, y, z, t) = \widehat{c}_{x1} + \widehat{c}_{x2}t + \widehat{c}_{x3}x + \widehat{c}_{x4}y + \widehat{c}_{x5}tx + \widehat{c}_{x6}ty \tag{4.8}$$

$$\widehat{W}_y(x, y, z, t) = \widehat{c}_{y1} + \widehat{c}_{y2}t + \widehat{c}_{y3}x + \widehat{c}_{y4}y + \widehat{c}_{y5}tx + \widehat{c}_{y6}ty \tag{4.9}$$

Based on this formulation, the basis function to be used in LSE are

$$h_1(x, y, z, t) = 1 \tag{4.10}$$

$$h_2(x, y, z, t) = t \tag{4.11}$$

$$h_3(x, y, z, t) = x \tag{4.12}$$

$$h_4(x, y, z, t) = y \tag{4.13}$$

$$h_5(x, y, z, t) = tx \tag{4.14}$$

$$h_6(x, y, z, t) = ty \tag{4.15}$$

Consider q number of aircraft gathering and sharing their local wind information. Each part of the basis function matrix is constructed based on the data from

each aircraft. Consider aircraft-i has gathered p_i number of local wind vector information at discrete times $\{t_{i1} \dots t_{ip_i}\}$. Then, **H**-matrix from aircraft-i at discrete time $k \geq t_{ip_i}$ is

$$\mathbf{H}_i(k) = \begin{bmatrix} 1 & t_{i1} & x_{i1} & y_{i1} & t_{i1}x_{i1} & t_{i1}y_{i1} \\ 1 & t_{i2} & x_{i2} & y_{i2} & t_{i2}x_{i2} & t_{i2}y_{i2} \\ \vdots & \vdots & \vdots & \vdots & \vdots & \vdots \\ 1 & t_{ip_i} & x_{ip_i} & y_{ip_i} & t_{ip_i}x_{ip_i} & t_{ip_i}y_{ip_i} \end{bmatrix} \in \mathbb{R}^{p_i \times 6} \tag{4.16}$$

Combining data from all the aircraft, the overall **H**-matrix is constructed as

$$\mathbf{H}(k) = \begin{bmatrix} H_1(k) \\ \vdots \\ H_q(k) \end{bmatrix} \in \mathbb{R}^{(p_i \times q) \times 6} \tag{4.17}$$

Wind Estimation Model-3 : This model has the structure of quadratic polynomial function of position as

$$\widehat{W}_x(x,y,z,t) = \widehat{c}_{x1} + \widehat{c}_{x2}\ x + \widehat{c}_{x3}\ y + \widehat{c}_{x4}\ xy + \widehat{c}_{x5}\ x^2 + \widehat{c}_{x6}\ y^2 \tag{4.18}$$

$$\widehat{W}_y(x,y,z,t) = \widehat{c}_{y1} + \widehat{c}_{y2}\ x + \widehat{c}_{y3}\ y + \widehat{c}_{y4}\ xy + \widehat{c}_{y5}\ x^2 + \widehat{c}_{y6}\ y^2 \tag{4.19}$$

The basis function to be used in LSE of EM-3 are

$$h_1(x,y,z,t) = 1 \tag{4.20}$$

$$h_2(x,y,z,t) = x \tag{4.21}$$

$$h_3(x,y,z,t) = y \tag{4.22}$$

$$h_4(x,y,z,t) = xy \tag{4.23}$$

$$h_5(x,y,z,t) = x^2 \tag{4.24}$$

$$h_6(x,y,z,t) = y^2 \tag{4.25}$$

Similarly, Consider q number of aircraft gathering and sharing their local wind information. Each part of the basis function matrix is constructed based on the data

from each aircraft. Consider aircraft-i has gathered p_i number of local wind vector information at discrete times $\{t_{i1} \dots t_{ip_i}\}$. Then, **H**-matrix from aircraft-i at discrete time $k \geq t_{ip_i}$ is

$$\mathbf{H}(k) = \begin{bmatrix} 1 & x_{i1} & y_{i1} & x_{i1}y_{i1} & x_{i1}^2 & y_{i1}^2 \\ 1 & x_{i2} & y_{i2} & x_{i2}y_{i2} & x_{i2}^2 & y_{i2}^2 \\ \vdots & \vdots & \vdots & \vdots & \vdots & \vdots \\ 1 & x_{ip_i} & y_{ip_i} & x_{ip_i}y_{ip_i} & x_{ip_i}^2 & y_{ip_i}^2 \end{bmatrix} \in \mathbb{R}^{p_i \times 6} \tag{4.26}$$

Combining data from all the aircraft, the overall **H**-matrix is constructed as

$$\mathbf{H}(k) = \begin{bmatrix} H_1(k) \\ \vdots \\ H_q(k) \end{bmatrix} \in \mathbb{R}^{(p_i \times q) \times 6} \tag{4.27}$$

Wind Estimation Model-4 : The structure of this model is represented by quadratic polynomial function of time and position as

$$\widehat{W}_x(x,y,z,t) = \widehat{c}_{x1} + \widehat{c}_{x2}\ t + \widehat{c}_{x3}\ x + \widehat{c}_{x4}\ y + \widehat{c}_{x5}\ tx \tag{4.28}$$

$$+ \ \widehat{c}_{x6}\ ty + \widehat{c}_{x7}\ xy + \widehat{c}_{x8}\ t^2 + \widehat{c}_{x9}\ x^2 + \widehat{c}_{x10}\ y^2 \tag{4.29}$$

$$\widehat{W}_y(x,y,z,t) = \widehat{c}_{y1} + \widehat{c}_{y2}\ t + \widehat{c}_{y3}\ x + \widehat{c}_{y4}\ y + \widehat{c}_{y5}\ tx \tag{4.30}$$

$$+ \ \widehat{c}_{y6}\ ty + \widehat{c}_{y7}\ xy + \widehat{c}_{y8}\ t^2 + \widehat{c}_{y9}\ x^2 + \widehat{c}_{y10}\ y^2 \tag{4.31}$$

The basis function of EM-4, based on this formulation, to be used in the LSE are

$$h_1(x,y,z,t) = 1 \tag{4.32}$$

$$h_2(x,y,z,t) = t \tag{4.33}$$

$$h_3(x,y,z,t) = x \tag{4.34}$$

$$h_4(x,y,z,t) = y \tag{4.35}$$

$$h_5(x,y,z,t) = tx \tag{4.36}$$

$$h_6(x,y,z,t) = ty \tag{4.37}$$

$$h_7(x,y,z,t) = xy \tag{4.38}$$

$$h_8(x,y,z,t) = t^2 \tag{4.39}$$

$$h_9(x,y,z,t) = x^2 \tag{4.40}$$

$$h_{10}(x,y,z,t) = y^2 \tag{4.41}$$

Similarly, Consider q number of aircraft gathering and sharing their local wind information. Each part of the basis function matrix is constructed based on the data from each aircraft. Consider aircraft-i has gathered p_i number of local wind vector information at discrete times $\{t_{i1} \dots t_{ip_i}\}$. Then, **H**-matrix from aircraft-i at discrete time $k \geq t_{ip_i}$ is

$$\mathbf{H}(k) = \begin{bmatrix} 1 & t_{i1} & x_{i1} & y_{i1} & t_{i1}x_{i1} & t_{i1}y_{i1} & x_{i1}y_{i1} & t_{i1}^2 & x_{i1}^2 & y_{i1}^2 \\ 1 & t_{i2} & x_{i2} & y_{i2} & t_{i2}x_{i2} & t_{i2}y_{i2} & x_{i2}y_{i2} & t_{i2}^2 & x_{i2}^2 & y_{i2}^2 \\ \vdots & \vdots & \vdots & \vdots & \vdots & \vdots & \vdots & \vdots & \vdots & \vdots \\ 1 & t_{ip_i} & x_{ip_i} & y_{ip_i} & t_{ip_i}x_{ip_i} & t_{ip_i}y_{ip_i} & x_{ip_i}y_{ip_i} & t_{ip_i}^2 & x_{ip_i}^2 & y_{ip_i}^2 \end{bmatrix} \in \mathbb{R}^{(p_i \times q) \times 10} \tag{4.42}$$

Combining data from all the aircraft, the overall **H**-matrix is constructed as

$$\mathbf{H}(k) = \begin{bmatrix} H_1(k) \\ \vdots \\ H_q(k) \end{bmatrix} \in \mathbb{R}^{(p_i \times q) \times 10} \tag{4.43}$$

4.1.1 Least Square Technique

The term "Least Squares (LS)" in mathematics is an approach to solving the overdetermined linear systems of equations by computing an approximate solution to the systems that minimize the sum of the squares of the residuals. The residuals depend on the difference between the approximated values and the actual values.

The linear regression or curve fitting and parameter estimation by LS scheme is one of the most basic and commonly used estimation techniques in diverse engineering applications such as structural reliability analysis [84], UAV [85], remote sensing [86], computer graphics [87]. This is because (i) it can easily and efficiently be implemented in computer, (ii) it is easy to understand and interpret without having advance mathematical background, and (iii) it provides optimal solution if all basic assumptions are valid. For example, if the system being studied is truly linear with additive uncorrelated normally distributed noise (of zero mean and constant variance), then the constants solved for by the least squares are in fact the most likely coefficients to have been used to generate the data [88].

In general, the LS algorithms consist of two steps : (i) predetermine the function with unknown parameters or coefficients that closely model the behavior of the process or physical quantity of interest and (ii) construct and solve the equation for the optimal coefficients. Theoretically, the first step is to construct the linear combination of basis functions, which are reasonable to describe the process, i.e., wind vector field in this research. Note that, the individual basis functions can be nonlinear functions as well. These functions are also known as "Approximation function" or "Approximant" in short. The most commonly used approximant is polynomial function [89]. Another approximant, which is widely used in parameter estimation of dynamic systems is exponential function of time. For stochastic processes or systems, the Guassian function is commonly used as the approximant.

4.1.1.1 Least Square Estimation for Wind Field Approximation

A wind vector field, particularly each component, can be considered as some unknown functions of position and time. The local wind vectors from multiple aircraft are "data" or "measurements" of these unknown functions at a set of discrete positions and times. Then, approximations for these unknown functions are defined as linear combinations of a set of basis functions as

$$w(x, y, z, t) \cong \sum_{i=1}^{n} c_i h_i(x, y, z, t) \tag{4.44}$$

where $w(x, y, z, t)$ is each of the components of the wind vector field, $h_i(x, y, z, t)$ are the basis functions and c_i are the set of unknown coefficients to be estimated. Then, the k^{th} measurement at position (x_k, y_k, z_k) and time t_k can be expressed as

$$\widetilde{w}_k = h_k c + e_k \tag{4.45}$$

where $\widetilde{w}_k = \widetilde{w}(x_k, y_k, z_k, t_k)$, $h_k = [h_1(x_k, y_k, z_k, t_k), \ldots, h_n(x_k, y_k, z_k, t_k)] \in \mathbb{R}^{1\times n}$, $c = [c_1, \ldots, c_n]^T \in \mathbb{R}^{n\times 1}$ and $e_k = e(x_k, y_k, z_k, t_k)$ is the residual error. For all k number of measurements put together, the matrix measurement equation is written as

$$\widetilde{W}_k = H_k c + E_k \tag{4.46}$$

where $\widetilde{W}_k \in \mathbb{R}^{k\times 1}$, $H_k \in \mathbb{R}^{k\times n}$, $E_k \in \mathbb{R}^{k\times 1}$, and $k \geq n$. By the LSE method, the unknown coefficients can be estimated as

$$\widehat{c}_k = (H_k^T H_k)^{-1} H_k^T \widetilde{W}_k \tag{4.47}$$

The residual is defined as the difference between what is actually measured and what would be measured if $c = \widehat{c}_k$, which can be expressed as

$$E_k = H_k \widehat{c}_k - \widetilde{W}_k \tag{4.48}$$

Substituting Eq. (4.47) in Eq. (4.48) yields the residual error at estimation time k.

$$E_k = H_k(H_k^T H_k)^{-1} H_k^T \widetilde{W}_k - \widetilde{W}_k \tag{4.49}$$

The sum of the squares of the residuals is calculated as

$$\|E_k\| = \sum_{i=1}^{k} E_i^2 \tag{4.50}$$

4.1.1.2 Least Square Estimation Algorithm

The LSE method as a global estimation method equally weighs each local wind data measured or estimated from the aircraft in the airspace of operation. The LSE algorithm is represented as follows

Algorithm : Least Squares Estimation

1: **Initialization.**

Read Local Wind Data : $W_{xj},\ W_{y_j},\ x_j,\ y_j,\ t_j$

where $j = 1, 2, \ldots, q$, which indicates the number of the aircraft in the vicinity.

2: **Estimation.**

[1] Construct H_k matrix, where $H_k \in \mathbb{R}^{pq \times l}$

where p is data size and l is a number of basis functions.

[2] Solve normal equation for $\widehat{c}_k$, where $\widehat{c}_k \in \mathbb{R}^{l \times 1}$.

$$\widehat{c}_k = (H_k^T H_k)^{-1} H_k^T \widetilde{W}_k$$

[3] Determine residual errors E_k, where $E_k \in \mathbb{R}^{pq \times 1}$

$$E_k = H_k(H_k^T H_k)^{-1} H_k^T \widetilde{W}_k - \widetilde{W}_k$$

[4] Find the least sum of the squares of the residuals

$$\|E_k\| = \textstyle\sum_{i=1}^{n} E_i^2$$

[5] Repeat steps 1-4 for each wind estimation model.

[6] Choose the results of the wind estimation model with the least residual error.

3: **End Estimation.**

Output the $\widehat{c}_k$ of the EM-m, where m indicates the estimation

model numbers with the least $\|E_k\|$.

4.1.1.3 Weighted Least Square Estimation (WLSE)

The LSE method discussed in the previous section is a global estimation technique. All data are considered evenly important and thus equally weighted. However, when the wind field information around the immediate trajectory of the aircraft is considered more important than the wind field information in the rest of the airspace, the weighted least square method is more appropriated for wind field estimation within the intended airspace of operation of aircraft. This can be implemented by (i) predetermine the intended airspace of the aircraft by using the predicted position of the owner aircraft at the next update time, (ii) determine the relative distance of other aircraft in the same airspace of operation with respect to the predicted owner aircraft position, and (iii) calculate weight based on the relative distance calculated form previous step.

There are many options for distance weighting functions, which are used in scattered data interpolation and approximation, reported in the literature. Ref. [90] introduced a simple inverse distance weighting function also referred to as "Shepard's Method"

$$G(d) = \frac{1}{d^p} \tag{4.51}$$

where $p > 0$, the most common choice of $p = 2$ and d is the relative distance. Ref. [91] utilizes Gaussian weighting function, this function is exponentially decay to zero with increasing d

$$G(d) = e^{-\frac{d^2}{h^2}} \tag{4.52}$$

where h is the spacing parameter which can be used to smooth out small features in the data. Ref. [92] presents Wendland weighting function, which is well defined in interval $d \in [0, h]$ and furthermore, $G(0) = 1, G(h) = 0, G'(h) = 0$ and $G''(h) = 0$.

$$G(d) = \left(1 - \frac{d}{h}\right)^4 \left(1 + \frac{4d}{h}\right) \tag{4.53}$$

Notice that all these weighting functions have the identical role of formulating points closer to the point of interest to be more important than points far away. In this research, "Shepard's Method" is used by specifying $p = 1$, i.e., the weighting function is inversely proportional to the relative distance from ownership aircraft intended position with the specified time horizon Δt_{LH} s. The point of interest is calculated by

$$x_{p_k} = x_k + V_k \cos(\mu_k)\Delta t_{LH} \tag{4.54}$$

$$y_{p_k} = y_k + V_k \sin(\mu_k)\Delta t_{LH} \tag{4.55}$$

where $x_{p_k},\ y_{p_k}$ are the point of interest or intended position of the ownership aircraft, x_k, y_k are position, $V_k,\ \mu_k$ are speed and heading angle of ownership aircraft at discrete time k, respectively.

Consider q number of aircraft gathering and sharing their local wind information. Once the point of interest is calculated, the relative distance of each aircraft from this point of interest at the time instant k is calculated by

$$d_{kj} = \sqrt{(x_{pi} - x_{kj})^2 + (y_{pi} - y_{kj})^2} \tag{4.56}$$

where $j = 1, 2, \ldots, q$.

Consider aircraft-i has gathered p_i number of local wind vector information at discrete times $\{t_{i1}, \ldots, t_{ip_i}\}$. Then, the weighted matrix of aircraft-i at discrete time $k \geq\ t_{ip_i}$ is calculated by

$$G_i(k) = \begin{bmatrix} \frac{1}{d_{i1}} & 0 & \cdots & 0 \\ 0 & \frac{1}{d_{i2}} & \ddots & \vdots \\ \vdots & \ddots & \ddots & 0 \\ 0 & \cdots & 0 & \frac{1}{d_{ip_i}} \end{bmatrix} \in \mathbb{R}^{p_i \times p_i} \tag{4.57}$$

Combining data from all the aircraft, the overall **G** - matrix is constructed as

$$\mathbf{G}(k) = \begin{bmatrix} G_1(k) & 0 & \cdots & 0 \\ 0 & G_2(k) & \ddots & \vdots \\ \vdots & \ddots & \ddots & 0 \\ 0 & \cdots & 0 & G_q(k) \end{bmatrix} \in \mathbb{R}^{(p_i \times q) \times (p_i \times q)} \tag{4.58}$$

By using WLSE method, the unknown coefficients, which are dependent upon relative distance, can be estimated by

$$\widehat{c}_k(d) = (H_k^T G(d) H_k)^{-1} H_k^T G(d) \widetilde{W}_k \tag{4.59}$$

Similar to the LSE method, the residual error is determined by Eq. (4.48). Substituting Eq. (4.59) in Eq. (4.48) yields the formulation for the residual error at estimation time k.

$$E_k = H_k (H_k^T G(d) H_k)^{-1} H_k^T G(d) \widetilde{W}_k - \widetilde{W}_k \tag{4.60}$$

Then, the sum of the squares of the residuals is calculated as

$$\|E_k\| = \sum_{i=1}^{k} E_i^2 \tag{4.61}$$

4.1.1.4 Weighted Least Square Estimation Algorithm

The WLSE is a local estimation method and weighs more heavily wind data gathered closer to the projected aircraft location as compared to wind data collected away from the projected aircraft position. This means that each aircraft may calculate a different wind field approximation even though from the same local wind measurements. The algorithm for a computer implementation of WLSE method is given below.

Algorithm : Weighted Least Squares Estimation

1: **Initialization.**

[1] Read local wind data : $W_{xj},\ W_{yj},\ x_j,\ y_j,\ t_j$

where $j = 1, 2, \ldots, q$, which indicates the number of

the aircraft in the vicinity.

[2] Read current aircraft position : $x_{kj},\ y_{kj}$

[3] Read ownership aircraft flight data : $x_k,\ y_k,\ V_k,\ \mu_k$

2: **Estimation.**

[1] Calculate predicted position of ownership aircraft for given

look-ahead time Δt_{LH}.

$$x_p = x_k + V_k \cos(\mu_k)\Delta t_{LH}$$

$$y_p = y_k + V_k \sin(\mu_k)\Delta t_{LH}$$

[2] Calculate relative distance from ownership predicted position

of others aircraft in the vicinity.

$$d_{kj} = \sqrt{(x_p - x_{kj})^2 + (y_p - y_{kj})^2}$$

[3] Calculate weight $G(d_k)_j$, which is a function of d_k.

of each aircraft in the vicinity.

$$G(d_k)_j = \tfrac{1}{d_{kj}}$$

[4] Construct H_k matrix, where $H_k \in \mathbb{R}^{pq \times l}$

where p is data size and l is a number of basis functions.

[5] Solve normal equation for $\widehat{c}_k(d_k)$, where $\widehat{c}_k(d_k) \in \mathbb{R}^{l \times 1}$.

$$\widehat{c}_k(d_k) = (H_k^T G(d_k) H_k)^{-1} H_k^T G(d_k) \widetilde{W}_k$$

[6] Determine residual errors E_k, where $E_k \in \mathbb{R}^{pq \times 1}$

$$E_k = H_k (H_k^T G(d_k) H_k)^{-1} H_k^T G(d_k) \widetilde{W}_k - \widetilde{W}_k$$

[7] Find the least sum of the squares of the residuals

$$\|E_k\| = \textstyle\sum_{i=1}^{n} E_i^2$$

[8] Repeat steps 1-7 for each wind estimation model.

[9] Choose the results of the wind estimation model with the least residual error.

3: **End Estimation.**

Output the $\widehat{c}_k$ of the EM-m, where m indicates the estimation

model numbers with the least $\|E_k\|$

4.2 Generation of Local Wind Data

In this research, the wind field estimation relies on local wind information from multiple aircraft flying in the area. This implies that the aircraft are used as wind sensors measuring local wind vectors at different locations within the same wind field. While there are efforts to directly measure wind vector by onboard sensors such as Doppler LIDAR (Light Detection and Ranging) [93], various methods are available to estimate wind an aircraft is exposed to using available onboard flight data sensors, as discussed in Section 1.3.1. In this research, a method presented in Ref. [1, 2] is used for wind estimation. This method assumes the availability of a GPS unit that provides the velocity of the aircraft relative to the inertial frame, an IMU that provides the orientation relative to the inertial frame, and an airdata sensor providing the velocity vector of the aircraft relative to the air in terms of airspeed, side slip angle and angle of attack. Using these data, the method can calculate the wind velocity vector that the aircraft is experiencing by using the kinematic relation between the velocity vectors.

4.2.1 Kinematics-based Local Wind Estimation [1, 2]

The velocity of an aircraft relative to the inertial frame can be written as the sum of (i) the velocity of the aircraft relative to the surrounding air and (ii) the velocity of the air relative to the inertial frame, which is, by definition, is the wind velocity vector. This leads to

$$V_{\underline{aircraft}} = V_{\underline{aircraft}} + V_{\underline{air}} \tag{4.62}$$
$$\underline{inertial} \qquad\quad \underline{air} \qquad\quad \underline{inertial}$$

where $V_{\underline{aircraft}}$ and $V_{\underline{air}}$ are usually expressed in the inertial frame while $V_{\underline{aircraft}}$ is conveniently written in the aircraft wind frame. Then, the relation given in Eq. (4.62)

is used to write the wind vector representation in terms of the representation of the other two vectors and the rotation matrices between these frames as

$$W_I = \dot{r}_B - \mathbf{R}_{BI}^T \mathbf{R}_{BW}^T [V\ 0\ 0]^T \tag{4.63}$$

where W_I is the representation of the wind vector in the inertial frame, $\dot{r}_B$ is the representation of the aircraft inertial velocity in the inertial frame, V is the airspeed, $\mathbf{R}_{BI}$ is the rotation matrix from inertial reference frame to the aircraft body frame and $\mathbf{R}_{BW}$ is the rotation matrix from wind frame to the aircraft body frame. An onboard GPS/IMU system will provide $\dot{r}_B$. $\mathbf{R}_{BI}$ is expressed in terms of Euler angles (ψ, θ, ϕ), which are provided by the IMU system. $\mathbf{R}_{BW}$ is expressed in terms of side slip angle, β and angle of attack, α. The triad (V, β, α) are obtained from an onboard airdata system.

4.2.2 Estimated Local Wind of Other Aircraft

The preceding section details how the local wind vector is estimated from the standard aircraft sensors on the ownership aircraft. In simulation, the ownership aircraft is modeled by 6-DOF equations of motion and controller and thus all necessary signals for local wind estimation are available. For the wind field estimation, local wind data from other aircraft in the vicinity are utilized. For these other aircraft, the simulation does not use full 6-DOF equations. Instead, only the kinematics equations are used to generate trajectories based on specified speed, flight path angle and heading angle. The position information at a given time from the aircraft trajectory is used in wind field models introduced in Chapter 2 to compute the local wind velocity vector. The local wind information from multiple aircraft are assumed to be shared with other aircraft in the same airspace for wind field estimation.

4.3 Simulation Results of Local Wind Estimation

4.3.1 Local Wind Estimation of Ownership Aircraft

The local wind vector estimation method is implemented in the simulation environment that includes the 6-DOF nonlinear equations of motion, introduced in Section 3.1. In the simulation runs for the evaluation of the wind estimation, two aircraft are flying in different trajectories within various wind fields. Each aircraft has onboard local wind estimation system running based on onboard measurements. This section presents the results of the wind estimation and the comparison with the actual wind vector computed from the wind field used in each simulation. In the simulations presented herein, the temporally and spatially varying wind fields are considered. The four different wind fields simulated are the ones introduced in Chapter 2.

In this simulation, two aircraft, Aircraft-1 and Aircraft-2 are flown by their respective controllers. Each controller is designed to fly the aircraft to follow airspeed, altitude and turn rate commands. The commanded altitude and speed for both aircraft are 7010 m and 190 m/s , respectively. The commanded turn rates are given to fly each aircraft through the flight paths shown in Fig. 4.1 as overlaid on each wind field. These figures also show, as contour lines, the variation of wind strength with position and time over 300×300 km area. The aircraft are assumed to be equipped with the sensors necessary for local wind vector estimation as described above. The details of the sensor measurements are tabulated in Table 4.1. While measurements are provided with high sampling rates, the wind vector calculations are updated only at every 10 seconds.

The simulation results are presented in Fig. 4.2. In simulations the wind vectors computed by the wind field models are multiplied by a factor before sent to the aircraft

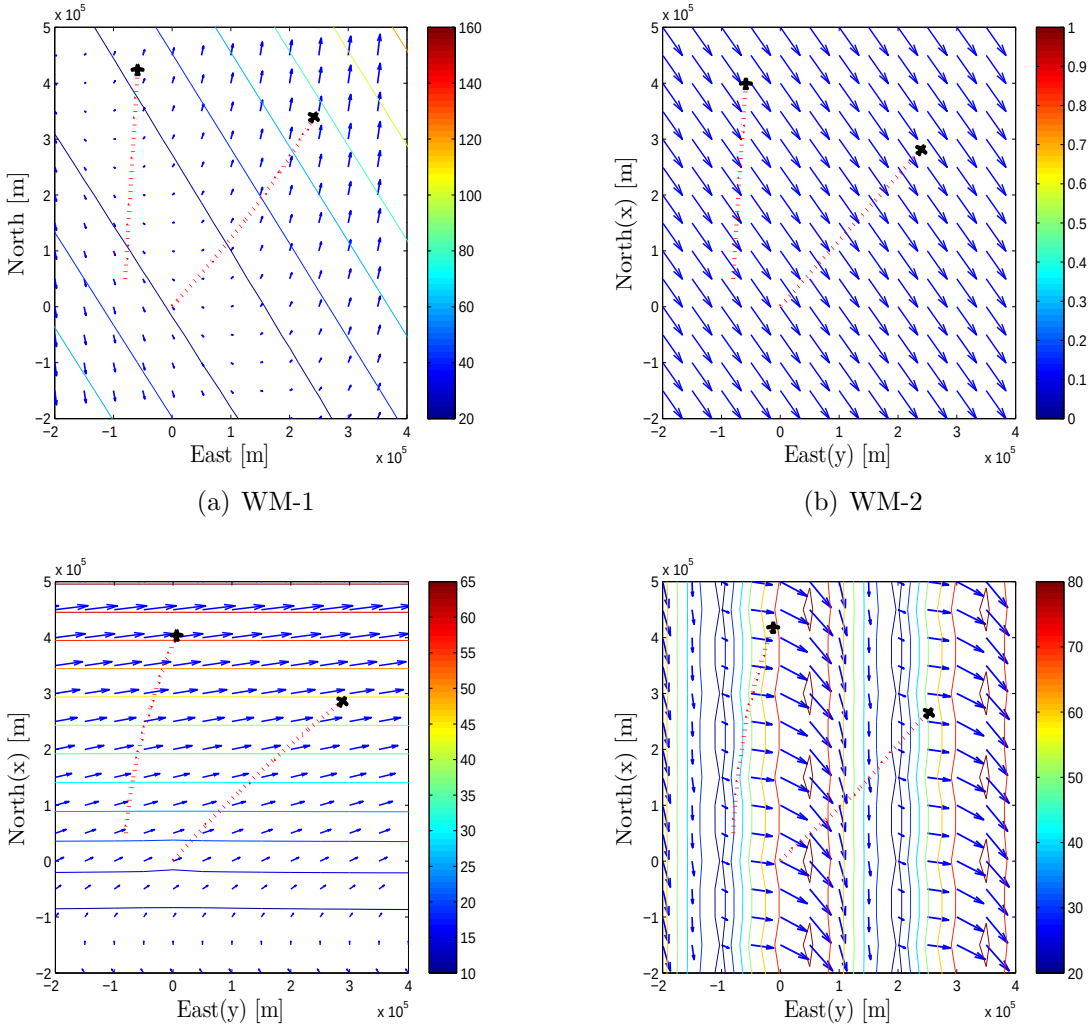

(a) WM-1

(b) WM-2

(c) WM-4

(d) WM-5

Figure 4.1. Aircraft-1 and -2 trajectories in WM-1 -2 -4 and -5.

dynamics module. This factor start from zero and goes to 1 as a step response of a first order transfer function with the time constant of 10 sec. This is done to ensure that the controller flying the aircraft can smoothly adjust the control inputs to their normal levels without causing any saturation in magnitude and rate. The choice of

Table 4.1. Details of sensor data [1, 2]

Measurements states and sampling rate				
Symbol	Description	Unit	Sensor	Sampling rate
$\dot{r}_B$	Inertial velocity	m/s	GPS/IMU	100 Hz
(ψ, θ, ϕ)	Euler's angle	deg	GPS/IMU	100 Hz
V	True airspeed	m/s	Airdata	20 Hz
(β, α)	Aerodynamic angle	deg	Airdata	20 Hz

10 sec for the time constant implies that the wind goes to its normal level after 50 sec.

Figures 4.2 (a)-(d) show the actual and estimated wind components for Aircraft-1 and Aircraft-2, respectively, flying in the wind field modeled by Wind Model-1, -2, -4, and -5. The top plots show wind component along x-axis, while the bottom plots present wind component along y-axis. As can be seen in these figures, multiple aircraft flying in different regions of a wind field experience different wind vectors. This information, when shared between aircraft, can help estimate a model for the entire wind field.

4.3.2 Local Wind Estimation of Other Aircraft

In simulations presented in this thesis, only Aircraft-1 and -2 use local wind estimation based on onboard flight data sensors. The other aircraft models are only kinematics based as explained in Section 4.2.2. In the simulation cases, theses aircraft are flying along straight lines with constant airspeed of 190 m/s at altitude of 7010 m but different heading angles.

The trajectories of the aircraft are represented in dash line overlaid on the spatially and temporally varying wind field, i.e., WM-1, -2, -4, and -5, as depicted

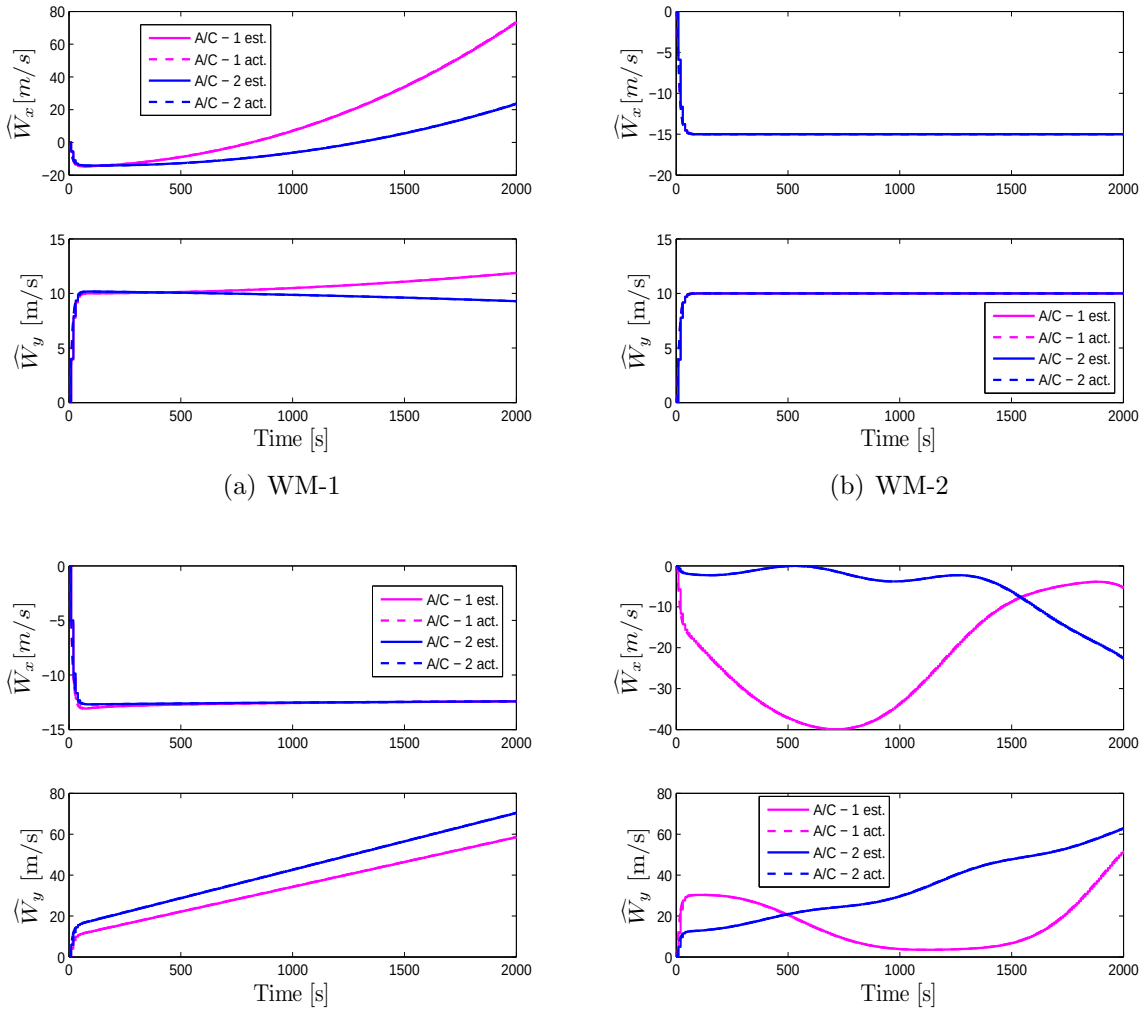

(a) WM-1 (b) WM-2

(c) WM-4 (d) WM-5

Figure 4.2. Estimated and actual local wind in WM-1 -2 -4 and -5.

in Figure 4.3 (a)-(d). The wind strength, which each aircraft expose to are shown in Fig. 4.4 (a)-(d), respectively.

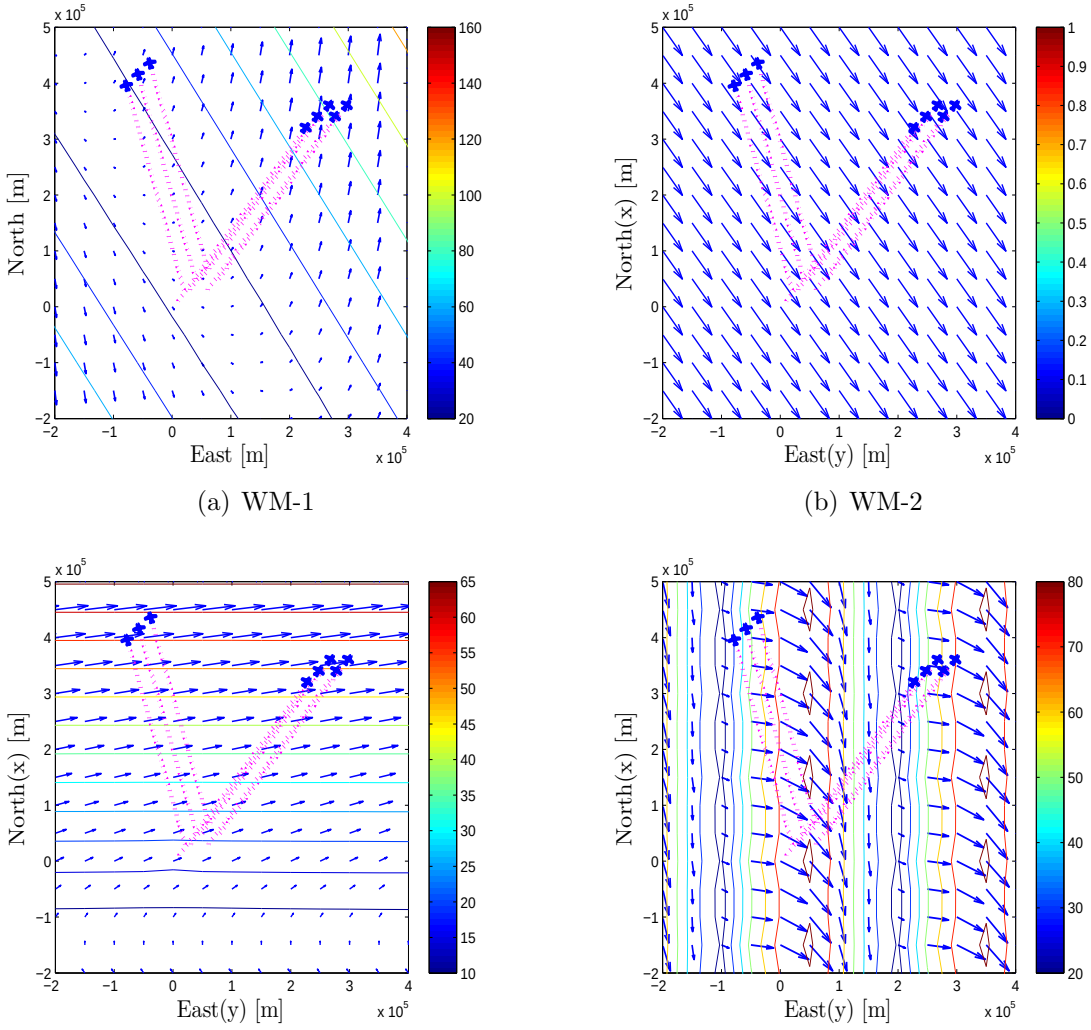

(a) WM-1

(b) WM-2

(c) WM-4

(d) WM-5

Figure 4.3. Aircraft -3 to -10 trajectories in WM-1 -2 -4 and -5.

4.4 Wind Field Estimation Simulation Results

The LSE and WLSE algorithms are implemented in simulation and various simulation cases are run for evaluating the algorithms. This section shows the simulations results of the wind field estimation. In the simulation cases presented here, ten aircraft fly with 190 m/s airspeed at 7010 m altitude with in a 300 $\times$ 300 km

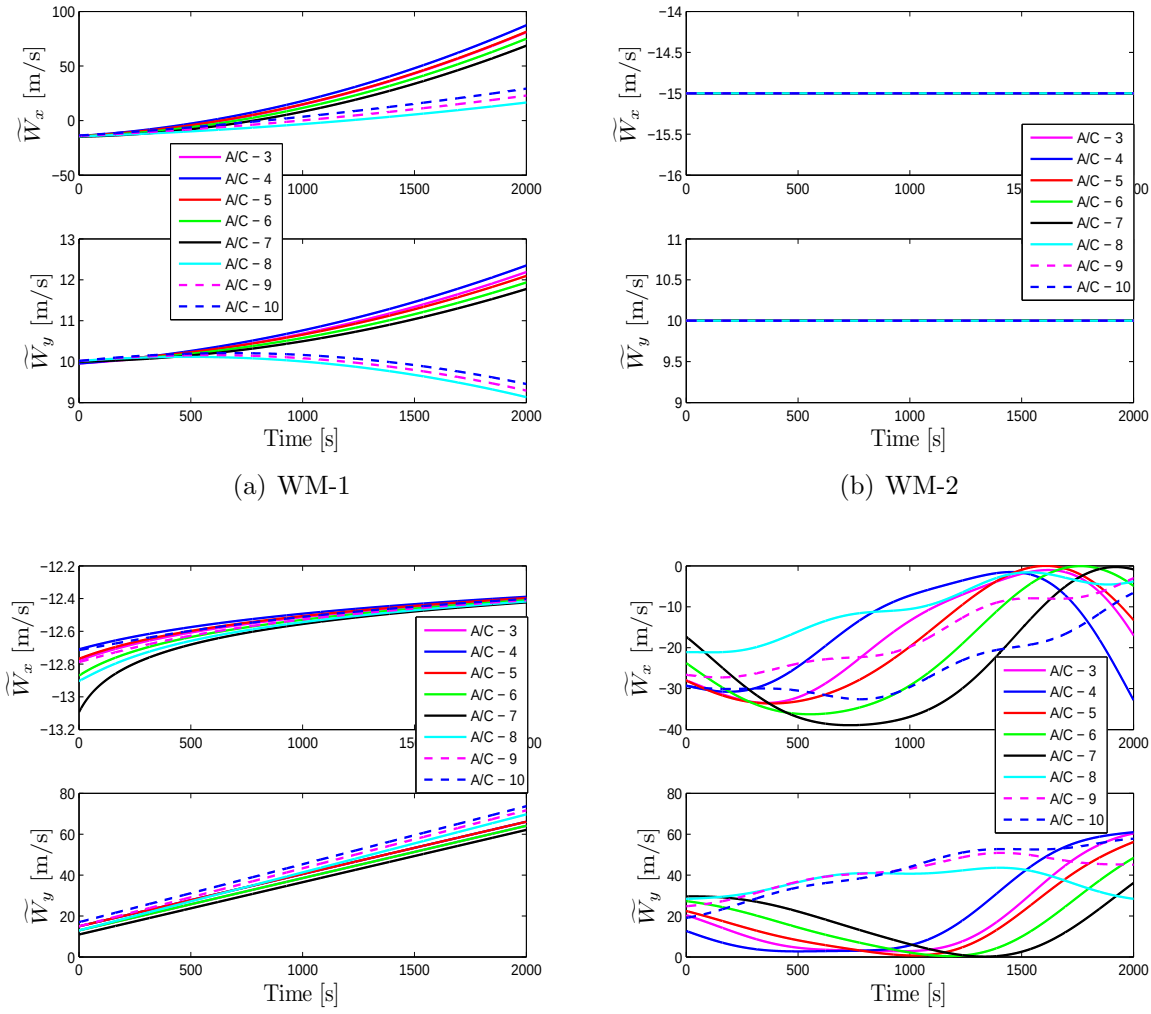

(a) WM-1

(b) WM-2

(c) WM-4

(d) WM-5

Figure 4.4. Estimated local wind in WM-1 -2 -4 and -5.

area. There are two trajectory patterns, flown by ten aircraft in the same airspace of operation. Aircraft positions at time $t = 100,\ 500,\ 1000$ and 2000 s are marked with small airplane icon and the paths are indicated by dashed-lines, overlaid on the wind fields, in Figs. 4.6 and 4.7. As stated earlier, each aircraft is assumed to broadcast its local wind vector estimation along with the position and time of the estimation.

The simulation cases are run with different wind field models introduced in Chapter 2. As stated then, the wind field models are used as both wind field "estimation model" and "simulation model". In each simulation case, different combinations of wind field models for "estimation" and "simulation" are used for evaluating the LSE and WLSE method. In each simulation case, the wind field estimation algorithm carries out parameter estimation for each model and chooses the estimation model with the least residual errors. This means that the estimation might be switching between estimation models depending on the value of their residual error.

The wind field estimation is updated every 10 s. The local wind is sampled every 1 s or sampling frequency of 1 Hz and the data size for local wind data storage of each aircraft is equal to 100 such that the dimension of $\mathbf{H}_k$ is 1000×3 for EM-1, 1000×6 for EM-2 and -3, and 1000×10 for EM-4, respectively. In each wind field, the ten aircraft are flown along two different patterns, pattern-1 and pattern-2, as shown in Figs. 4.5.a and 4.5.b, respectively.

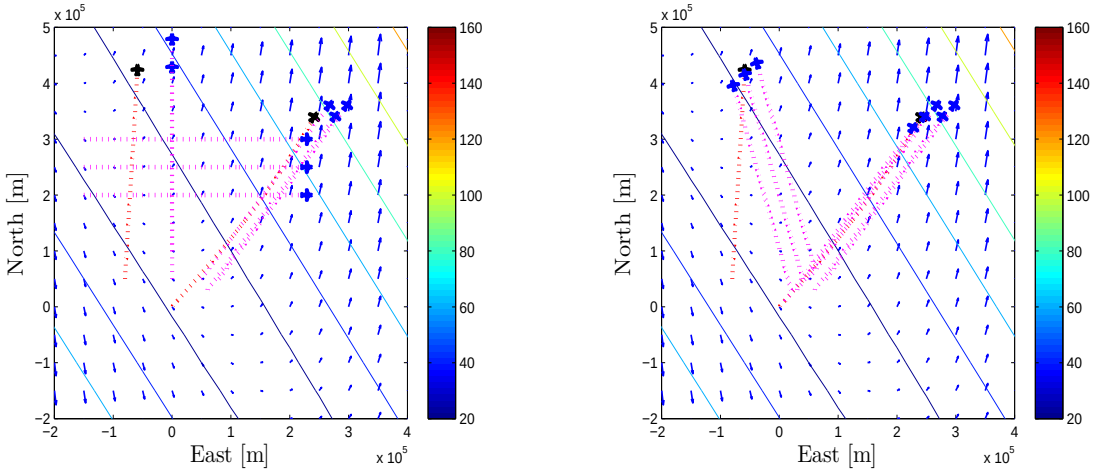

(a) Trajectory pattern - 1 (b) Trajectory pattern - 2

Figure 4.5. Aircraft trajectory patterns-1 and -2 .

4.4.1 Wind Field Model-1 Case

4.4.1.1 Least Square Estimation Results

In this simulation case, spatially and temporally varying horizontal wind vector field is generated by WM-1, when $z = 7010$ m, $x_0 = 300$ and $y_0 = 300$. The mean wind components are $W_{x0}(z,t) = -10$ m/s and $W_{y0}(z,t) = 15$ m/s and $A(z,t) = 19 \times 10^{-6} + 5 \times 10^{-8}t, B(z,t) = -5 \times 10^{-7} + 1 \times 10^{-6}t, C(z,t) = 15 \times 10^{-7} + 1 \times 10^{-8}t, E(z,t) = -15 \times 10^{-7} + 5 \times 10^{-9}t$. This WM-1 captures the wind speed variation ranging from $20 - 80$ m/s in this simulation, which is run for 2000 s.

Figures 4.6 and 4.7-(a)-(d) shows the snapshots of the positions of and the paths traveled by ten aircraft flying in spatially and temporally varying horizontal wind field represented by WM-1, through trajectory patterns-1 and -2, at different times, $t = 100,\ 500,\ 1000$ and 2000 s, respectively. Since the wind is varying with position and time, the aircraft flying in different region and different time are exposed to the different wind strength as shown by the contour lines.

The performance of the wind field estimation algorithms are shown in Figures 4.8 and 4.9 while the aircraft flying in WM-1 through trajectory pattern-1 and -2, shown in Figs. 4.6 and 4.7, respectively. Subfigures (a) indicates the wind estimation model with the least residual error by the EM number. Fig. 4.8 (a) shows that EM-4 is always the estimation model with the least residual error while aircraft flying in WM-1 along trajectory pattern-1. However, Fig. 4.9 (a) shows that, when aircraft flying through trajectory pattern-2, EM-4 is the best model initially, but the residual error of EM-2 becomes the smallest after a while. It is also interesting to note that x-component switches between EM-4 and EM-2 while y- component stays with EM-2. This shows that the x- and y-components may be computed using different estimation models because an estimation model may have the least residual error in x- component

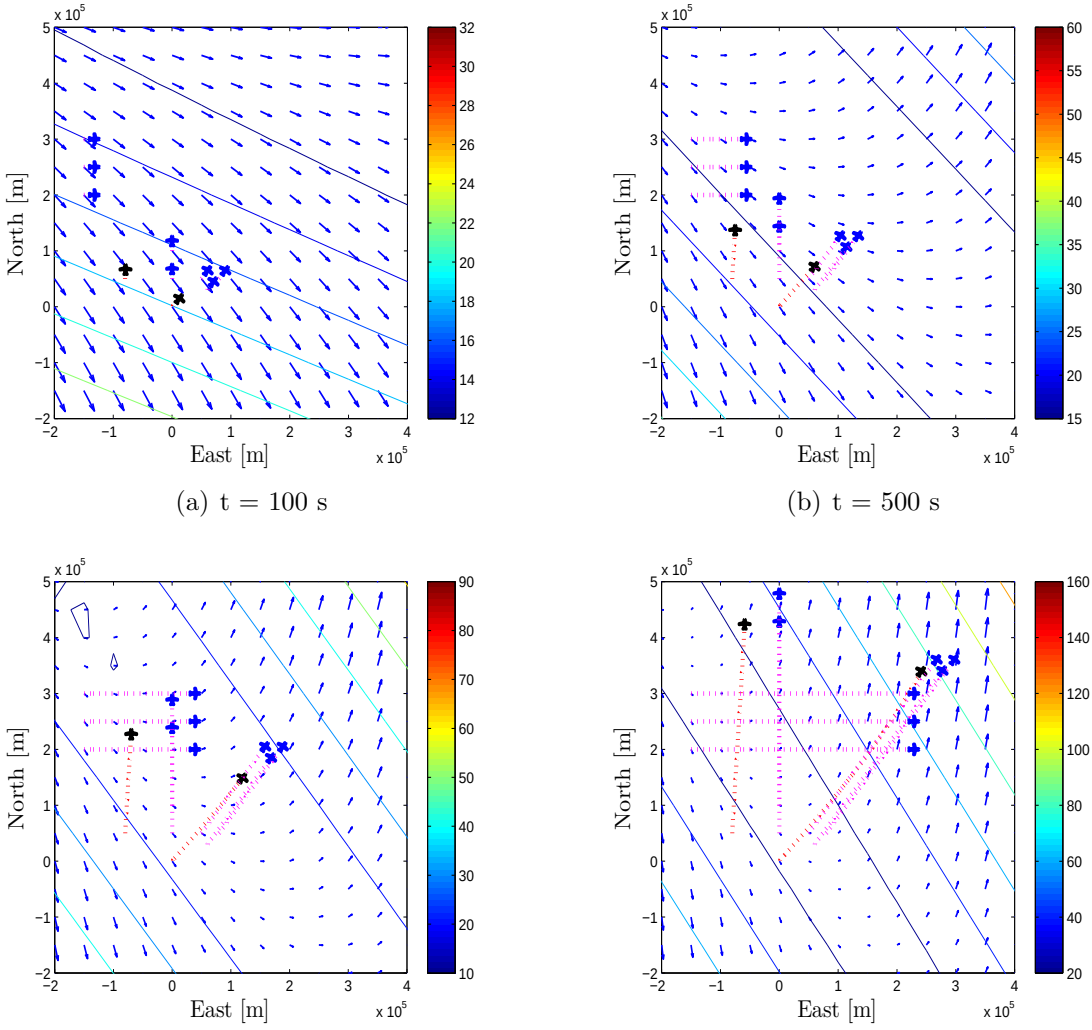

(a) t = 100 s

(b) t = 500 s

(c) T = 1000 s

(d) T = 2000 s

Figure 4.6. Aircraft trajectory pattern-1 in WM-1.

while another for y-component. Subfigures (b) shows the smallest residual error while Subfigures (c) presents the comparison of the residual errors from all four estimation models. Both Figs. 4.8 (c) and 4.9 (c) show that the switching between EM-4 and EM-2 occurs when estimation error becomes very small compared to the values earlier in the simulation. This may bring up an argument for improving the overall estimation

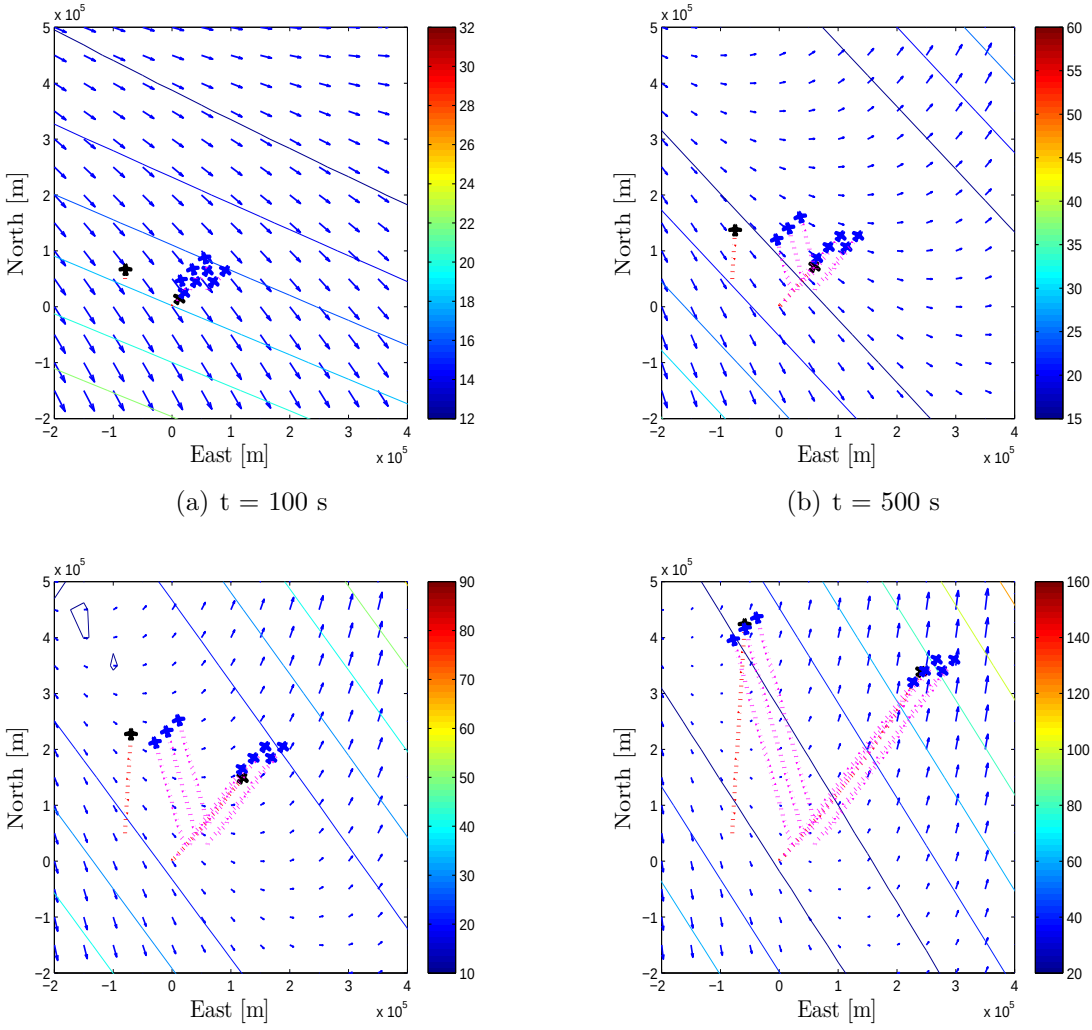

(a) t = 100 s

(b) t = 500 s

(c) T = 1000 s

(d) T = 2000 s

Figure 4.7. Aircraft trajectory pattern-2 in WM-1.

performance by adding a logic to prevent unnecessary switching when the difference in estimation error is less than a threshold. However, this is left for future work. Subfigures (d) show the comparison of the estimated local wind and the actual local wind along the trajectory of Aircraft-1.

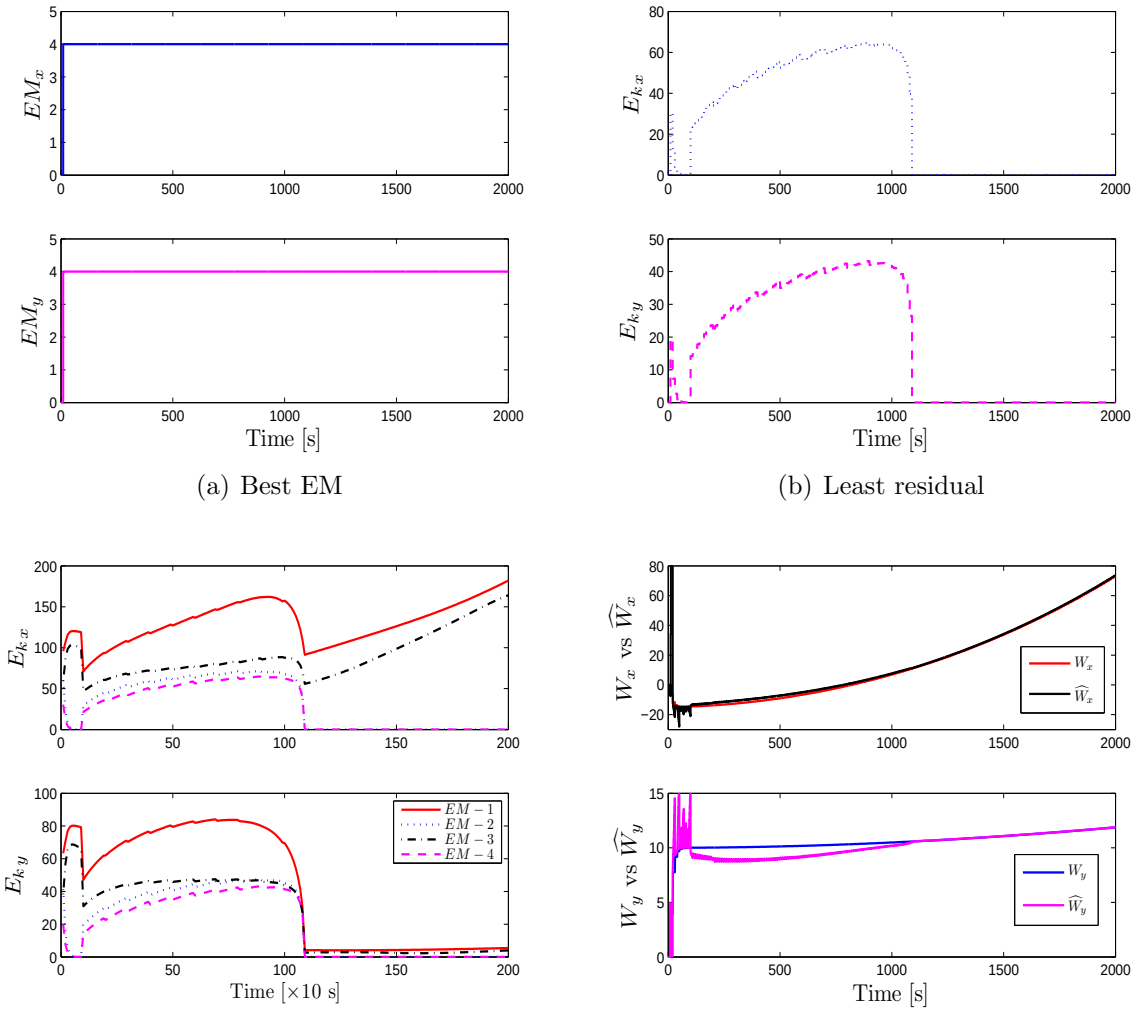

(a) Best EM

(b) Least residual

(c) Residuals

(d) Measured vs Estimated

Figure 4.8. Wind estimation by LSE in WM-1 trajectory pattern-1.

4.4.1.2 Weighted Least Square Estimation Results

In the previous section, the performance of wind field estimation based on LSE are presented. In this section, the performance of the WLSE wind field estimation algorithms are shown in Figures 4.10 and 4.11 while the aircraft are flying in WM-1 through trajectory pattern-1 and -2, similar to the LSE case, shown in Figs. 4.6 and

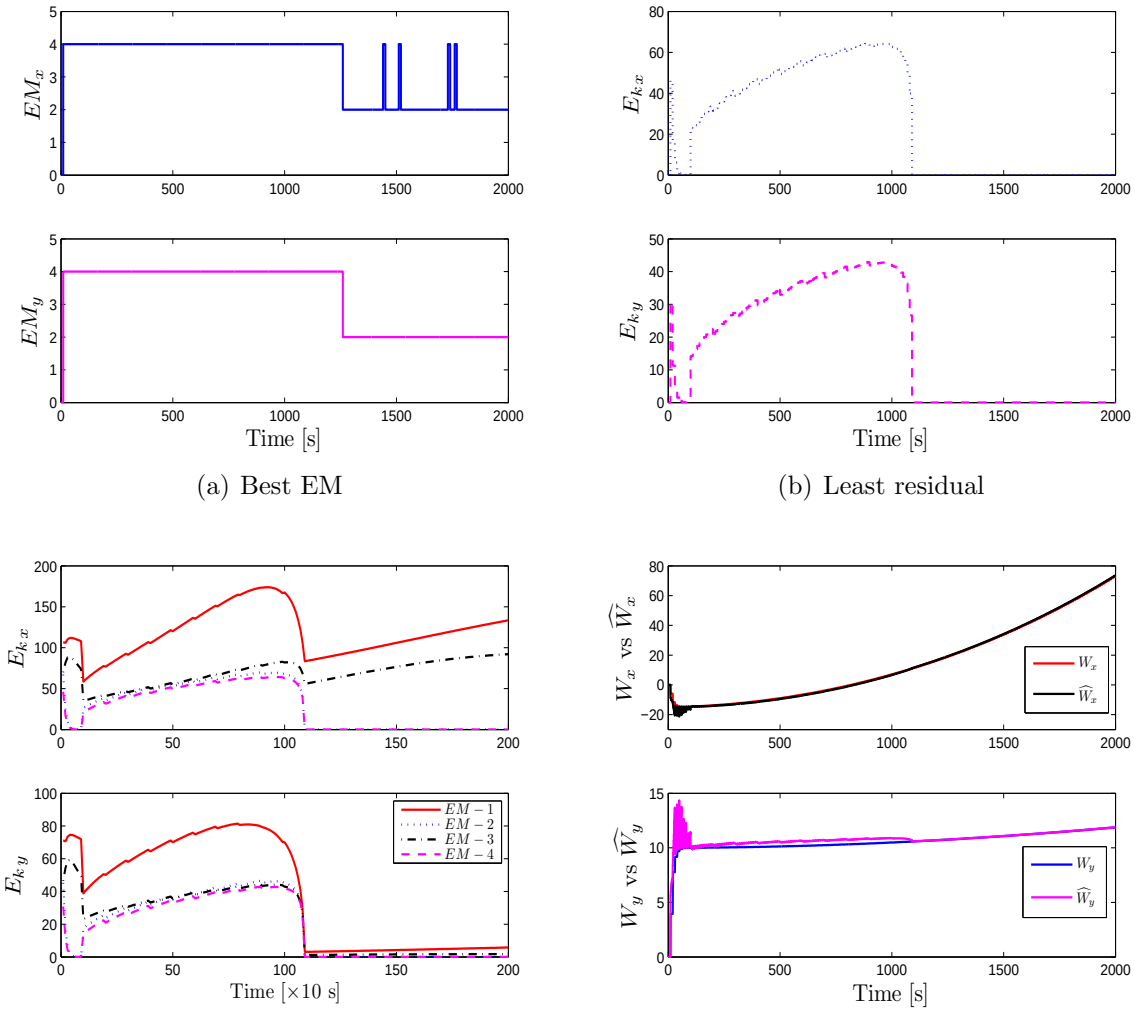

(a) Best EM

(b) Least residual

(c) Residuals

(d) Measured vs Estimated

Figure 4.9. Wind estimation by LSE in WM-1 trajectory pattern-2.

4.7. Subfigures (a) indicates the wind estimation model with the least residual error by the EM number. Unlike LSE, Figs. 4.10 (a) and 4.11 (a) show that the estimation model with the least estimation error switches between all four models while aircraft flying in WM-1 through both trajectory pattern-1 and -2. It is also interesting that x-component switches between wind models occur more frequently than y-component.

This shows that the x- and y-components are probably computed using different estimation models. Subfigures (b) shows the smallest residual error while Subfigures (c) presents the comparison of the residual errors from all four estimation models. Similarly as discussed in the LSE case, the future work to improve the overall estimation performance to prevent unnecessary switching among estimation models also applies to the WLSE case. Subfigures (d) show the comparison of the estimated local wind and the actual local wind along the trajectory of Aircraft-1.

4.4.2 Wind Field Model-4 Case

4.4.2.1 Least Square Estimation Results

In this simulation case, the spatially and temporally varying horizontal wind vector field is generated by WM-4, when $z = 7010$ m, $x_0 = 300$ and $y_0 = 300$, the mean wind components are $W_{x0}(z,t) = -10$ m/s and $W_{y0}(z,t) = 15 + 1 \times 10^{-2}t$ m/s and the coefficients are $A(z,t) = 1 \times 10^{-1}, B(z,t) = 1 \times 10^{-2}t, C(z,t) = D(z,t) = 1, E(z,t) = 1 \times 10^{-6}$. This WM-4 captures the wind speed variation ranging from $10 - 65$ m/s in this simulation, which is run for 2000 s.

Figures 4.12 and 4.13-(a)-(d) show the snapshots of the positions of and the paths traveled by ten aircraft flying in the spatially and temporally varying horizontal wind field represented by WM-4, through trajectory patterns-1 and -2, at different times, $t = 100,\ 500,\ 1000$ and 2000 s, respectively. Since the wind is varying with position and time, the aircraft flying in different region and different time is exposed to different wind strengths as shown by the contour lines.

The performance of the wind field estimation algorithms are shown in Figures 4.14 and 4.15 while aircraft are flying in WM-4 through trajectory pattern-1 and -2, which are similar to the WM-1 case, shown in Figs. 4.12 and 4.13, respectively.

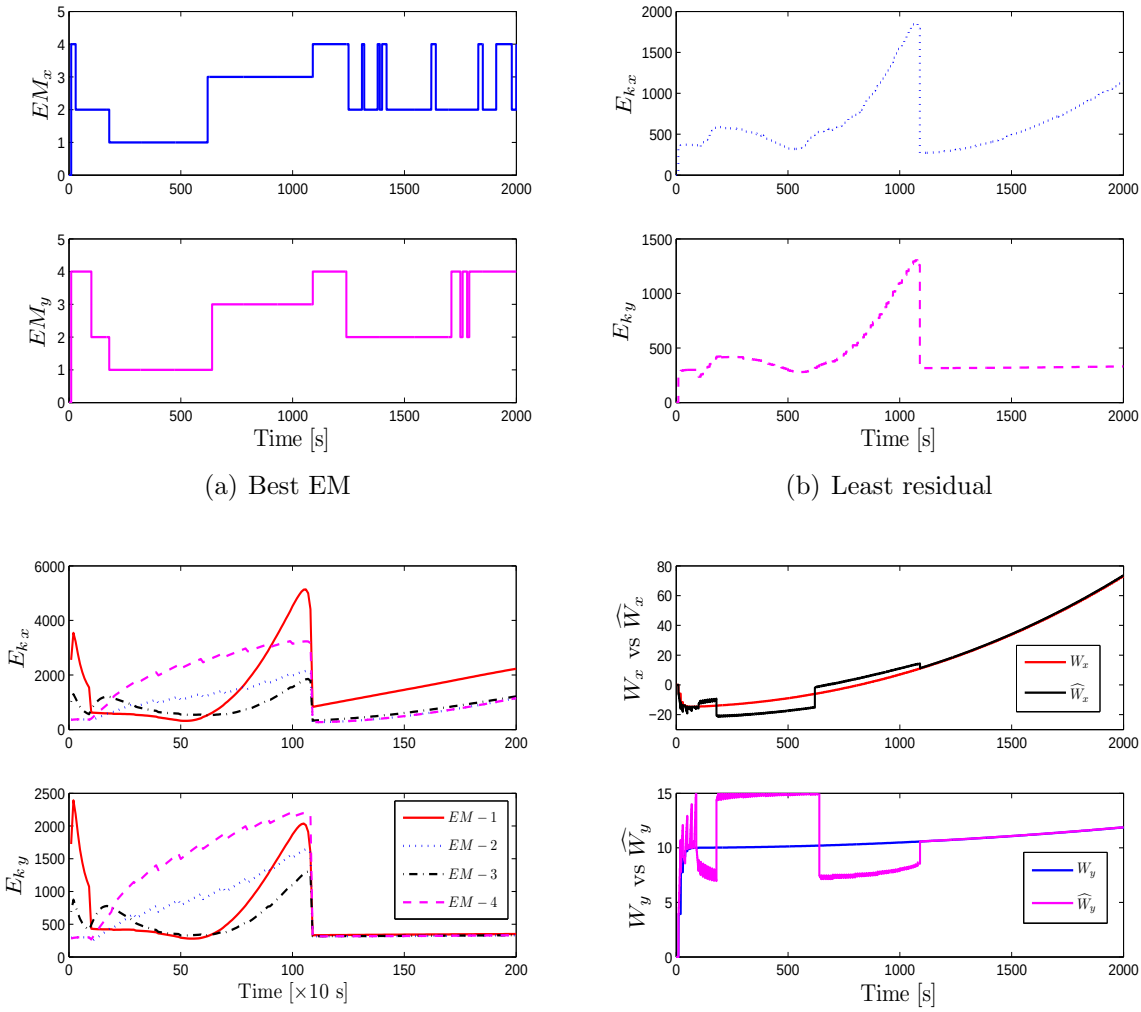

(a) Best EM

(b) Least residual

(c) Residuals

(d) Measured vs Estimated

Figure 4.10. Wind estimation by WLSE in WM-1 trajectory pattern-1.

Subfigures (a) indicates the wind estimation model with the least residual error by the EM number. Fig. 4.14 (a) and 4.15 (a) show that EM-4 is always the estimation model with the least residual error while the aircraft fly in WM-4 through both trajectory pattern-1 and -2 in x-component. However, in y-component, EM-4 is the best model initially, but the residual error of EM-2 becomes the smallest after a while.

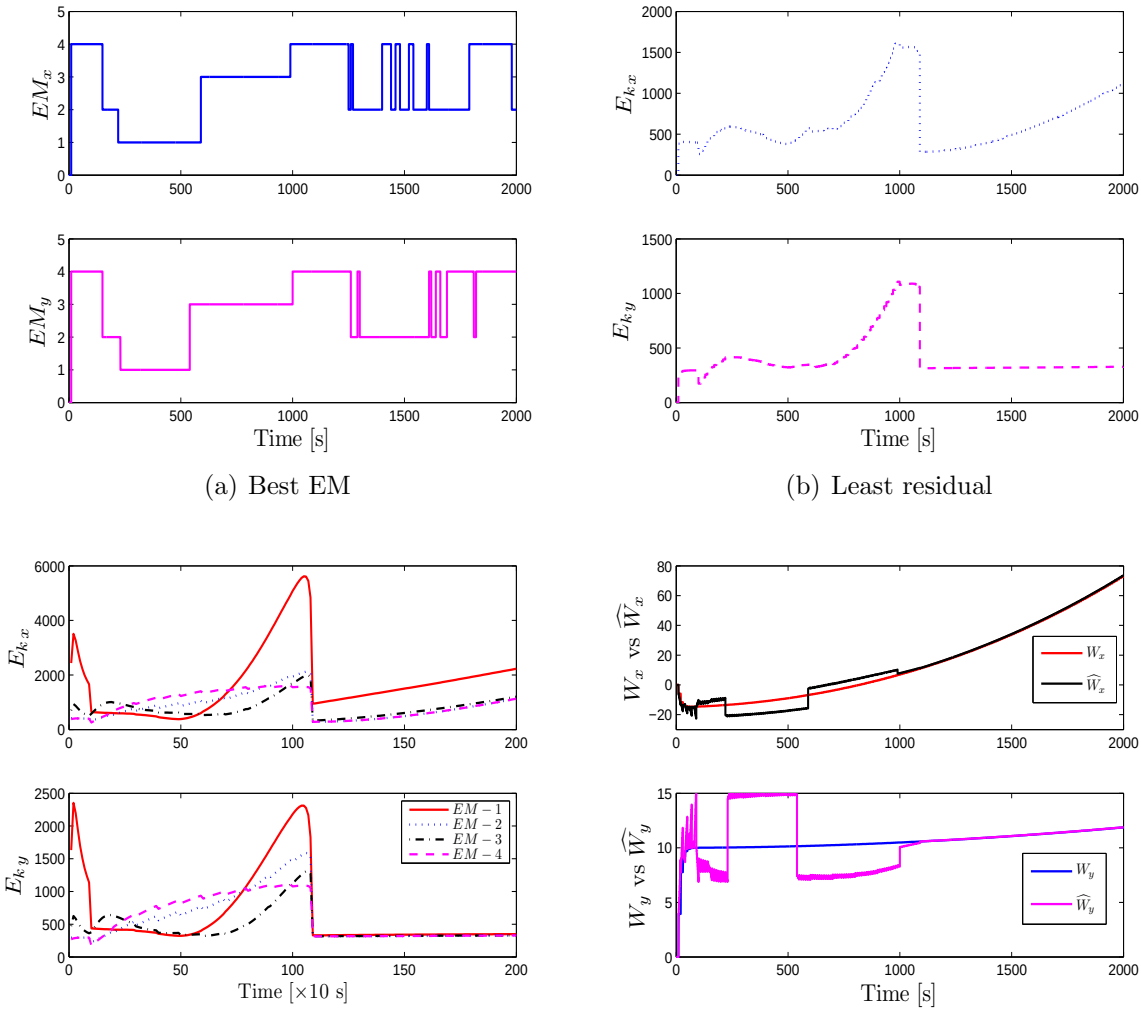

(a) Best EM

(b) Least residual

(c) Residuals

(d) Measured vs Estimated

Figure 4.11. Wind estimation by WLSE in WM-1 trajectory pattern-2.

Furthermore, Fig. 4.15 (a) shows y- component, while aircraft flying in trajectory pattern-1, switches between EM-2 and EM-4 during short duration because at that time the estimation error of EM-4 becomes smaller than the estimation error value of the EM-2. Subfigures (c) presents the comparison of the residual errors from all four estimation models. Both Figs. 4.14 (c) and 4.15 (c) show that the switching between

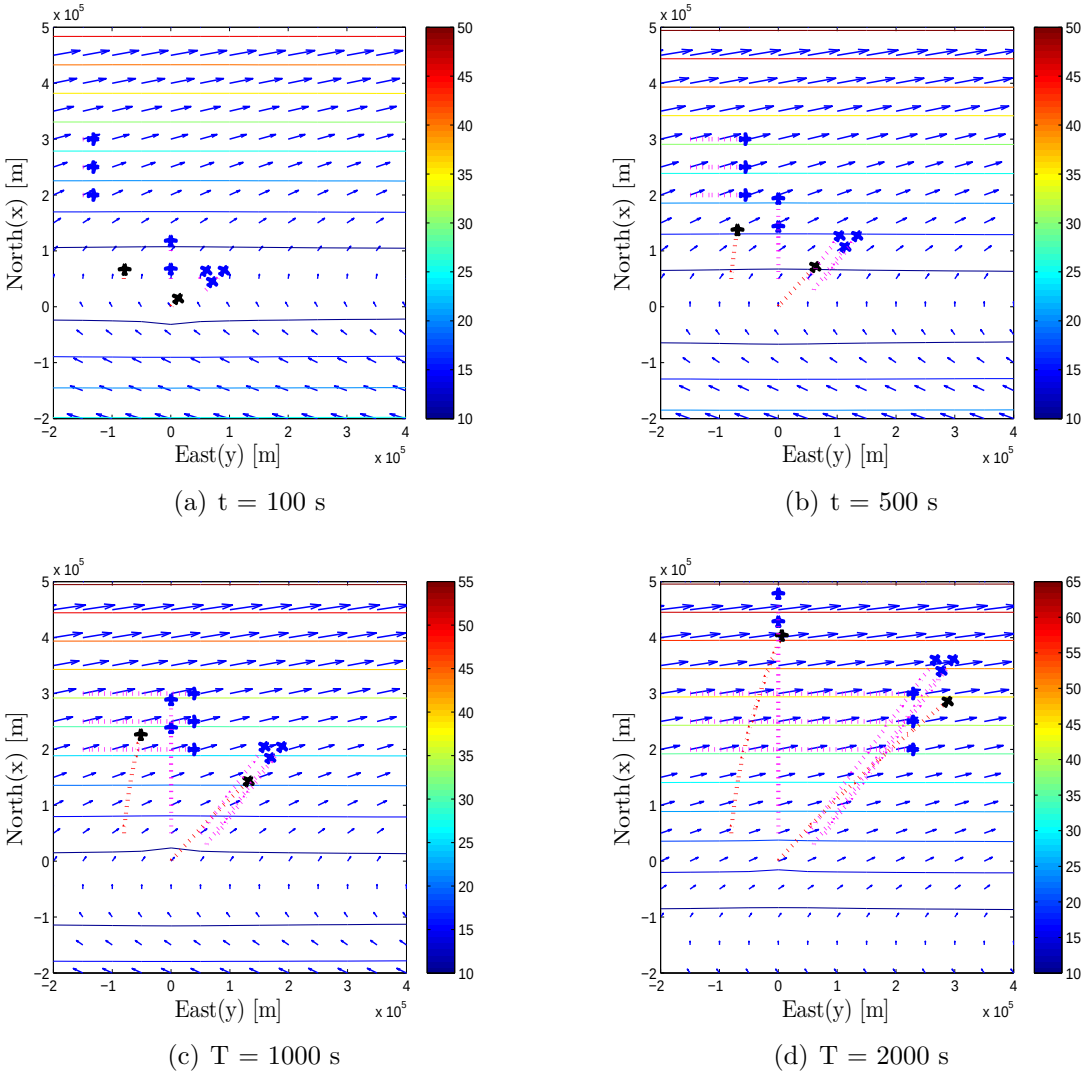

(a) t = 100 s

(b) t = 500 s

(c) T = 1000 s

(d) T = 2000 s

Figure 4.12. Aircraft trajectory pattern-1 in WM-4.

EM-4 and EM-2 occurs when the estimation error becomes very small compared to the values earlier in the simulation. This obvious results again would be improved by adding a logic to prevent unnecessary switching when the difference in estimation error is less than a threshold. Subfigures (d) show the comparison of the estimated local wind and the actual wind along the trajectory of Aircraft-1.

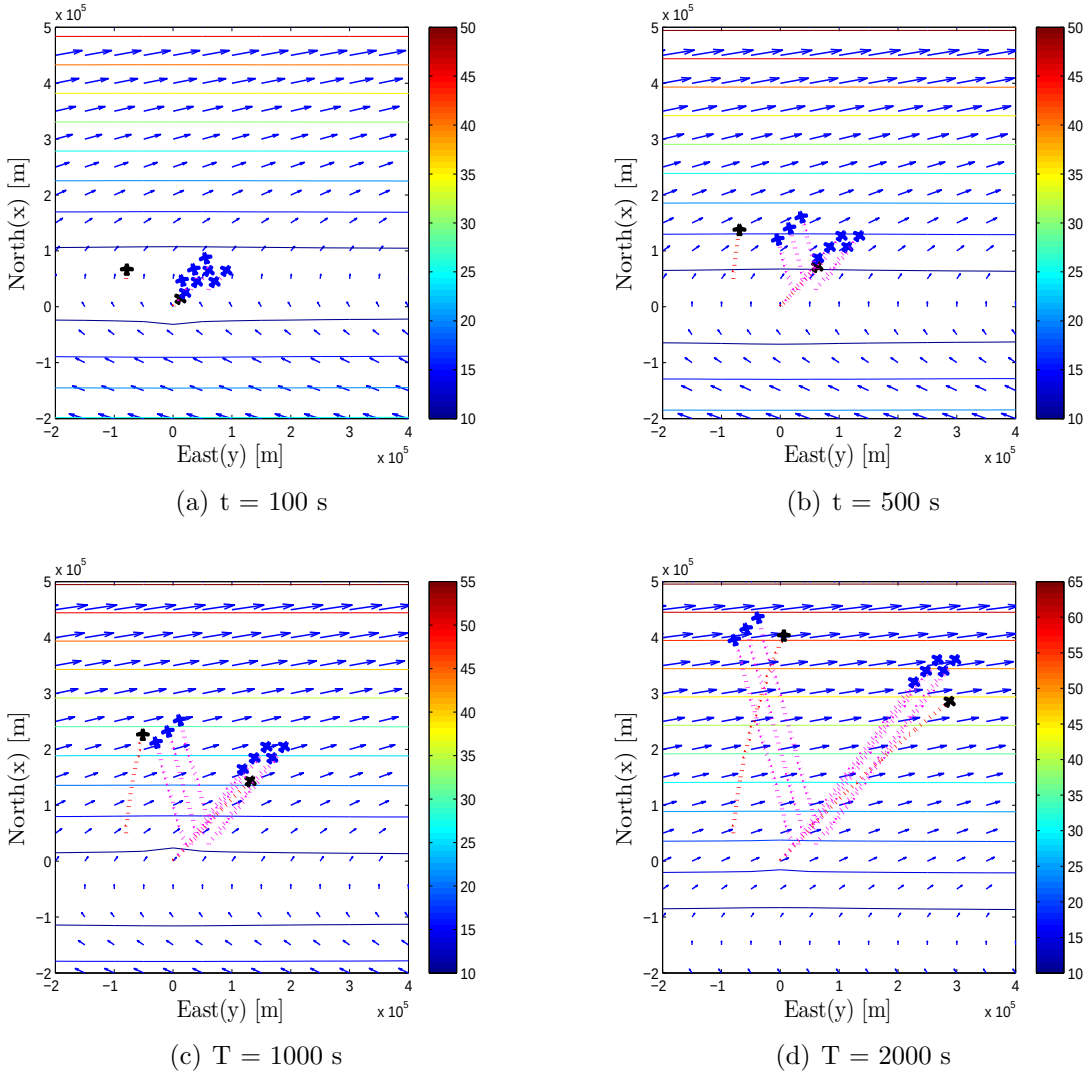

(a) t = 100 s

(b) t = 500 s

(c) T = 1000 s

(d) T = 2000 s

Figure 4.13. Aircraft trajectory pattern-2 in WM-4.

4.4.2.2 Weighted Least Square Estimation Results

The performance of the wind field estimation algorithms based on WLSE are shown in Figures 4.16 and 4.17 while the aircraft are flying in the WM-4 through trajectory pattern-1 and -2, shown in Figs. 4.12 and 4.13, respectively. Subfigures (a) show that the best wind estimation model (i.e., the one with the smallest least

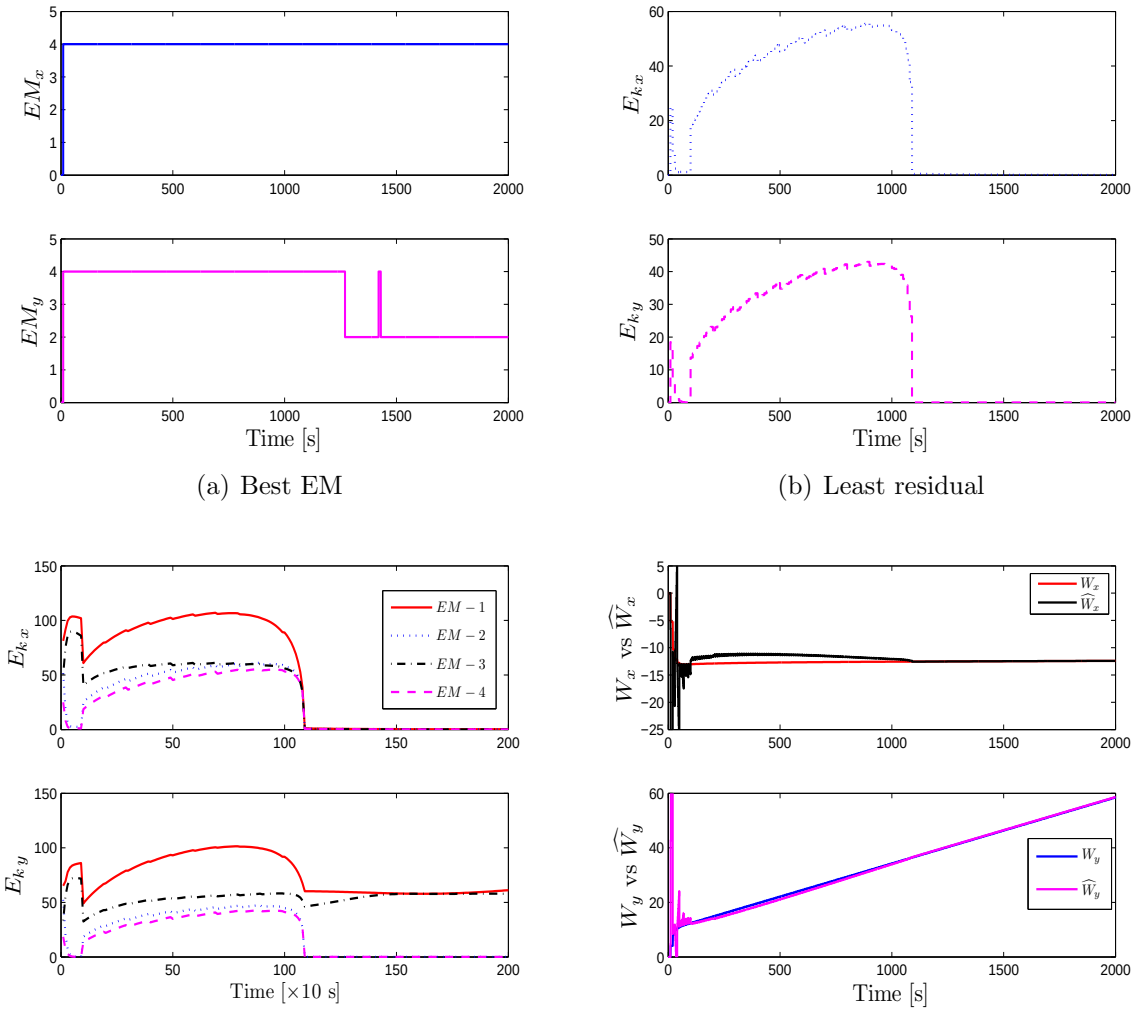

(a) Best EM

(b) Least residual

(c) Residuals

(d) Measured vs Estimated

Figure 4.14. Wind estimation by LSE in WM-4 trajectory pattern-1.

square error) switches between all estimation models. Again, the best models for x- and y-components are not necessarily the same. For example, Figs. 4.16 (a) and 4.17 (a) has EM-1 for x-component and EM-4 (mostly) for y-component during the last phase of the simulations. Subfigures (c) presents the comparison of the residual errors from all four estimation models. Both Figs. 4.16 (c) and 4.17 (c) show that the

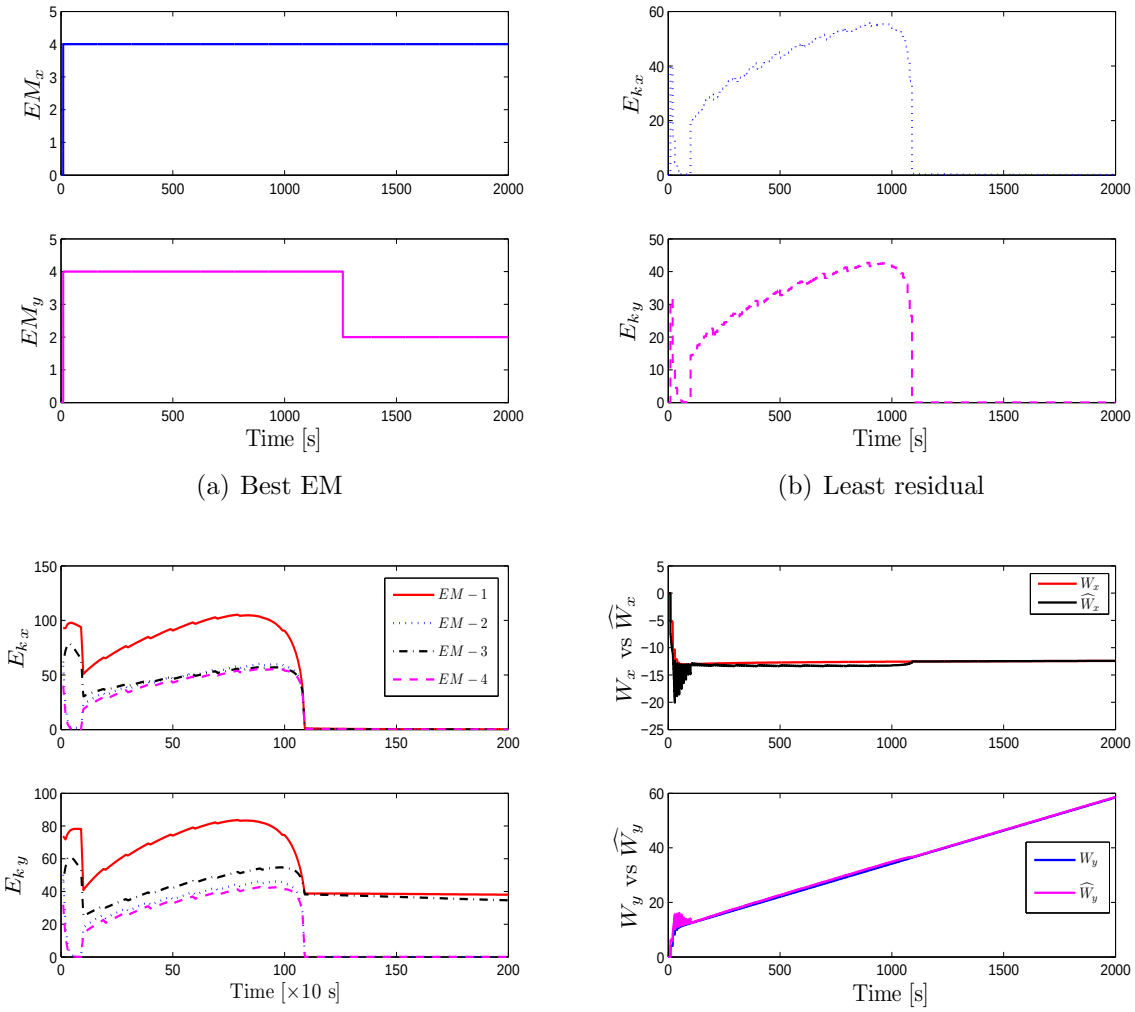

(a) Best EM

(b) Least residual

(c) Residuals

(d) Measured vs Estimated

Figure 4.15. Wind estimation by LSE in WM-4 trajectory pattern-2.

switching among all four estimation models occur when the estimation error becomes very small compared to the values earlier in the simulation. This phenomenon can be avoided, if considered detrimental, by adding a logic to prevent unnecessary switching when the difference in estimation error is less than a threshold. Subfigures (d) show

the comparison of the estimated local wind and the actual wind along the trajectory of Aircraft-1.

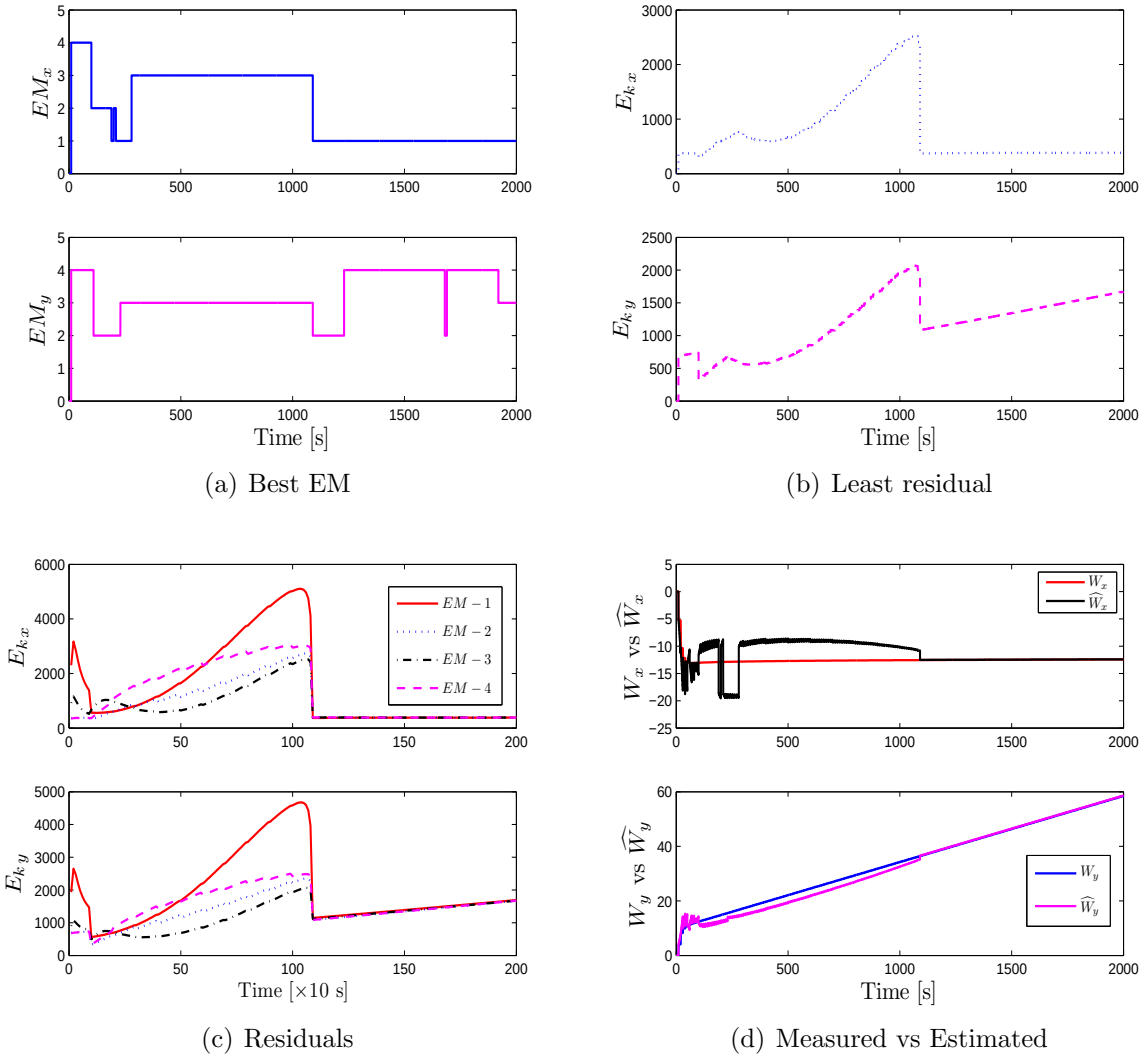

(a) Best EM

(b) Least residual

(c) Residuals

(d) Measured vs Estimated

Figure 4.16. Wind estimation by WLSE in WM-4 trajectory pattern-1.

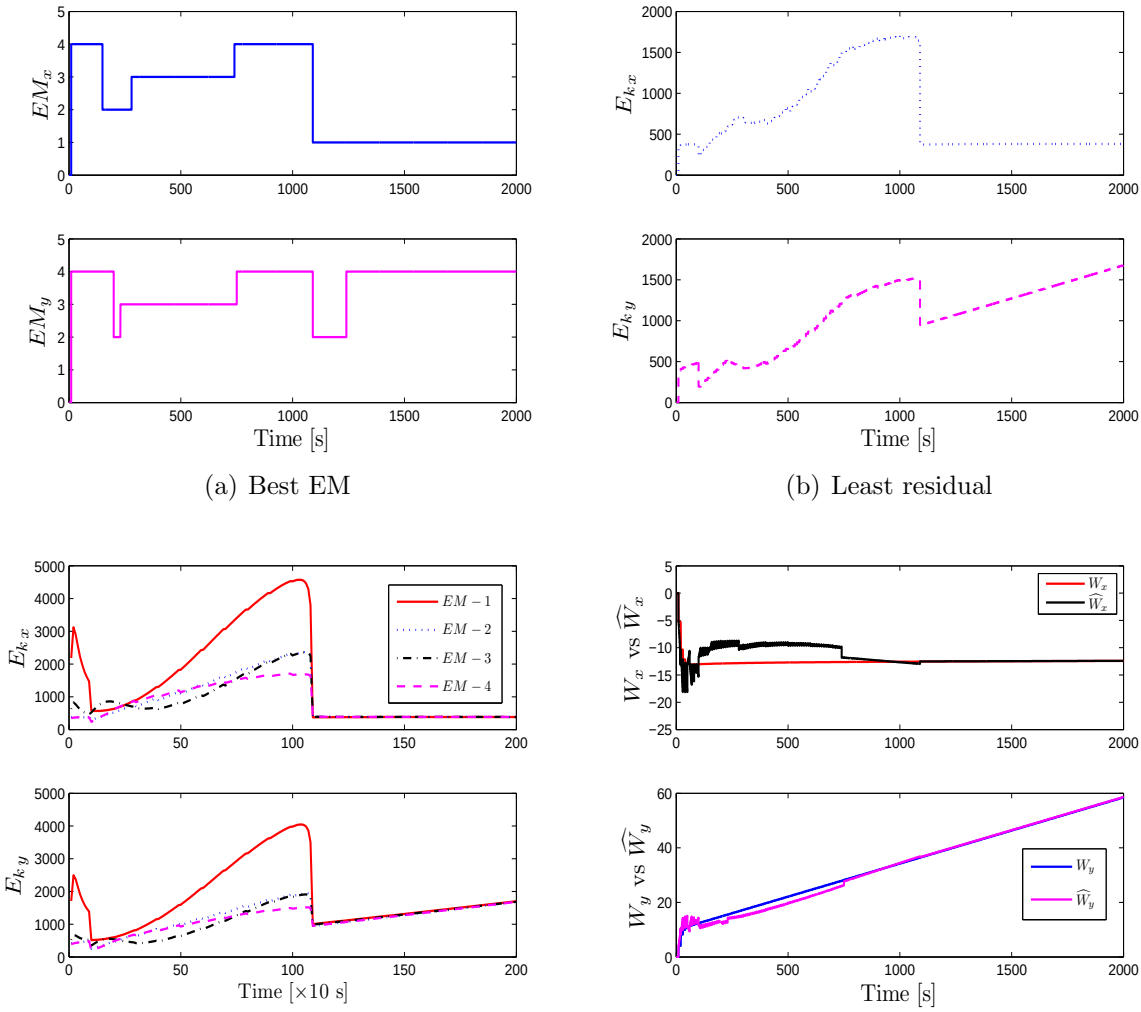

(a) Best EM

(b) Least residual

(c) Residuals

(d) Measured vs Estimated

Figure 4.17. Wind estimation by WLSE in WM-4 trajectory pattern-2.

4.4.3 Wind Field Model-5 Case

4.4.3.1 Least Square Estimation Results

In this simulation case, the experiment is simulated with the spatially and temporally varying horizontal wind vector field is generated by WM-5 when $z = 7010$ m, the wave length $\lambda = 3 \times 10^5$ and the wave speed $W_{wave}(z,t) = 15 + e^{\frac{1}{180}t} + 1 \times 10^{-2}t$

m/s, in order to investigate the performance of wind field estimation algorithms based on LSE in the nonlinear wind vector field.

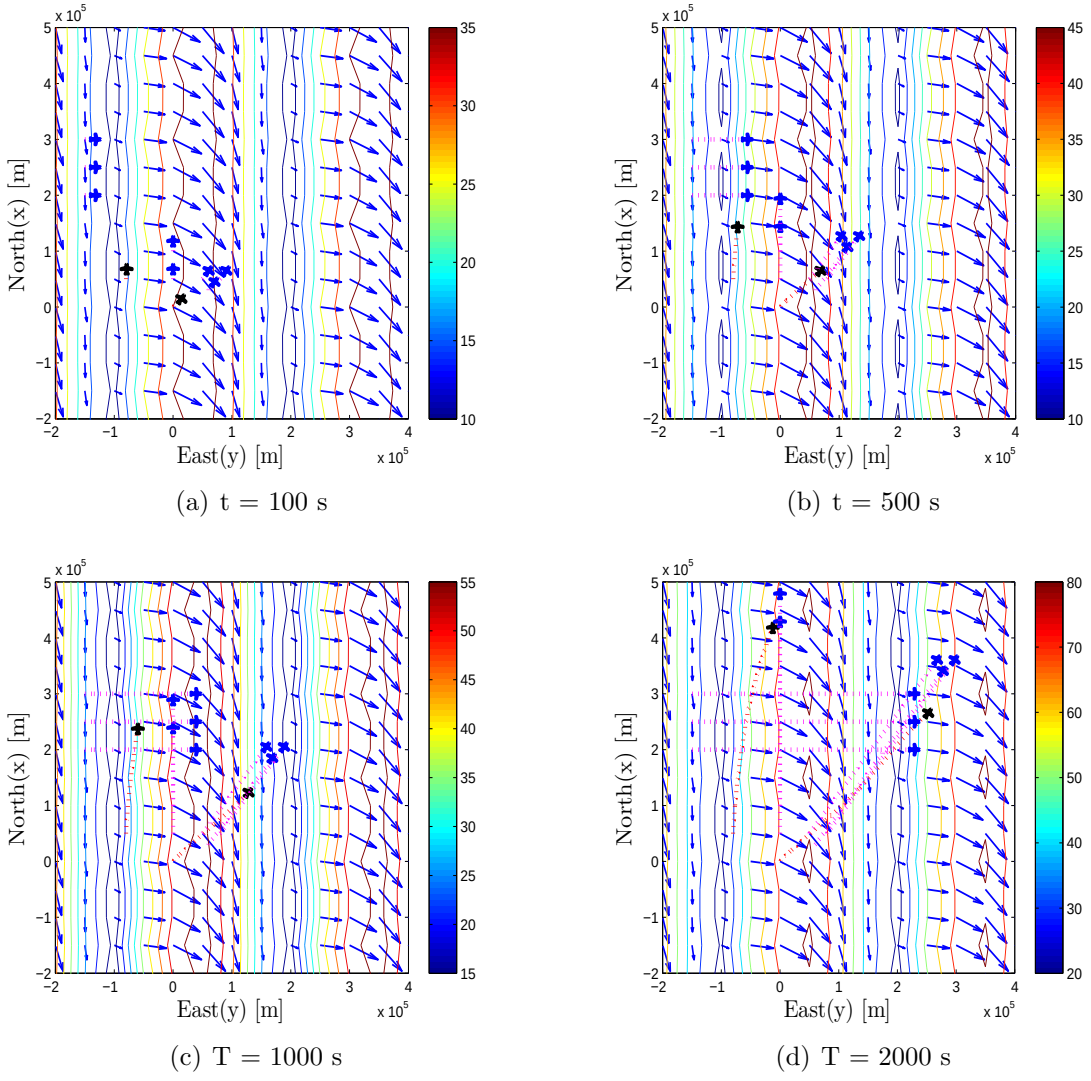

(a) t = 100 s (b) t = 500 s

(c) T = 1000 s (d) T = 2000 s

Figure 4.18. Aircraft trajectory pattern-1 in WM-5.

Figures 4.18 and 4.19-(a)-(d) shows the snapshots of the positions of and the paths traveled by ten aircraft flying in spatially and temporally varying horizontal

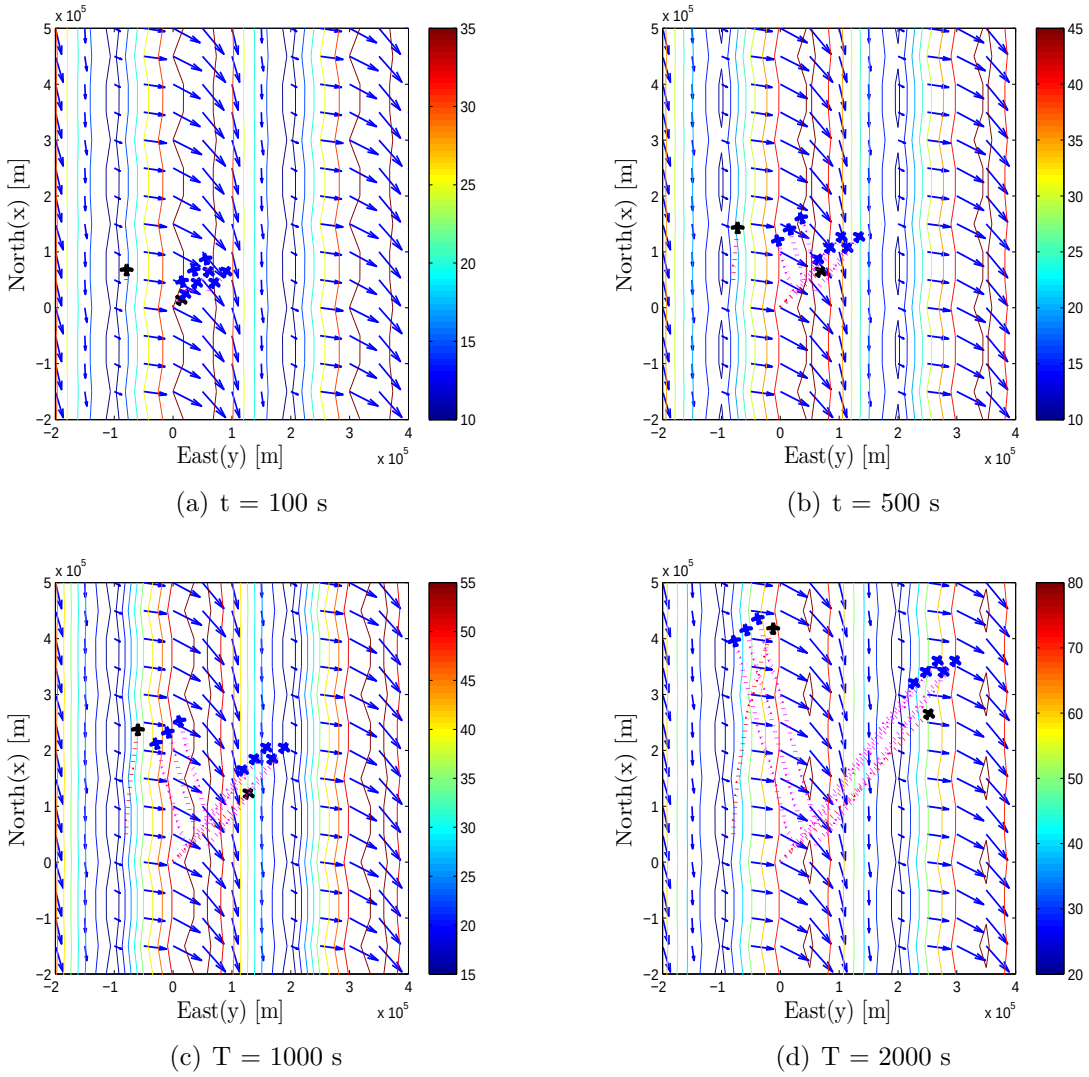

(a) t = 100 s

(b) t = 500 s

(c) T = 1000 s

(d) T = 2000 s

Figure 4.19. Aircraft trajectory pattern-2 in WM-5.

wind field represented by WM-5, through trajectory pattern-1 and -2, at different times, $t = 100,\ 500,\ 1000$ and 2000 s, respectively. Since the wind is varying with position and time, the aircraft flying in different region and different time will be exposed to the different wind strength and direction as shown by contour lines.

The performance of the wind field estimation algorithms are shown in Figures 4.20 and 4.21 while the aircraft are flying in WM-5 through trajectory pattern-1 and -2, shown in Figs. 4.18 and 4.19, respectively. Subfigures (a) indicates the wind estimation model with the least residual error by the EM number. Figs. 4.20 (a) and 4.21 (a) show that EM-4 is always the estimation model with the least residual error while the aircraft fly in WM-5 along both trajectory pattern-1 and -2 and in both x- and y-component. Subfigures (b) shows the smallest residual error while Subfigures (c) presents the comparison of the residual errors from all four estimation models. Subfigures (d) show the comparison of the estimated local wind and actual wind along the trajectory of Aircraft-1. Fig. 4.21 (d) shows an interesting result that, while the aircraft flying through the trajectory pattern-2, the difference between the estimated wind and actual wind components along x-axis is smaller than that when the aircraft flying through the trajectory pattern-1. This indicates the the benefit of collecting wind data from aircraft spread more over the area of operation.

4.4.3.2 Weighted Least Square Estimation Results

The performance of wind field estimation by implementing WLSE algorithms are shown in Figures 4.22 and 4.23 while the aircraft are flying in WM-5 through trajectory pattern-1 and -2, shown in Figs. 4.18 and 4.19, respectively. Subfigures (a) indicates the wind estimation model with the least residual error by the EM number. Fig. 4.22 (a) shows that the best estimation model switches between all estimation models when aircraft fly through trajectory pattern-1 while Fig. 4.23 (a) indicates that the best model is EM-4 in the first half of the simulation and switches between all four in the rest of the simulation. Subfigures (b) shows the smallest residual error while Subfigures (c) presents the comparison of the residual errors from all four estimation models.

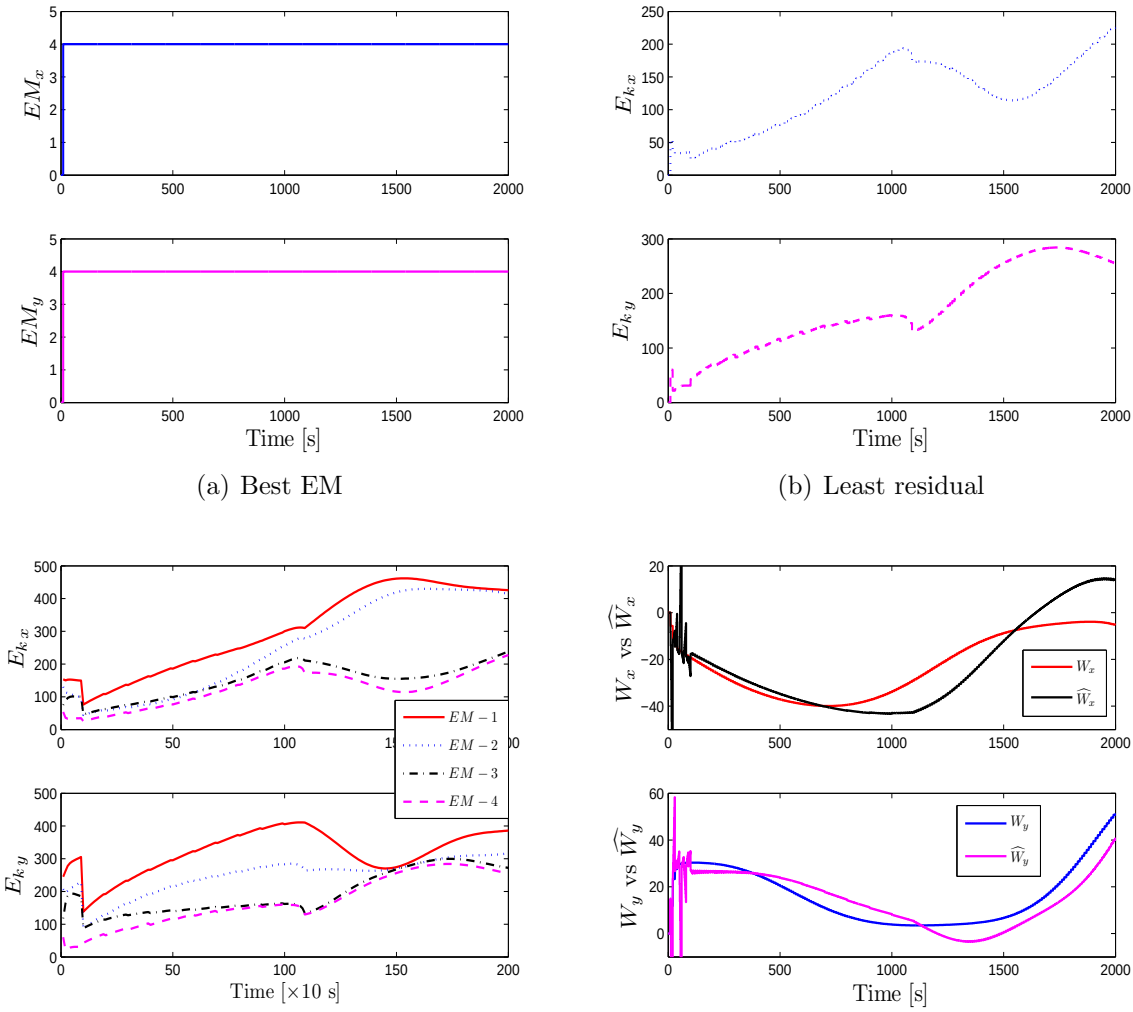

(a) Best EM

(b) Least residual

(c) Residuals

(d) Measured vs Estimated

Figure 4.20. Wind estimation by LSE in WM-5 trajectory pattern-1.

Both Figs. 4.22 and 4.23 show the discontinuous jumps in the estimated wind components when the estimation model switches to EM-1. This implies that the wind field estimation model with the smallest residual error does not necessarily give the best local wind vector estimation along a specific trajectory even in the case

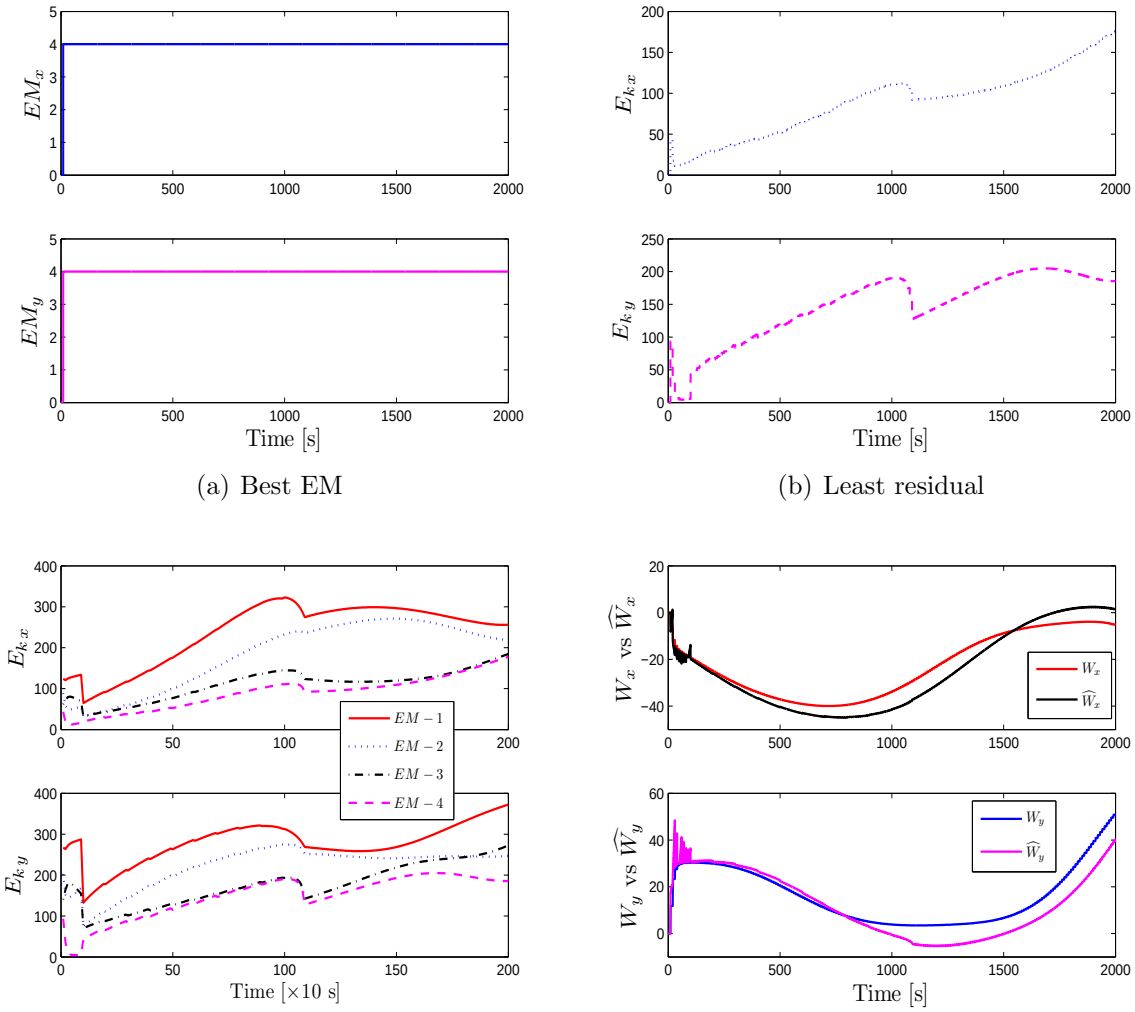

(a) Best EM

(b) Least residual

(c) Residuals

(d) Measured vs Estimated

Figure 4.21. Wind estimation by LSE in WM-5 trajectory pattern-2.

of weighted LSE. The switching among the different estimation models should be improved.

An estimation performance comparison between the LSE and WLSE shows that the WLSE shows a better estimation in the sense that error between the estimated wind and the actual wind along a trajectory is usually smaller. However, the WLSE

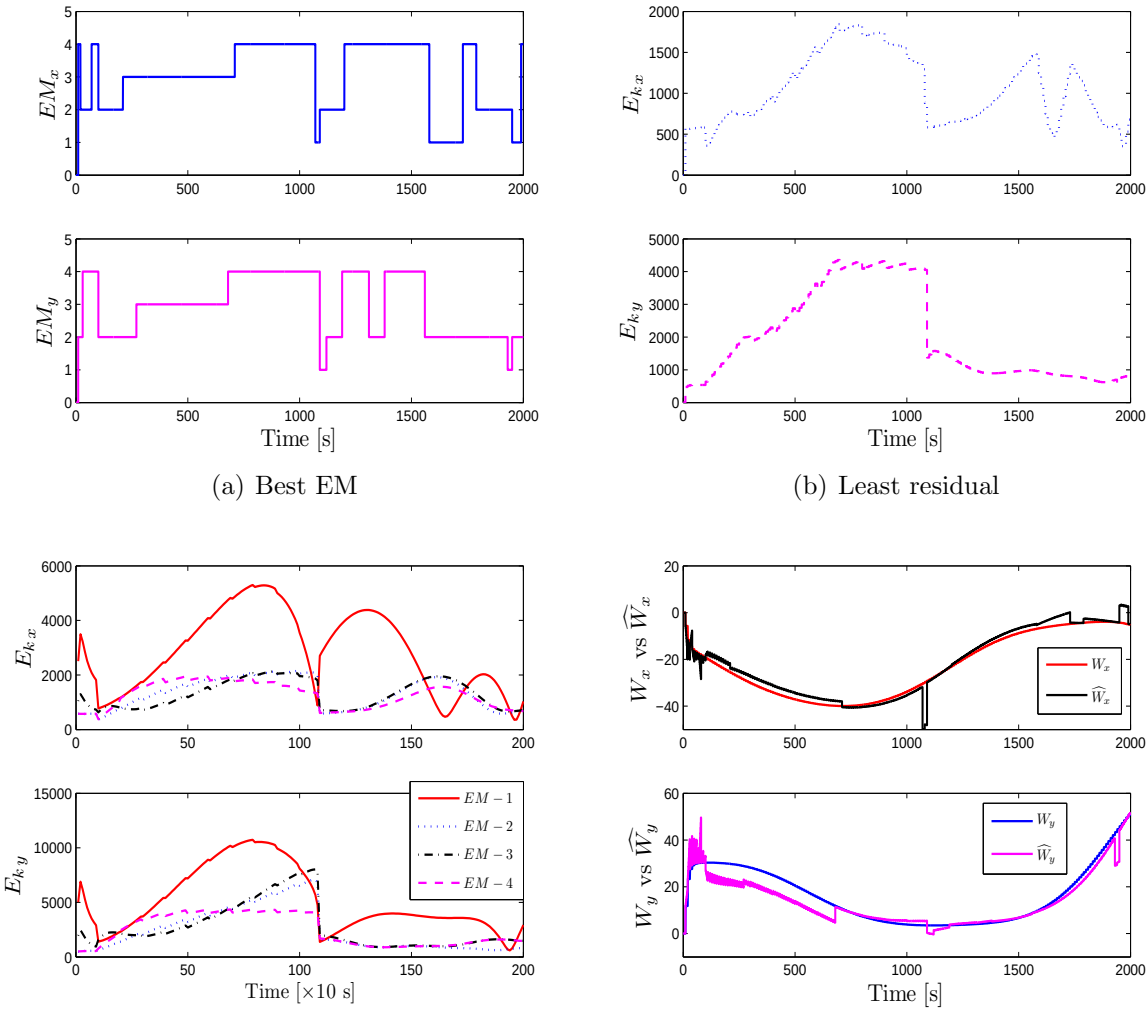

(a) Best EM

(b) Least residual

(c) Residuals

(d) Measured vs Estimated

Figure 4.22. Wind estimation by WLSE in WM-5 trajectory pattern-1.

methods result in more frequent switching between the estimation models, which causes discontinuity in the estimated local wind components.

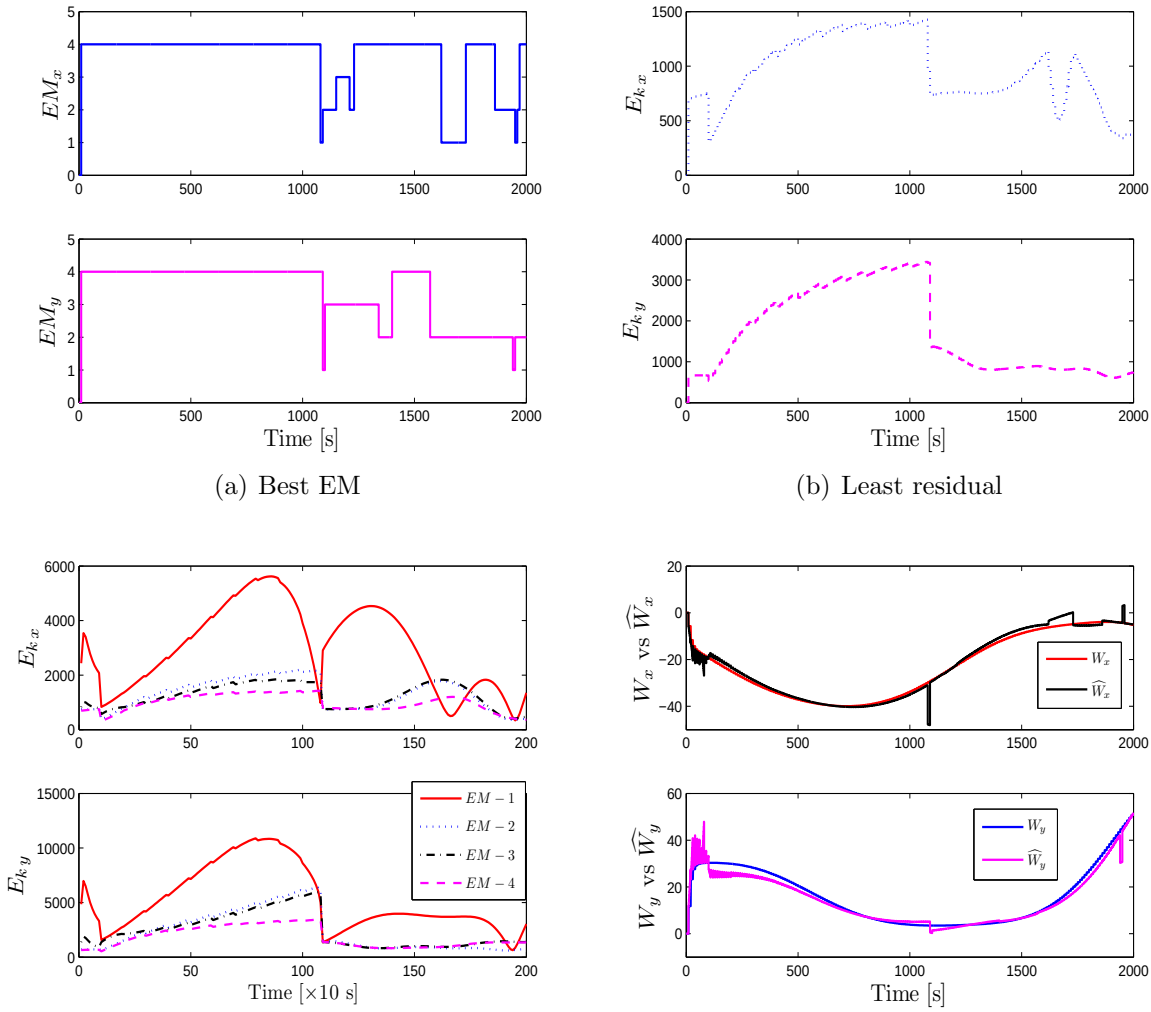

(a) Best EM

(b) Least residual

(c) Residuals

(d) Measured vs Estimated

Figure 4.23. Wind estimation by WLSE in WM-5 trajectory pattern-2.

Chapter 5

TRAJECTORY PREDICTION

The recent growth of air transportation system and demand to integrate Unmanned Aircraft System (UAS) into the national airspace system (NAS) in near future, will result in overcrowded sky. However, safe, orderly and efficient air navigation for every party should not be compromised [94]. The air traffic management (ATM) and the air traffic control (ATC) have the key roles to these issues and counter measures have been researched and experimented for decades. Among the solutions considered is to obtain the accurate knowledge of intended aircraft motion and hence its intended trajectory in the intended area of operation.

The knowledge of intended aircraft trajectory within some look ahead time (e.g., 2 minutes for short term or greater than 20 minutes for long term) will enhance the situational awareness for both pilot and ATC. The intended aircraft trajectory is the output of the trajectory prediction algorithms, which are the core processes that reside in both advanced airborne (Flight Management System (FMS)) and ground - based decision support tool (DST). The aircraft trajectory prediction or the prediction of four-dimensional (4D) aircraft trajectories are the key fundamental information for many advance ATC and ATM concepts [95]. The advanced DSTs are the promising solution to overcome the human factor limitation to deal with increasing capacity of the aircraft in the sky, in order to guarantee safety and efficiency of air navigation. Additionally, the trajectory prediction plays an important role in the light aircraft, gliders [96] and unmanned aircraft system (UAS) [97] application, which is expected

to be integrated into NAS in near future, for example, in conflict detection and avoidance capability for safety operations.

It is obvious that the predictability of aircraft trajectory or the accuracy of the predicted trajectory from trajectory prediction algorithms will improve the effectiveness of DST, which is trajectory based operation (TBO), reduce fuel consumption and emissions [62]. However, the prediction is never perfect due to several sources of error as presented in [23]. Inaccurate wind information is the major source of aircraft trajectory prediction error. Additionally, the lack of flight and aircraft intent information will result in aircraft trajectory prediction error as well.

5.1 Overview of Trajectory Prediction Process

The discrete equations given in Section 3.2.3 are propagated using the 4^{th} order Runge-Kutta method. The propagation starts from the current time and runs through the whole "prediction period" specified by the "look ahead time". The precision of propagation is specified by the "update rate". Fig. 5.1 demonstrates the input-output interface of the trajectory prediction module in simulation. The trajectory prediction requires the following for propagation of the equations:

1) Aircraft parameters such as mass, wing span, wing reference area.

2) The current values of the aircraft state variables ($V,\ \gamma,\ \mu,\ x,\ y,\ z$).

3) The input variables ($\zeta,\ \alpha,\ q,\ \delta_e,\ \delta_r,\ T$) specified through the whole prediction period. The variations of the input variables through the prediction period can be specified if the aircraft intent information is available. Otherwise, the inputs are assumed to stay at their current values.

4) Wind components ($\hat{W}_x,\ \hat{W}_y,\ \hat{W}_z$) and derivatives ($\dot{\hat{W}}_x,\ \dot{\hat{W}}_y,\ \dot{\hat{W}}_z$) computed by the estimated wind field model.

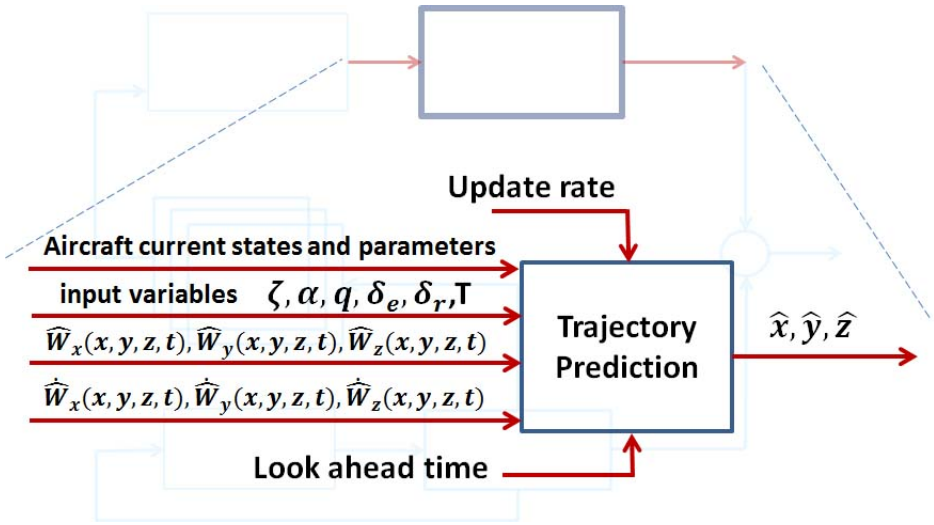

Figure 5.1. Trajectory prediction process block diagram.

This trajectory prediction process, which incorporates intent information and estimated wind field in the prediction process is summarized in the form of an algorithm as follows.

Algorithm : Trajectory Prediction with Intents and Estimated Wind Information

1: **Initialization.**

Read Initial States : $x_0,\ y_0,\ z_0,\ V_0,\ \gamma_0,\ \mu_0$

Read Initial Input/Control Variables : $\delta_{T_0},\ \delta_{e_0},\ \alpha_0,\ q_0,\ \zeta_0$

Read Estimated Wind : $\widehat{W}_x,\ \widehat{W}_y,\ \widehat{W}_z,\ \widehat{\dot{W}}_x,\ \widehat{\dot{W}}_y,\ \widehat{\dot{W}}_z$

2: **Prediction.**

Propagate the states from $t_k\ \rightarrow\ t_k + \Delta t_{LH}$

Check if the predicted states require flight mode change.

[1] Yes : Go to nominal condition analysis

Find when this event occurs? Assign as t_b

Recalculate the input/control variables based-on intent information

Propagate the states from $t_b - 1\ \rightarrow\ \Delta t_{LH}$

Store the result from $t_k\ \rightarrow\ t_k + \Delta t_{LH}$

Go to next step

[2] No : Go to next step

3: **End Prediction.**

Output the predicted position

5.2 Nominal Condition Analysis

The trajectory prediction process consists of the propagation of the PMM-based equations of motion throughout the prediction period. For the solution of the differential equations, the initial conditions of the state variables are set to the current values and the control variables are kept constant at the current values throughout the propagation period. This implies that the aircraft is assumed to continue flying in the current flight mode throughout the whole prediction period. The intent information may reveal that the aircraft will change flight mode within the prediction period.

This may be a time-based schedule or an event-based mode change. In the case of a mode change, the control variables should not be kept at their current values and need to be recalculated. The recalculation of the control variables requires a nominal or trimmed condition analysis if it is assumed that the second mode of flight is a trimmed flight condition. At the time of the mode change, for a selected set of state variables, the values of the state variables right before the mode change are used as the nominal values of the states in the second flight mode. Based on these nominal state variables and the nature of the flight mode, a trimmed condition analysis is carried out to determine the required nominal values of the control variables in the second mode of flight. For example, an aircraft is flying in straight-level flight and its known intent is to switch to a steady-state turn with a specified turn rate and speed at the same constant altitude when the aircraft reaches a certain position. If the predicted trajectory of the steady straight-level flight reaches the specified position within the prediction period, a trim analysis of the steady turn flight is carried out to determine the required nominal values of the control variables. The values of these control variables and the state variables at the time of the flight mode switch are used to propagate the PMM-based equations of motion in the rest of the prediction period.

The trimmed condition analysis is carried out with a specified speed V and yaw rate $\dot{\mu}$. The pitch rate q is set to zero and the angle of attack α is set to a constant. Further, the flights in this research are limited to constant altitude, which implies that $\dot{z} = 0$. Then, the PMM-based equations of motion in Eq. (5.1)-(5.3) yield three

algebraic equations for the trimmed flight specified, which are solved for the control variables ($\delta_{T_0},\ \delta_{e_0},\ \zeta_0$).

$$\begin{aligned} 0 &= K_{PM1}\delta_T - K_{PM2}V^2 - K_{PM3}\alpha^2 V^2 \\ &- g\sin(\gamma) \end{aligned} \tag{5.1}$$

$$\begin{aligned} 0 &= K_{PM4}V + K_{PM5}\alpha V + K_{PM6}(\alpha - \alpha_{ref})^2 V \\ &+ K_{PM7}q + K_{PM8}\delta_e V - \frac{g}{V}\cos(\gamma) \end{aligned} \tag{5.2}$$

$$\begin{aligned} 0 &= K_{PM4}\frac{\sin(\zeta)}{\cos(\gamma)}V + K_{PM5}\frac{\sin(\zeta)}{\cos(\gamma)}\alpha V \\ &+ K_{PM6}\frac{\sin(\zeta)}{\cos(\gamma)}(\alpha - \alpha_{ref})^2 V + K_{PM7}\frac{\sin(\zeta)}{\cos(\gamma)}q \\ &+ K_{PM8}\frac{\sin(\zeta)}{\cos(\gamma)}\delta_e V \end{aligned} \tag{5.3}$$

where

$$\begin{aligned} K_{PM1} &= \frac{T_{max}}{m} \quad K_{PM2} = \frac{\rho S C_{D_0}}{2m} \quad K_{PM3} = \frac{\rho S C_{D_{\alpha^2}}}{2m} \\ K_{PM4} &= \frac{\rho S C_{L_0}}{2m} \quad K_{PM5} = \frac{\rho S C_{L_\alpha}}{2m} \quad K_{PM6} = \frac{\rho S C_{L_{\alpha^2}}}{2m} \\ K_{PM7} &= \frac{\rho S c C_{L_q}}{4m} \quad K_{PM8} = \frac{\rho S C_{L_{\delta_e}}}{2m} \end{aligned}$$

5.3 Simulation Results

5.3.1 Utilization of Spatially Varying Wind in TP

The simulation cases presented here are the same as those presented in Section 4.4.2.1 where wind field estimation was performed. Two different simulation cases are run with Wind Model-4 but its parameters are set differently. The second case has stronger wind (25% of the aircraft airspeed) overall compared to the first case (13%). There are 10 aircraft flying in the area and the trajectory prediction is carried out for Aircraft-1 and -2. The role of the other aircraft in the simulation is to provide local wind information for wind field estimation. No intent information is used for

trajectory prediction in the simulation presented in this section. That is, the aircraft inputs are assumed to stay constant at their current values. The trajectory predictions are performed in two cases: (i) wind information formulated in the estimated wind field models is used in the propagation of the equations and (ii) it is assumed that there is no wind and thus the wind terms are ignored in the propagation equations although the aircraft are flying in the presence of the spatially varying wind. The "look ahead time" and "update rate" are set to be 120 sec and 10 sec, respectively. Fig. 5.2 shows a comparison of simulation results of trajectory prediction of Aircraft-1

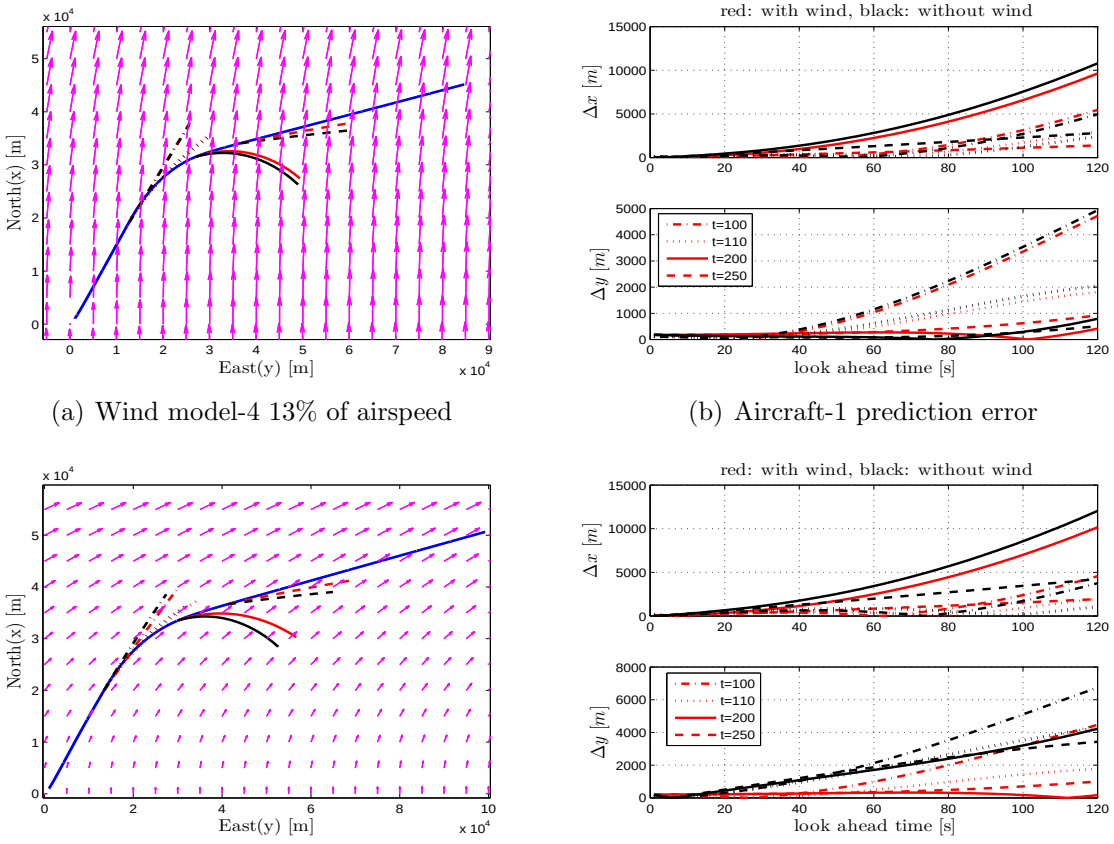

(a) Wind model-4 13% of airspeed

(b) Aircraft-1 prediction error

(c) Wind model-4 25% of airspeed

(d) Aircraft-1 prediction error

Figure 5.2. Comparison of predicted and actual trajectories and prediction errors.

in spatially varying wind according to Wind Model-4. Note that 4^{th} order Runge-Kutta method is used to propagate the aircraft states. Fig. 5.2-(a) shows the actual trajectory and the predicted trajectories at 4 different points, i.e., (i) right before the turn starts, $t = 100\ s$, (ii) right after the turn starts, $t = 110\ s$, (iii) right before the turn ends, $t = 200\ s$, and (iv) right after the turn ends, $t = 250\ s$. Note that the magnitude of the wind is approximately 13% of the aircraft speed at those points. Note also that two predicted trajectories are shown for each of these four times. The red ones are the trajectories predicted with the estimated wind field included in the propagation while the black ones are the trajectory predictions done under the assumption of no wind although the aircraft is subject to spatially varying wind. Fig. 5.2-(b) shows the prediction errors in x- and y-axes. The prediction errors are computed by comparing predicted aircraft position at a time with the position the aircraft actually ends up at the specified time.

Fig. 5.2-(c) and 5.2-(d) show the same comparisons when the aircraft flies within a stronger wind field. the magnitude of the wind vectors the aircraft experiences are about 25% of the aircraft speed as opposed to 13% in Fig. 5.2-(a) and 5.2-(b). The comparisons in both wind conditions show that the incorporating wind effect in trajectory prediction improves the accuracy. Further, the degradation in prediction accuracy is shown to be worse in stronger wind field when the wind field information is not used in propagation of the equations.

Fig. 5.3 shows the prediction errors in xy-graph. The prediction error are computed as the difference between the actual trajectory and the predicted trajectory computed at 200 s, right before the turn ends. For each case, the prediction error starts from the origin as that is the initial time for the prediction. As time progress, the corresponding point in each curve moves away from the origin. The last points in each curve represents the prediction error after 120 s as that is the look ahead

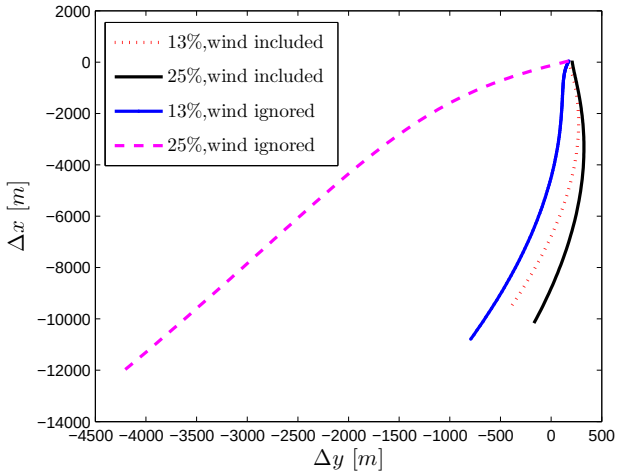

Figure 5.3. Comparison of prediction error of Aircraft-1 at $t = 200$ s.

time. The most important observation from Fig. 5.3 is about the sensitivity of the prediction to wind strength. When the trajectory prediction includes wind field information, the trajectory prediction is more robust as opposed to the cases where trajectory prediction is done without wind considered. This can be seen by the fact that "25%, wind ignored" curve moves very far away from "13%, wind ignored" curve while "25%, wind included" stays relatively close to "13%, wind included."

5.3.2 Utilization of Spatially and Temporally Varying Wind in TP

This section presents various simulation cases of trajectory prediction with both intent and wind field information included.

5.3.2.1 Flight Plan and Intents

In the simulation cases presented below, the aircraft starts flying from point A with coordinates $(x_A, y_A) = (100, -100)$ with heading angle μ_A in a straight level flight with constant speed and at constant altitude. The intent of the aircraft is to start a steady level turn with a constant turn rate $\dot{\mu}_{(B,C)}$ when its x-coordinate

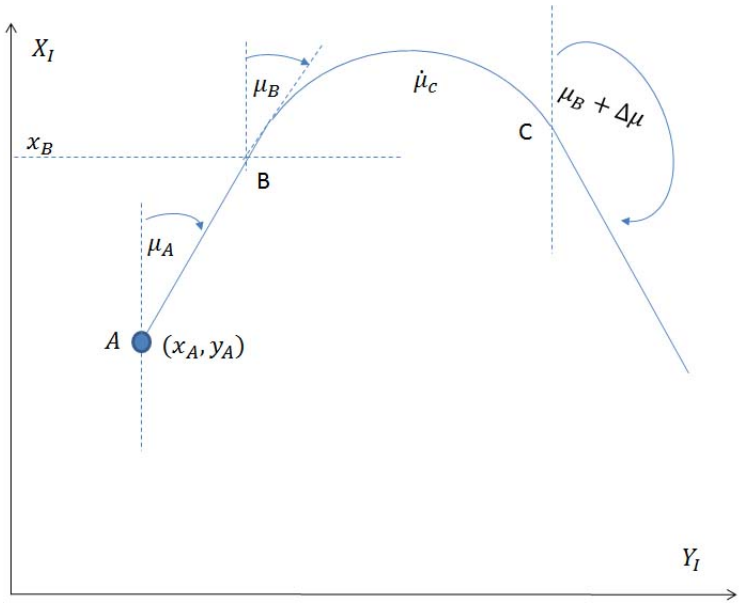

Figure 5.4. Sketch of the intended flight trajectory.

reaches $x_B = 2.471 \times 10^5$. The aircraft intends to continue on the steady turn with a constant turn rate of $\dot{\mu}_c$ until its heading changes by $\Delta\mu$. After this point, the intent of the aircraft is to switch back to steady straight level flight. The depiction of the intended flight path is shown in Fig. 5.4 and the parameters of the intended flight simulated in this section are given in Table 5.1.

Table 5.1. Details of flight plan and intents

Flight plan and intents		
Flight segment	Description	Intents ([m/s], [m], [deg/s], [deg])
$A \rightarrow B$	Straight flight	Constant speed, altitude, and heading $V_c = 190$, $z_c = 7010$, $\mu_c = 0$
$B \rightarrow C$	Turning flight	Constant speed, altitude, and turn rate $V_c = 190$, $z_c = 7010$, $\dot{\mu}_c = 0.4$, $\Delta\mu = 90$
$C \rightarrow$	Straight flight	Constant speed, altitude, and heading $V_c = 190$, $z_c = 7010$

In all simulation cases, ten aircraft fly in the same airspace of operation, which covers an area of 500×500 km. All aircraft fly at a constant altitude of 7010 m with constant speed of 190 m/s. The trajectory prediction is carried out for Aircraft-1. The role of the other aircraft in the simulation is to provide local wind information for wind field estimation, which is implemented by WLSE. The parameter used in the mathematical model of Aircraft-1 represent KC-135 aircraft. The trajectory predictions are performed in four cases, as described in Table 5.2, depending on whether the wind field estimation and/or intent information are included in trajectory propagation. In all four cases, the "look ahead time" and "update rate" are set to be 120 sec and 10 sec, respectively.

Table 5.2. Four trajectory prediction cases based on whether wind field estimation and/or intent information included in propagation

Case	Wind field Estimation	Intent Information
i	NO	NO
ii	YES	NO
iii	NO	YES
iv	YES	YES

5.3.2.2 Wind Field Model-1 Case

In the following simulation case presented, all 10 aircraft are exposed to a spatially and temporally varying wind field as modeled by WM-1 as described in Section 2.1 and shown in Fig. 5.5. The magnitude of the wind Aircraft-1 is exposed to in simulation is approximately 13% of its airspeed. Fig. 5.5 also shows the paths of the ten aircraft by dashed lines and directions by the airplane.

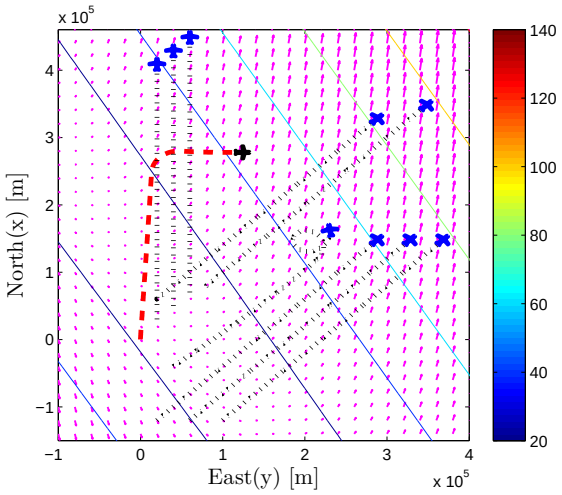

Figure 5.5. Paths of ten aircraft in simulation. The path of Aircraft -1 is red dashed line.

Figs. 5.6-(a) and 5.6-(b) show the comparison of the predicted trajectories in the four cases described in Table 5.2 with the actual trajectory. Fig. 5.6-(a) shows the trajectory predictions computed at $t = 1320$ sec. During this prediction period, the aircraft switches from the first straight level flight mode to the turn mode. Fig. 5.6-(b) shows the same computed at $t = 1580$ sec and, during this prediction period, the aircraft moves from turn flight mode to the second straight level flight mode.

Figs. 5.7-(a) and 5.7-(b) show the prediction errors during the prediction period until the look ahead time ($\Delta t_{LH} = 120$ sec), in terms of along-track and cross-track errors, for all four cases. Fig. 5.7-(a) shows along-track and cross-track errors computed at $t = 1320$ sec. Fig. 5.7-(b) shows the same prediction errors computed at $t = 1580$ sec. This plots clearly show the benefit of including intent and wind information in trajectory prediction.

Fig. 5.8 shows the prediction errors in xy-graph. The prediction errors are computed as the difference between the actual trajectory and predicted trajectory at $t = 1320$ and 1580 sec. For each case, the prediction error starts from the origin as

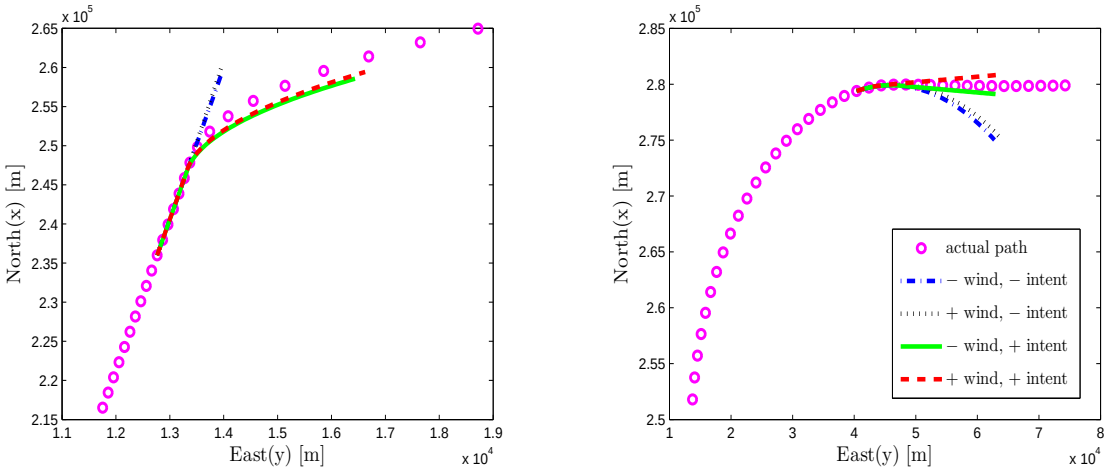

(a) t = 1320 s (b) t = 1580 s

Figure 5.6. Predicted trajectory cases versus actual trajectory.

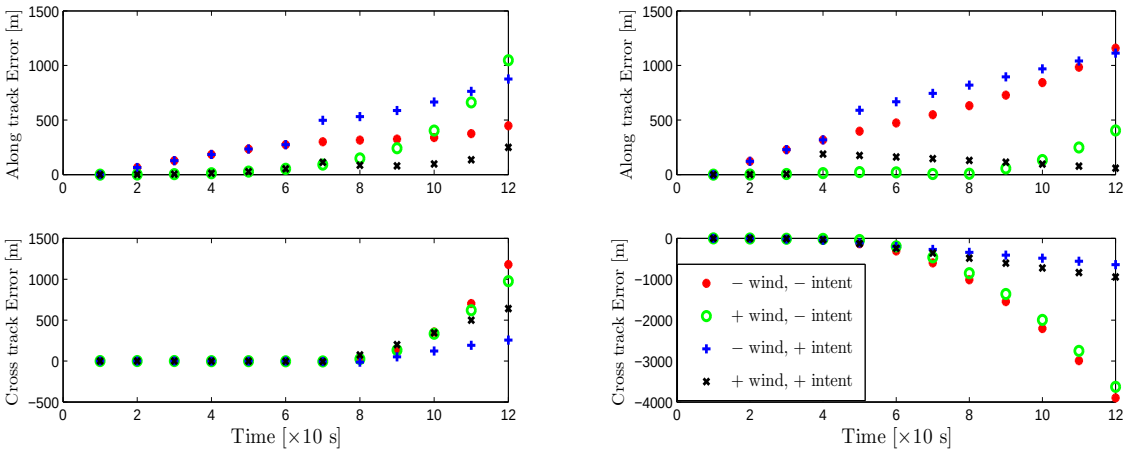

(a) t = 1320 s (b) t = 1580 s

Figure 5.7. Trajectory prediction errors for all four cases.

that is the initial time for prediction. As time progresses, the corresponding point in each curve moves away from the origin. The last points in each curve represents the prediction error after 120 sec as that is the look ahead time. The most important observation from Fig. 5.8 is about the sensitivity of the prediction accuracy to wind and intent information. When the trajectory prediction includes wind field and intent

information, the trajectory prediction is more accurate as opposed to the cases where trajectory prediction is done without wind and with or without intent information considered. For example, this can be seen in Fig. 5.8-(a) by the fact that "− wind, − intent" and "− wind, + intent" and "− wind, − intent" curve moves very far away from the origin while "+ wind, + intent" curve stay relatively close to the origin.

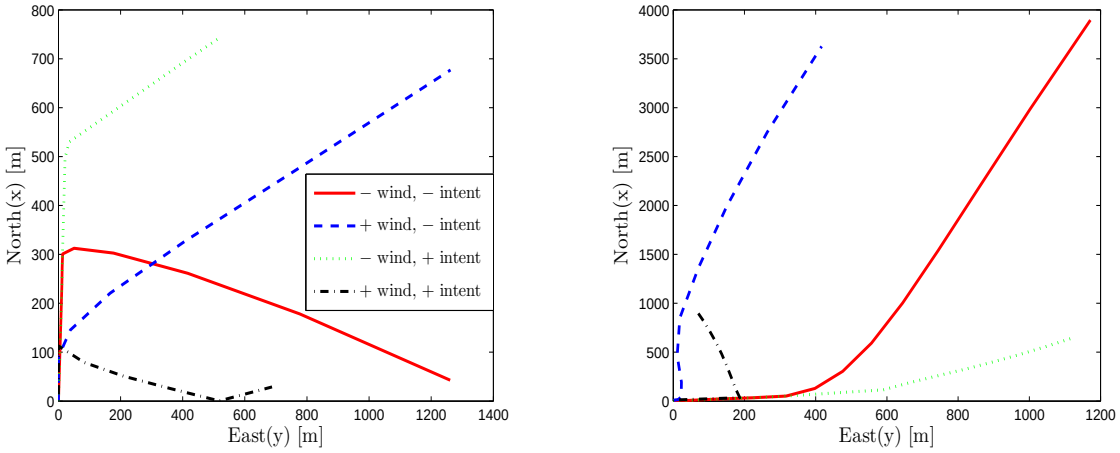

(a) t = 1320 s (b) t = 1580 s

Figure 5.8. Comparison of trajectory prediction error of Aircraft-1.

5.3.2.3 Wind Field Model-4 Case

In the following simulation case presented, all 10 aircraft are exposed to a spatially and temporally varying wind field as modeled by WM-4 as described in Section 2.4 and shown in Fig. 5.9. The magnitude of the wind Aircraft-1 is exposed to in simulation is approximately 21% of its airspeed. Fig. 5.9 also shows the paths of the ten aircraft by dashed lines and directions by the airplane.

Figs. 5.10-(a) and 5.10-(b) show the comparison of the predicted trajectories in the four cases described in Table 5.2 with the actual trajectory. Fig. 5.10-(a) shows

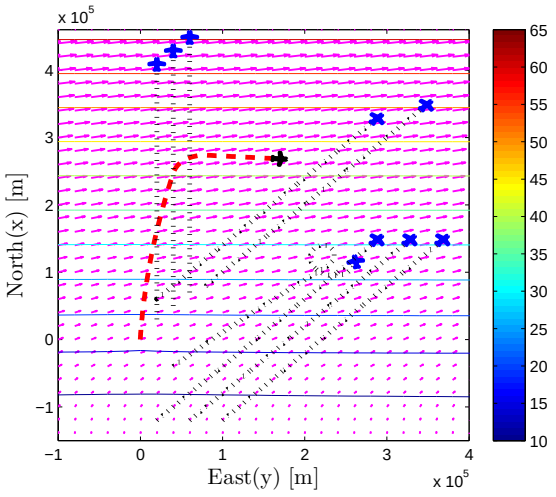

Figure 5.9. Paths of ten aircraft in simulation. The path of Aircraft-1 is red dashed line..

the trajectory predictions computed at $t = 1320$ sec. During this prediction period, the aircraft switches from the first straight level flight mode to the turn mode. Fig. 5.10-(b) shows the same computed at $t = 1550$ sec and, during this prediction period, the aircraft moves from turn flight mode to the second straight level flight mode.

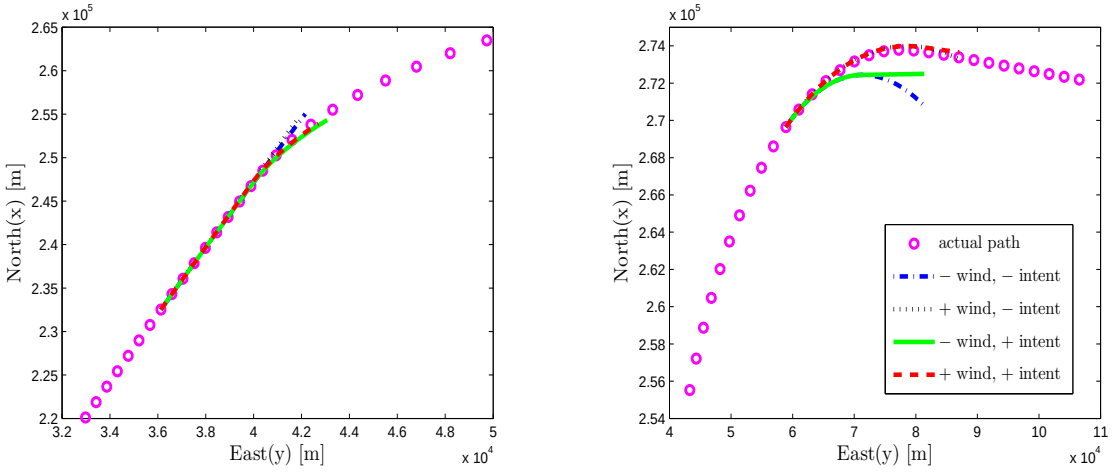

(a) t = 1320 s (b) t = 1550 s

Figure 5.10. Predicted trajectory cases versus actual trajectory.

Figs. 5.11-(a) and 5.11-(b) show the prediction errors during the prediction period until the look ahead time ($\Delta t_{LH} = 120$ sec), in terms of along-track and cross-track errors, for all four cases. Fig. 5.11-(a) shows along-track and cross-track errors computed at $t = 1320$ sec. Fig. 5.11-(b) shows the same prediction errors computed at $t = 1550$ sec.

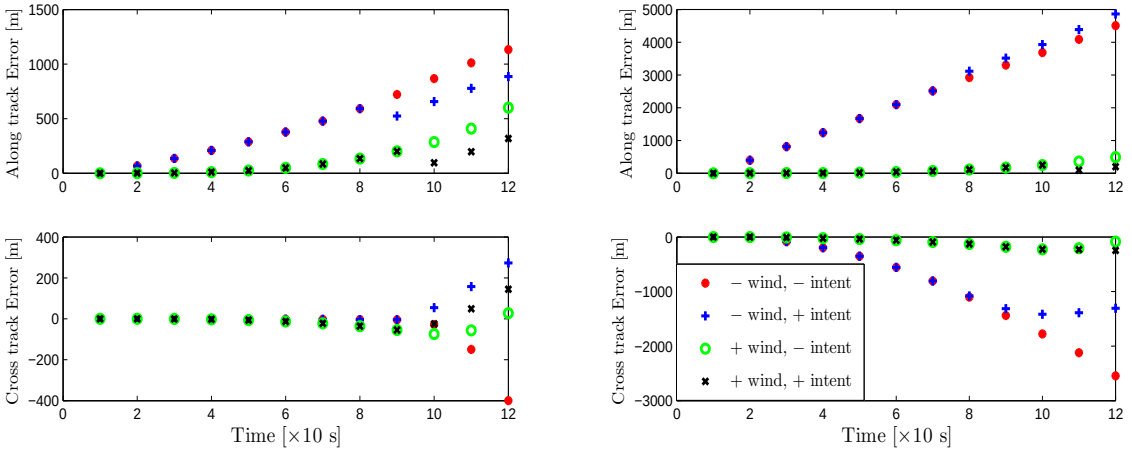

(a) t = 1320 s (b) t = 1550 s

Figure 5.11. Trajectory prediction errors for all four cases.

Fig. 5.12 shows the prediction errors in xy-graph. The prediction errors are computed as the difference between the actual trajectory and predicted trajectory computed at $t = 1320$ and 1550 sec. For each case, the prediction error starts from the origin as that is the initial time for prediction. As time progresses, the corresponding point in each curve moves away from the origin. The last points in each curve represents the prediction error after 120 sec as that is the look ahead time. The most important observation from Fig. 5.12 is about the sensitivity of the prediction accuracy to wind and intent information. When the trajectory prediction includes wind field and intent information, the trajectory prediction is more accurate as opposed to

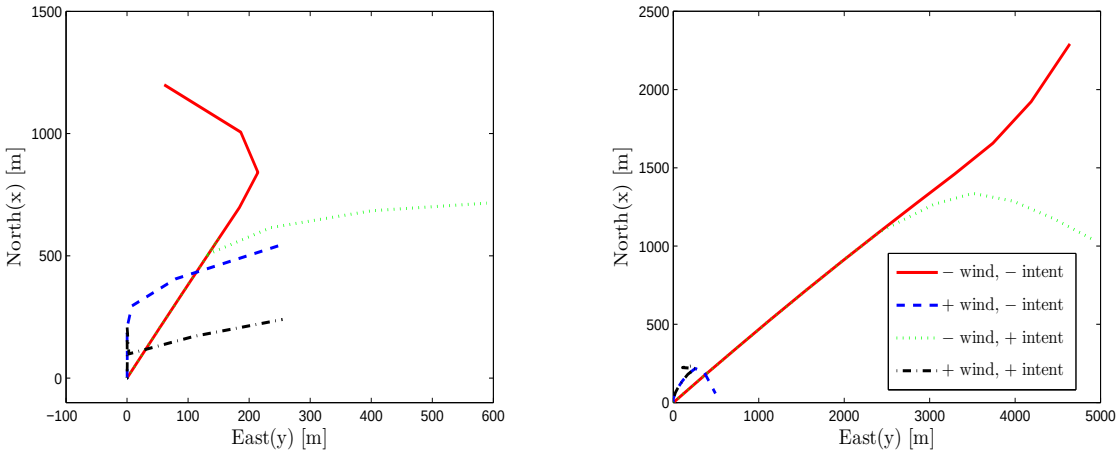

(a) t = 1320 s (b) t = 1550 s

Figure 5.12. Comparison of trajectory prediction error of Aircraft-1.

the cases where trajectory prediction is done without wind and with or without intent information considered. For example, this can be seen in Fig. 5.12-(a) by the fact that "− wind, − intent" and "− wind, + intent" and "− wind, − intent" curve moves very far away from the origin while "+ wind, + intent" curve stays close to the origin.

Chapter 6

INPUT PREDICTION

Rapid growth in air transportation along with plans for integration UAS into civilian airspace requires better situational awareness for both air traffic controllers and onboard pilots in terms of flight trajectories of aircraft relative to each other. Information about aircraft current positions and intended trajectories can help mitigate the risk of conflict and collision between aircraft operating in the same airspace. In the case of an emergency such as engine failure or loss of control surface effectiveness, it becomes imperative to compute feasible trajectories in order to determine alternative landing fields. Accuracy and reliability of trajectory prediction enhanced by the information of wind variation will improve the performance of various tasks such as conflict detection and avoidance, and planning of emergency landing.

In some cases, instead of computing the trajectory of an aircraft, a predefined trajectory is given to aircraft to fly. For example, when conflict with another aircraft is detected, conflict avoidance algorithms compute new trajectories for the aircraft to follow to avoid the conflict. Another example is the emergency landing situation mentioned above. Once an emergency occurs and emergency landing is required, a trajectory is prescribed for the aircraft to follow to the emergency landing site. There are cases where military aircraft are required to follow a prescribed trajectory, for example, in combat maneuvers or in rendezvous with other aircraft such as in aerial refueling. The feasibility of such prescribed trajectories requires the control surface deflections and engine thrust to be within their saturation and rate limits. This leads to the problem of "input prediction" which is to compute the required control surface

deflections and engine thrust for the aircraft to fly through the prescribed trajectory. The feasibility of a given trajectory depends on atmospheric wind conditions as much as the capabilities of the aircraft. Thus, in this problem, too, the information of wind field will improve the prediction of required input variation.

The aircraft trajectory prediction, which can be considered as an application of conventional (forward) simulation techniques. In that case, the equations of motion, generally linear or nonlinear differential equations, are solved starting with initial conditions for prescribed time variations of input variables, or forcing terms, as studied in Chapter 5. In the problem of trajectory prediction, for prescribed future variation of the input variables, the forward simulation techniques determine how the aircraft states will vary in the immediate future by solving the differential equations starting from the current aircraft states. In other problems, the inverse is desired. Namely, the trajectory of the aircraft is prescribed and the question is to determine the required input variation for the aircraft to follow the prescribed trajectory. Such methods are referred to as "inverse simulation" or "input prediction" [63]. By using the concept of inverse simulation, the feasibility of a desired trajectory can be determined in terms of whether the variations of control variables will be within their saturation and rate limits. This analysis can be made more precise by taking into account the effect of wind on aircraft trajectory, which will benefit from knowledge of the wind variation, i.e. the wind field, in the airspace of operation.

This chapter applies the iterative differentiation-based inverse simulation method [98] to predict required input variation for a KC-135R aircraft to fly a prescribed trajectory in the presence of spatially and temporally varying wind. The iterative differentiation method is selected in this research because of its computational feasibility. The input prediction procedure carried out in this research incorporates the

wind field estimation as detailed in Chapter 4 into the inverse simulation to account for the effect of the wind on the required control variation.

Two versions of input prediction are developed: (1) for offline implementation and (2) online implementation. The simulation cases of both methods presented here are to demonstrate the benefits of including estimated wind information in inverse simulation for input prediction.

6.1 Prescribed Trajectory for Inverse Simulation

The first step of inverse simulation is to specify the desired trajectory, which is the input to any inverse simulation model. There are various ways to prescribe aircraft trajectory or flight maneuvers. The most common and natural method is to specify the position of the aircraft with respect to the inertial frame as a function of time, i.e., $x(t)$, $y(t)$ and $z(t)$ [99]. This can also be done by specifying path of the CM of the aircraft in the inertial frame and the speed of the aircraft along the path or in terms of the heading angle $\mu(t)$ and flight path angle $\gamma(t)$. Another aspect of the prescribed trajectory is to specify or determine the variation of the aircraft attitude or orientation, which influences the trajectory of the CM through changing the direction of the applied forces and moments [100].

6.2 Off-line Case

Specific steps followed for input prediction are listed below.

1) The desired trajectory is defined, as depicted in Fig. 6.1, in terms of the initial heading angle $\mu(0)$, the length of the first straight flight leg l_1, the change in heading $\Delta\mu$ in a circular turn with a specified lateral offset h_{os} and the length of the 2^{nd} straight flight leg l_2. Note that for a race track maneuver, the heading angle

change $\Delta\mu$ should be 180 degrees. This method facilitates the formulation of a path in inertial frame.

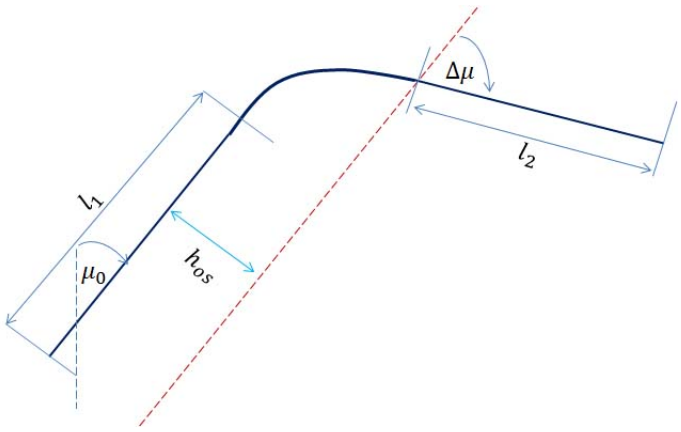

Figure 6.1. Desired trajectory specification.

2) The aircraft speed $V_I(t)$ along the path from the first step is specified. Note that V_I is the speed relative to the inertial frame. Thus, the path and the resultant trajectory are fixed in inertial frame regardless of the wind condition.

3) For the turn segment of the trajectory, the heading angle rate is computed by

$$\dot{\mu} = \frac{V_I}{h_{os}}[1 - \cos(\Delta\mu)] \tag{6.1}$$

where h_{os} is positive for right turns and negative for left turns. Integration of Eq. (6.1) will give the time variation of heading angle $\mu(t)$. For the straight flight legs, $\dot{\mu} = 0$. The translation between the straight flights and turns are managed by smoothing the $\dot{\mu}$ through a first-order filter.

4) Setting the flight path angle $\gamma(t) = 0$, for flight at constant altitude, the desired trajectory in terms of position $(x(t),\ y(t),\ z(t))$ within the inertial frame is obtained by integrating Eq. (3.31)-(3.33) in Section 3.2.1.

5) The attitude variation along the trajectory is determined as follows. First of all, yaw angle is assumed to be equal to the heading angle, i.e., $\psi(t) = \mu(t)$. The pitch angle is assumed to be constant. Specifically, for the flight cases considered, $\theta(t) = 0$. For the straight legs, the bank angle is set to be zero, $\phi(t) = 0$. During the turns, the bank angle is computed, with the assumption of steady-state coordinated turn, by

$$\phi = \arctan \frac{(V\dot{\mu})}{g} \tag{6.2}$$

For the details of derivation, see in Ref. [101].

6) Once the Euler angles and their time-derivatives are specified, the angular velocity components ($p,\ q,\ r$) are calculated by rotational kinematics such as in Eq. (3.9)-(3.11).

7) Using all the variables specified or computed in the earlier steps in solving algebraic equations given in Section 3.3.3 yields the angle of attack α, side slip angle β, and more importantly the control/input variables ($\delta_e,\ \delta_a,\ \delta_r,\ \delta_T$). Solution to the nonlinear algebraic equations are obtained using MATLAB's command *fsolve*. The wind components and their derivatives needed for the solution of the algebraic equations are obtained from the wind field model used in the simulations.

6.2.1 Simulation Results

Various simulation cases are run to predict the required control input variation (aerodynamic control surface deflections and thrust setting) for a KC-135 aircraft to fly through a racetrack maneuver with a specified speed within a spatially varying wind field. Through this process, feasibility of a prescribed trajectory is determined. The predicted input variations are compared against the saturation and rate limits of the corresponding control variable. This reveals the feasibility if all control predictions

are within saturation and rate limits. If a control variable is predicted to violate saturation or rate limits, this can lead to concluding the infeasibility of the prescribed trajectory. That is, the aircraft can not fly the desired trajectory.

In the following subsections, two different sets of simulation runs are presented. The first set includes input predictions for different speed and turn rates of the race track maneuver. The second set shows the effect of different wind fields on the predicted input variations.

6.2.1.1 Simulation with Different Speed and Turn Rates

Two sets of simulations are presented in this section. (1) Two cases with speed of 180 and 220 m/s. (2) Two cases with turn rates of 0.89 and 3.52 deg/s. The desired trajectories have constant altitude of 7010 m. The flights will take place within spatially varying wind fields generated by Wind Model-1. The paths within the inertial frame are shown in Fig. 6.2-(a) and (b) along with the wind vector fields. Fig. 6.3 shows the input predictions in all four cases. Figs. 6.3 also shows the predicted input in case of flying the same maneuver in the absence of wind. Figs. 6.3(a) and 6.3(b) show the input predictions with the two different speeds. As expected, the figures show that higher speed requires higher control surface deflections during the turns. Further, the effect of wind exposure can be clearly seen through a comparison between "wind" and "no wind" cases. Figs. 6.3(c) and 6.3(d) show the input predictions with the two different turn rates. As also expected, shaper turns require larger control surface deflections and higher thrust setting. Effect of the wind exposure can also be clearly seen in these cases. However, certain behaviors observed in control predictions in these cases are difficult to explain. For example, while the aircraft makes a right turn with both 180 and 220 m/s, aileron and rudder deflections show opposite signs in Fig. 6.3(a). Another example is in the thrust response. Fig. 6.3(b) shows thrust

decrease during turn when speed is 180 m/s. These observations reveals the need to investigate the solutions obtained from fsolve commands as fsolve command generates solutions that are highly dependent on the initial guesses.

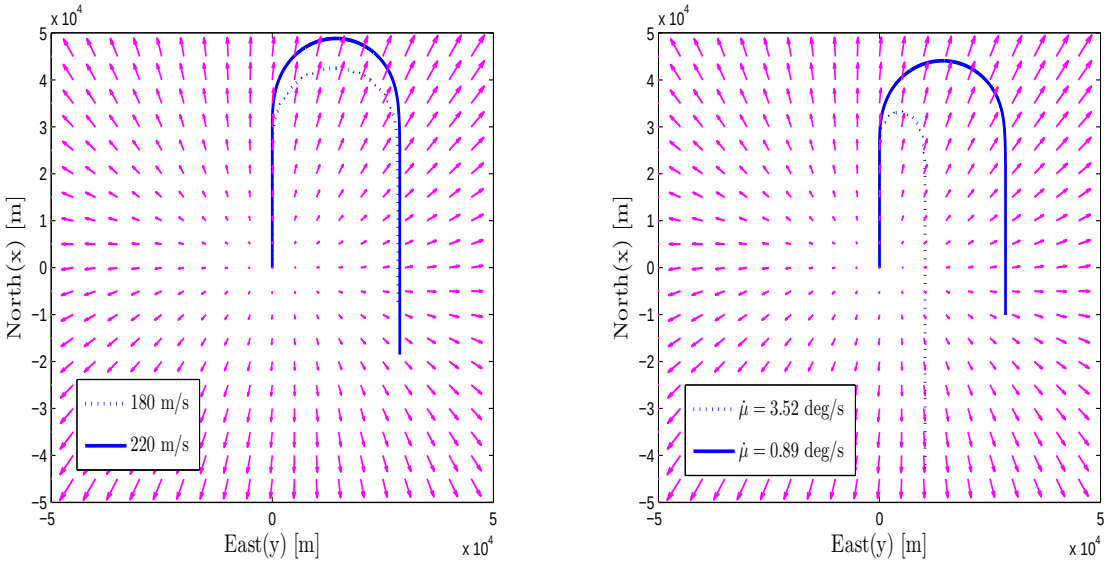

(a) Different airspeed (b) Different turn radius

Figure 6.2. Prescribed trajectories with different constant airspeed and turn rates.

6.2.1.2 Simulations with Different Wind Fields

In this section, aircraft is required to make a racetrack maneuver in different wind fields. The desired speed along the racetracks is 190 m/s and the altitude is 7010 m. The turn rates are 3.52 deg/s. The racetracks are shown in Figs. 6.4(a) and (b) overlaid on Wind Model-1 and Wind Model-3 wind fields, respectively. The coefficients of Model-1 are $D = 4 \times 10^{-6}$, $F_1 = 3 \times 10^{-4}$, $F_2 = 5 \times 10^{-4}$, and $\zeta = 5 \times 10^{-7}$. The coefficients of Model-3 are $A(z,t) = -2 \times 10^{-5}$, $B(z,t) = -2 \times 10^{-5}$, $C(z,t) = 2 \times 10^{-5}$, and $E(z,t) = -2 \times 10^{-5}$.

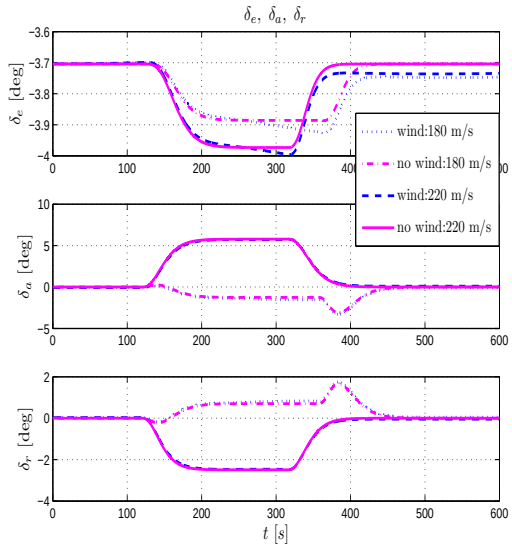

(a) Control surface deflections

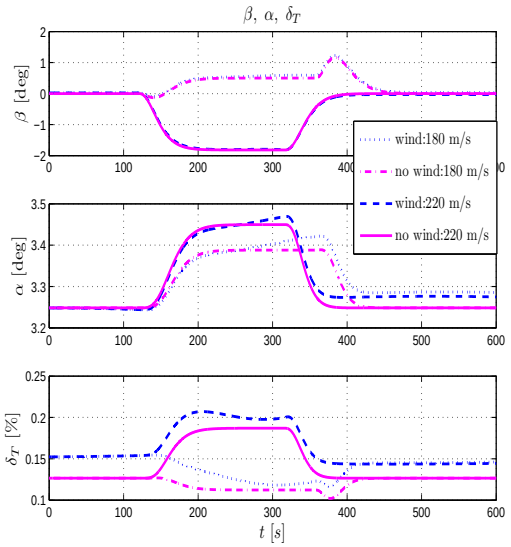

(b) Thrust, β, α

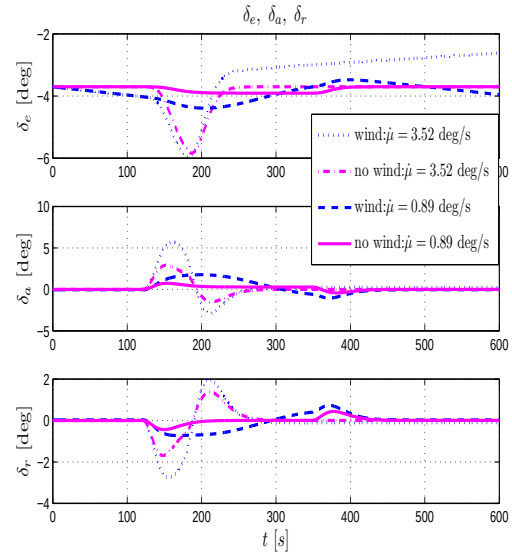

(c) Control surface deflections

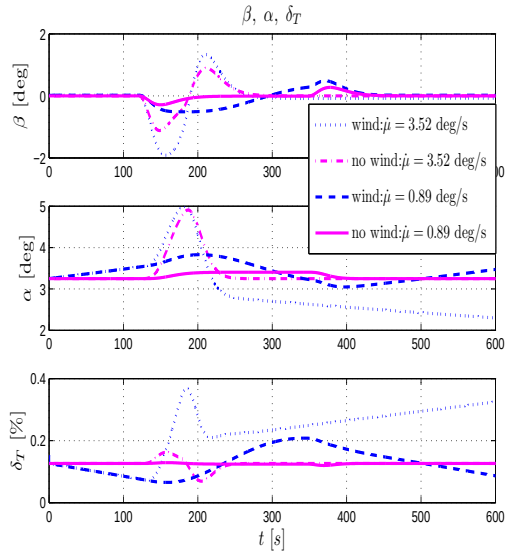

(d) Thrust, β, α

Figure 6.3. Predicted input variables and aerodynamic's angle.

Fig. 6.5 shows the input predictions for the aircraft flying in the absence of wind, within Model-1 wind field and within Model-3 wind field. The plots clearly show the

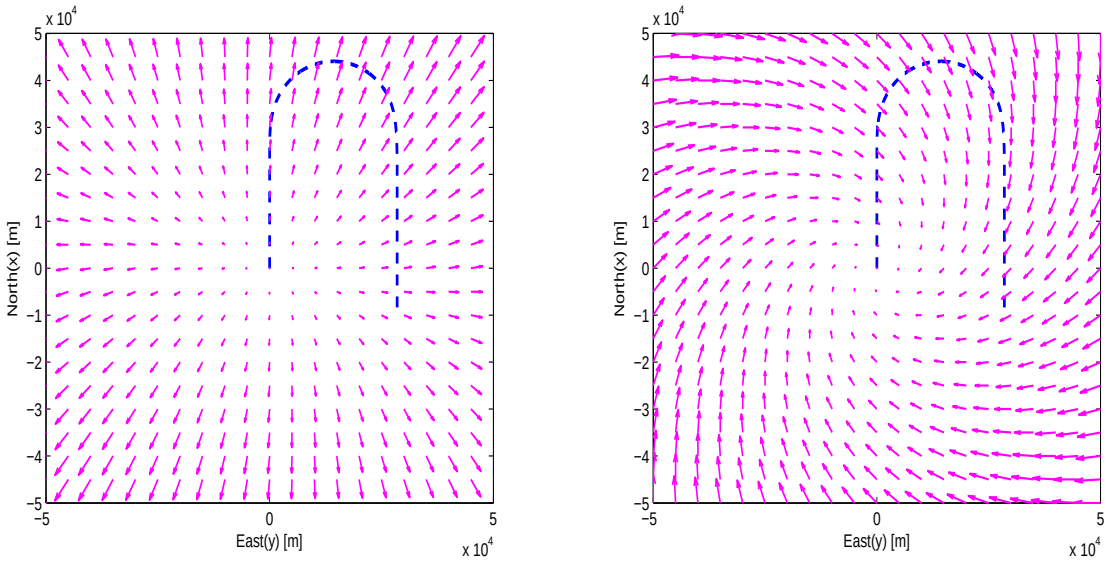

(a) Wind Model-1 (b) Wind Model-3

Figure 6.4. Prescribed trajectories in different wind field model.

effect of the presence of wind and the structure of the wind field on the required inputs for an aircraft to fly through a desired trajectory. Further, a stronger wind (Wind Model-3 in this case) requires larger input variables to complete a turn. However, the direction of the wind as much as the magnitude affects the input prediction. For example, if the aircraft happens to be flying in a tail wind region, the required thrust is lower as can be seen in Fig. 6.5(b) in the case of Wind Model-1.

If the same racetrack maneuver is to be executed in a much stronger wind field such as the one shown in Fig. 6.6, the required control/input variation may exceed the saturation limits. The wind field shown in Fig. 6.6 is generated by Wind Model-4 with parameters $A = 1.5$, $B = C = D = 1$, and $E = 10 \times 10^{-4}$. In this wind field, the magnitude of the wind can go as high as 50% of the desired speed. Fig. 6.7 shows that very large control surface deflections are required to execute the desired maneuver. In fact, the required aileron and rudder deflections exceed their limits. Further, the

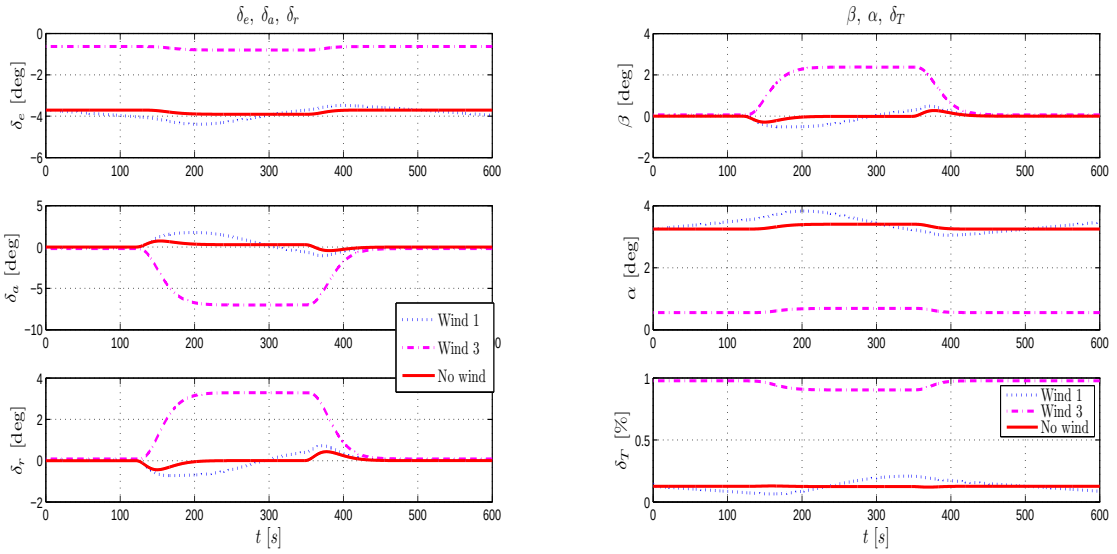

(a) Predicted control surfaces

(b) Predicted thrust setting

Figure 6.5. Predicted control surface deflections comparison in Wind Model-1 and -3.

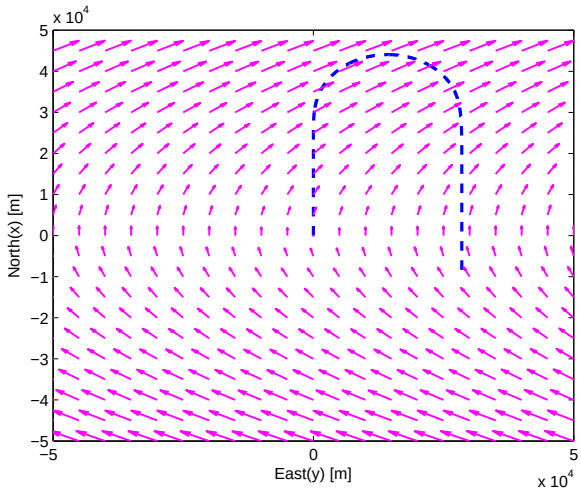

Figure 6.6. Prescribed trajectory in strong Wind Model-4.

required thrust saturates at the lower limit. If the wind field is adequately estimated and the estimated wind field is properly used in input prediction, this maneuver would not be initiated because the control saturation would be accurately predicted.

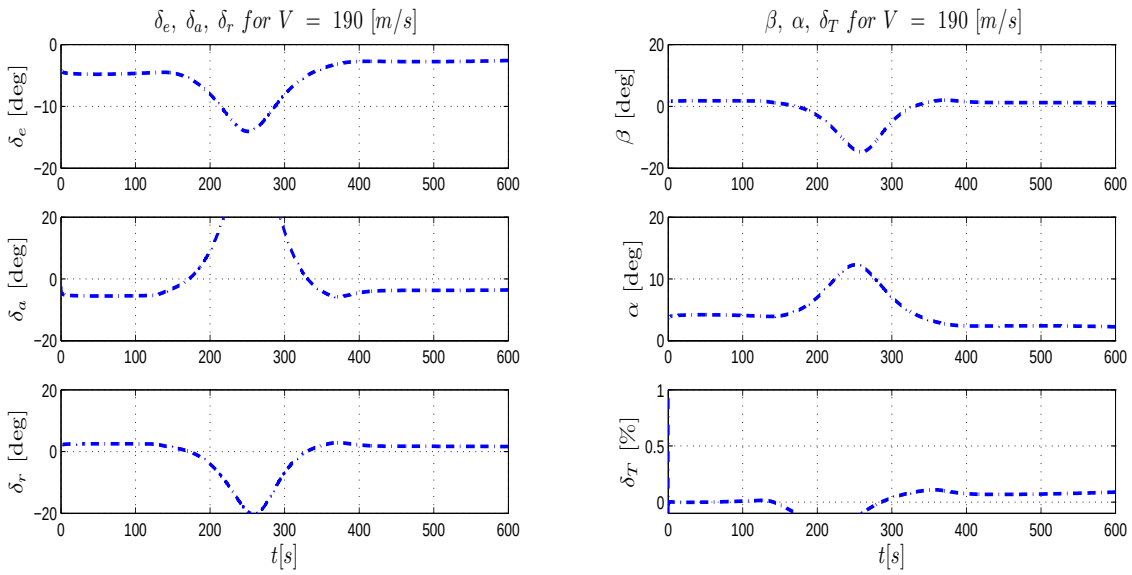

(a) Wind mode-4 (b) Wind mode-4

Figure 6.7. Predicted input in strong wind that would lead to input saturation.

6.3 Online Case

This section presents the details of online input prediction (IP) through inverse simulation and its implementation in simulation. The particular emphasis is on input prediction for aircraft flying in a spatially and/or temporally varying wind field. The simulation cases presented investigate the feasibility of a KC-135 aircraft to fly through (i) an accelerating-decelerating rectilinear trajectory and (ii) a racetrack trajectory. While the aircraft flies through the prescribed trajectory, it will be exposed to spatially and/or temporally varying wind vector. To account for this effect on the input prediction, the inverse simulation procedure will process the estimated wind field to compute the local wind vector along the prescribed trajectory.

6.3.1 Accelerating-Decelerating Rectilinear Trajectory

Accelerating-decelerating rectilinear trajectory represents a flight condition along a straight line in the inertial frame with varying airspeed. This type of flight maneu-

ver needs to be executed for various reasons such as to maintain a desired separation with other aircraft or to avoid conflict with aircraft while maintaining current heading and altitude. The variation of the speed while the aircraft moving along a straight line is modeled as [102]

$$V(t) = \begin{cases} V_0 & \text{for } t < t_1 \text{ or } t > t_2 + T_2 \\ V_0 + \frac{V_0}{16}(\cos(3\pi(\frac{t-t_1}{T_1})) - 9\cos(\pi(\frac{t-t_1}{T_1})) + 8) & \text{for } t_1 \leq t < t_1 + T_1 \\ V_0 + V_d & \text{for } t_1 + T_1 \leq t \leq t_2 \\ V_0(1 - \frac{V_0}{16}(\cos(3\pi(\frac{t-t_1}{T_1})) - 9\cos(\pi(\frac{t-t_1}{T_1})) + 8)) & \text{for } t_2 \leq t \leq t_2 + T_2 \end{cases} \tag{6.3}$$

where V_0 is the ground speed of the aircraft at the start of IP precess, V_d is the total increase (decrease if negative), and t_1, T_1, t_2, and T_2 are time parameters to specify the times of start, duration and end of speed change. Fig. 6.8 shows a speed change profile based on Eq. (6.3) when $t_1 = 5$ s, $t_2 = 65$ s, and $T_1 = T_2 = 20$ s, $V_d = 20$ m/s.

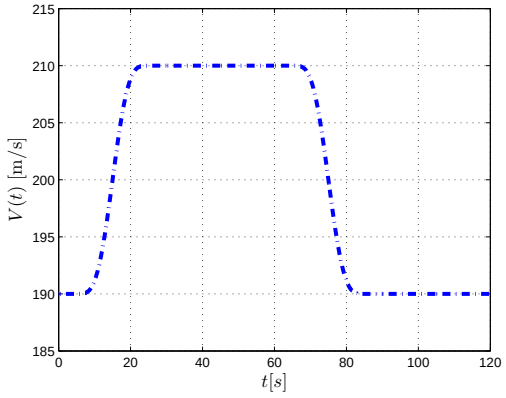

Figure 6.8. Airspeed variation with time.

As depicted in Fig. 6.9, for an accelerating-decelerating prescribed trajectory starting from point O at x_0, y_0, z_0, the current aircraft states such as airspeed, heading angle, flight path angle, position and altitude are used for initial conditions.

Starting from these initial conditions and using the specified airspeed variation, the translational kinematics equation is used to generate the prescribed trajectory within the prediction period, specified by time horizon, t_{LH}. For rectilinear trajectory, the heading and flight path angles are kept constant at their current values.

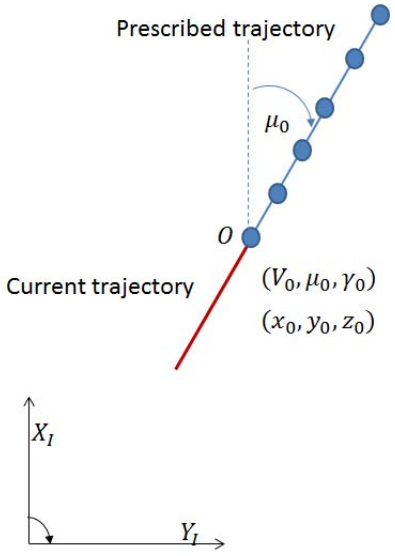

Figure 6.9. Prescribed accelerating-decelerating rectilinear trajectory.

6.3.2 Curvilinear Trajectory

This type of trajectory is typical for aircraft performing a turn maneuver. There are several ways to describe a turn maneuver such as, constant turn radius, constant bank angle or constant turn rate. Turning maneuvers are part of normal aircraft operation such as holding pattern for safe separation or flying a racetrack maneuver in aerial refueling. They can also be part of a critical operation such as in conflict or collision avoidance.

In this research, the prescribed turning trajectory is modeled by specifying the variation of heading rate as a function of time. This function is adopted from Ref. [102], which used it to represent the roll angle variation with time for turn maneuvers,

$$\dot{\mu}(t) = \begin{cases} 0 & \text{for } t < t_1 \text{ or } t > t_2 + T_2 \\ \frac{\dot{\mu}_d}{16}(\cos(3\pi(\frac{t-t_1}{T_1})) - 9\cos(\pi(\frac{t-t_1}{T_1})) + 8) & \text{for } t_1 \leq t < t_1 + T_1 \\ \dot{\mu}_d & \text{for } t_1 + T_1 \leq t \leq t_2 \\ \dot{\mu}_d(1 - \frac{\dot{\mu}_d}{16}(\cos(3\pi(\frac{t-t_1}{T_1})) - 9\cos(\pi(\frac{t-t_1}{T_1})) + 8)) & \text{for } t_2 \leq t \leq t_2 + T_2 \end{cases} \tag{6.4}$$

where $\dot{\mu}_d$ is the maximum desired value of the heading angle rate, t_1 and t_2 are times at the start and end of maneuver, T_1 and T_2 are time for transition from straight flight maneuver to turning maneuver and from turning maneuver to straight flight maneuver, respectively. The maximum turn rate $\dot{\mu}_d$ is computed by

$$\dot{\mu}_d = \frac{V_I}{h_{os}}[1 - \cos(\Delta\mu)] \tag{6.5}$$

based on constant speed V_I, desired heading change $\Delta\mu$ and lateral offset h_{os} during the turn, where h_{os} is positive for right turns and negative for left turns.

The curvilinear trajectory is used for defining a prescribed racetrack maneuver as depicted in Fig. 6.10. As done in the previous section, the prescribed trajectory is initialized using the current state variables of the aircraft. The turn is defined by the pertaining parameters included in Eq. (6.4) and (6.5). An example of the heading rate variation is shown in Fig. 6.11. For a racetrack maneuver, the heading angle change $\Delta\mu$ should be 180 degrees. Fig. 6.11 shows the heading rate variation with time horizon of $t_{LH} = 350$ s. The start and end times of the turn are $t_1 = 100$ s and $t_2 = 214$ s, the transition time durations are $T_1 = T_2 = 30$ s. The lateral offset $h_{os} = 2.747 \times 10^4$ m and $V_I = 190$ m/s.

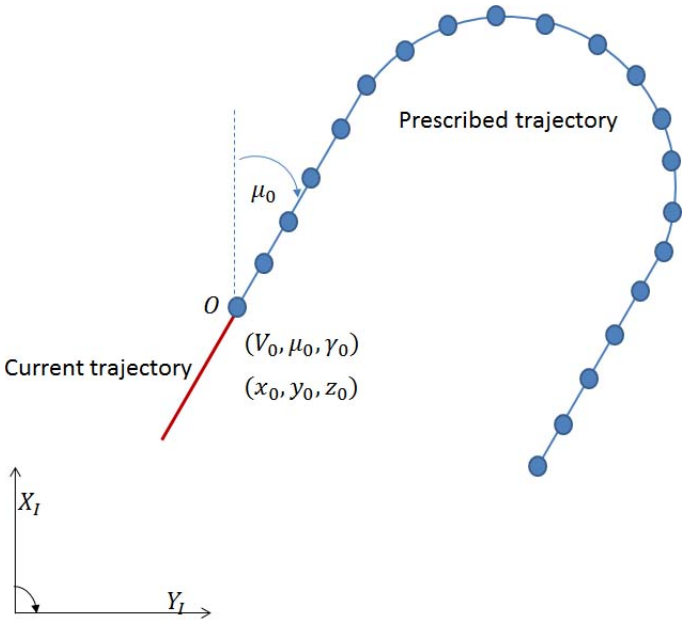

Figure 6.10. Prescribed racetrack trajectory.

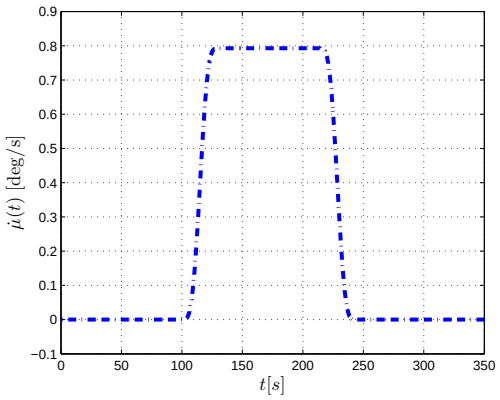

Figure 6.11. Heading rate variation with time.

6.3.3 Calculation of Prescribed Trajectory Variables

In the previous section, the prescribed trajectory is defined in terms of time variation of ground speed, heading and flight path angles as well as their derivatives. This section details the procedure to calculate the other variables of the prescribed trajectory.

In Eqs. (3.61)-(3.63) and (3.67)-(3.69), the variables are V, β, α, ψ, θ, ϕ, δ_a, δ_e, δ_r, and δ_T. Given a prescribed trajectory, four of these ten variables should be computed and then the six equations will be solved for the remaining six variable. Since the objective herein is to predict the input variable, four should be the control variables and the other two are selected to be β and α. This means that V, ψ, θ and ϕ should be determined from the prescribed trajectory. In the six equations, values of the variables needed from the previous discrete time $V_{(n-1)}$, $\beta_{(n-1)}$, $\alpha_{(n-1)}$, $\psi_{(n-1)}$, $\theta_{(n-1)}$, $\phi_{(n-1)}$ are known at current discrete time from the computation of the previous discrete time.

1) The prescribed trajectory is defined and calculated from the translational kinematics equation as

$$\dot{x} = V_I \cos\gamma_I \cos\mu_I \tag{6.6}$$

$$\dot{y} = V_I \cos\gamma_I \sin\mu_I \tag{6.7}$$

$$\dot{z} = -V_I \sin\gamma_I \tag{6.8}$$

where $\dot{x}, \dot{y}, \dot{z}$ are the aircraft ground velocity components expressed in the inertial frame, V_I is the speed relative to inertial frame, γ_I is the flight path angle, μ_I is the heading angle.

2) For the turning segment of the trajectory, the heading angle rate is computed by

$$\dot{\mu}_I = \frac{V_I}{h_{os}}[1 - \cos(\Delta\mu_I)] \tag{6.9}$$

where h_{os} is positive for right turns and negative for left turns. Integration of Eq. (6.9) will give the time variation of heading angle $\mu_I(t)$. For the straight flight legs, $\dot{\mu}_I = 0$.

3) For flight at the constant altitude, $\gamma_I = 0$, the desired trajectory in terms of position $(x(t), y(t), z(t))$ within the inertial frame is obtained by integrating Eq. (6.6)-(6.8).

4) Differentiating Eq. (6.6)-(6.8) in order to obtain the inertial acceleration as

$$\ddot{x} = \dot{V}_I \cos\gamma_I \cos\mu_I - V_I\dot{\gamma}_I \sin\gamma_I \cos\mu_I - V_I\dot{\mu}_I \cos\gamma_I \sin\mu_I \tag{6.10}$$

$$\ddot{y} = \dot{V}_I \cos\gamma_I \sin\mu_I - V_I\dot{\gamma}_I \sin\gamma_I \sin\mu_I + V_I\dot{\mu}_I \cos\gamma_I \cos\mu_I \tag{6.11}$$

$$\ddot{z} = -\dot{V}_I \sin\gamma_I - V\dot{\gamma}_I \cos\gamma_I \tag{6.12}$$

where $\ddot{x}, \ddot{y}, \ddot{z}$ are the acceleration components of the aircraft's CM with respect to the inertial frame.

5) As stated earlier, V, ψ, θ and ϕ should be determined from the prescribed trajectory. In the following, the procedure to calculate these variables are explained.

5.1) The components of aircraft ground velocity in inertial frame, formulated in Eqs. (6.6)-(6.8), can also be written in terms of the velocity with respect to air and the wind velocity vector as Eq. (6.13)

$$\begin{bmatrix} \dot{x} \\ \dot{y} \\ \dot{z} \end{bmatrix} = \mathbf{R}_{WG}^T \begin{bmatrix} V \\ 0 \\ 0 \end{bmatrix} + \begin{bmatrix} W_x \\ W_y \\ W_z \end{bmatrix} \tag{6.13}$$

which leads to

$$\dot{x} - W_x(x,y,z,t) = V\cos\gamma\cos\mu \tag{6.14}$$

$$\dot{y} - W_y(x,y,z,t) = V\cos\gamma\sin\mu \tag{6.15}$$

$$\dot{z} - W_z(x,y,z,t) = -V\sin\gamma \tag{6.16}$$

where $\dot{x}, \dot{y}, \dot{z}$ are computed from Eqs. (6.6)-(6.8) and W_x, W_y, W_z from the approximate model of the wind velocity vector field. Thus, these equations are solved to lead to

$$\tan\mu = \frac{\dot{y} - W_y}{\dot{x} - W_x} \tag{6.17}$$

$$\sin\gamma = \frac{-(\dot{z} - W_z)}{V} \tag{6.18}$$

$$V = \sqrt{(\dot{x} - W_x)^2 + (\dot{y} - W_y)^2 + (\dot{z} - W_z)^2} \tag{6.19}$$

5.2) With V computed in the previous step, the following steps are to compute the other three variables ψ, θ, ϕ from the prescribed trajectory. This will be done first by determining the angles of the wind frame, (μ, γ, ξ) with respect to the inertial frame. Note that μ and γ are already computed in the previous step. Thus, only ξ, "the roll angle of the frame" is left to be computed. For this, a method introduced in [103, 104] is used. The applied force vector for atmospheric flight consists of two parts, which are the aerodynamic/propulsive force and the weight as

$$\underline{\mathrm{f}} = \underline{\mathrm{A}}_w + m\underline{\mathrm{g}} \tag{6.20}$$

where $\underline{\mathrm{f}}$ is the resultant force acting at the aircraft CM, $\underline{\mathrm{A}}_w$ is aerodynamic/propulsive force, which will be represented later in wind frame and $\underline{\mathrm{g}}$ is the gravitational force vector, which will be represented in local frame. Note from the definitions of the reference frames in Appendix A, the local frame, which is moving with the aircraft, is always parallel to the inertial frame. Newton's 2^{nd} Law implies that

$$f = ma_{cw} \tag{6.21}$$

where f is the representation of the applied force vector in wind frame, m is the mass of aircraft and a_{cw} is the representation of acceleration of aircraft's CM in wind frame. Since $(\ddot{x}, \ddot{y}, \ddot{z})$, computed in Eqs. (6.10)-(6.12), are the components of the acceleration vector in the inertial frame and a_{cw} is the representation of the same vector in the wind frame, they are related through the rotation matrix from local frame (always aligned with the inertial frame) to the wind frame as

$$a_{cw} = \mathbf{R}_{WG} \begin{bmatrix} \ddot{x} \\ \ddot{y} \\ \ddot{z} \end{bmatrix} \tag{6.22}$$

where $\mathbf{R}_{WG}$ the rotation matrix from local frame to wind frame is expressed in terms of (μ, γ, ξ) as

$$\mathbf{R}_{WG} = \begin{bmatrix} \cos\gamma\cos\mu & \cos\gamma\sin\mu & -\sin\gamma \\ -\cos\xi\sin\mu & \cos\xi\cos\mu & \sin\xi\cos\gamma \\ +\sin\xi\sin\gamma\cos\mu & \sin\xi\sin\gamma\sin\mu & \\ \sin\xi\sin\mu & -\sin\xi\cos\mu & \cos\xi\cos\gamma \\ +\cos\xi\sin\gamma\cos\mu & +\cos\xi\sin\gamma\sin\mu & \end{bmatrix} \tag{6.23}$$

which is the rotation matrix constructed using 3-2-1 sequence of elementary rotations with angles μ around the 3^{rd} axis, γ around the 2^{nd} axis and ξ around the 1^{st} axis. Note that the 1^{st} axis of the wind frame is, by definition, along the "air velocity" vector. Note that (μ, γ, ξ) are the angles of the wind frame, which is attached to the velocity of the aircraft with respect to the air, they depend on the wind velocity vector as well as the orientation (ψ, θ, ϕ) of body frame with respect to the inertial frame rotation matrix. The representation of aerodynamic/propulsive force vector $\underline{A}_w$ in the wind frame is

$$A_w = -\begin{bmatrix} D \\ S \\ L \end{bmatrix} + \mathbf{R}_{WB}\begin{bmatrix} T_x \\ T_y \\ T_z \end{bmatrix} = \begin{bmatrix} A_x \\ A_y \\ A_z \end{bmatrix} \tag{6.24}$$

where $D,\ S,\ L$ are drag, side force and lift, and $T_x,\ T_y,\ T_z$ are the thrust components in the body frame, $A_x,\ A_y,\ A_z$ are the aero/propulsive force components in wind frame and $\mathbf{R}_{WB}$ is the rotation matrix from body frame to wind frame.

Eq. (6.20) written in terms of the vector representations becomes

$$f = A_w + m\mathbf{R}_{WG} \begin{bmatrix} 0 \\ 0 \\ g \end{bmatrix} \tag{6.25}$$

which yields

$$f = \begin{bmatrix} A_x \\ A_y \\ A_z \end{bmatrix} + mg \begin{bmatrix} -\sin\gamma \\ \sin\xi\cos\gamma \\ \cos\xi\cos\gamma \end{bmatrix} \tag{6.26}$$

Differentiation of Eq. (6.13) leads to

$$\begin{bmatrix} \ddot{x} \\ \ddot{y} \\ \ddot{z} \end{bmatrix} = \dot{\mathbf{R}}_{WG}^T \begin{bmatrix} V \\ 0 \\ 0 \end{bmatrix} + \mathbf{R}_{WG}^T \begin{bmatrix} \dot{V} \\ 0 \\ 0 \end{bmatrix} + \begin{bmatrix} \dot{W}_x \\ \dot{W}_y \\ \dot{W}_z \end{bmatrix} \tag{6.27}$$

Rotational kinematics for rotational matrix from the local frame to wind frame implies

$$\dot{\mathbf{R}}_{WG} = \mathbf{S}(\omega_{WG})\mathbf{R}_{WG} \tag{6.28}$$

where ω_{WG} is the angular velocity of the wind frame with respect to the local frame represented in wind frame as

$$\omega_{WG} = \begin{bmatrix} p_w \\ q_w \\ r_w \end{bmatrix} \tag{6.29}$$

Taking transpose yields

$$\dot{\mathbf{R}}_{WG}^T = \mathbf{R}_{WG}^T\mathbf{S}^T(\omega_{WG}) = -\mathbf{R}_{WG}^T\mathbf{S}(\omega_{WG}) \tag{6.30}$$

where $\mathbf{S}^T(\omega_{WG}) = -\mathbf{S}(\omega_{WG})$ since it is a skew-symmetric matrix. Substituting Eq. (6.30) in Eq. (6.27) leads to

$$\begin{bmatrix} \ddot{x} \\ \ddot{y} \\ \ddot{z} \end{bmatrix} = -\mathbf{R}_{WG}^T \mathbf{S}(\omega_{WG}) \begin{bmatrix} V \\ 0 \\ 0 \end{bmatrix} + \mathbf{R}_{WG}^T \begin{bmatrix} \dot{V} \\ 0 \\ 0 \end{bmatrix} + \begin{bmatrix} \dot{W}_x \\ \dot{W}_y \\ \dot{W}_z \end{bmatrix} \tag{6.31}$$

where

$$\mathbf{S}(\omega_{WG}) = \begin{bmatrix} 0 & r_w & -q_w \\ -r_w & 0 & p_w \\ q_w & -p_w & 0 \end{bmatrix} \tag{6.32}$$

Multiplying both side of Eq. (6.31) with $\mathbf{R}_{WG}$, yields

$$\mathbf{R}_{WG} \begin{bmatrix} \ddot{x} \\ \ddot{y} \\ \ddot{z} \end{bmatrix} = -\mathbf{S}(\omega_{WG}) \begin{bmatrix} V \\ 0 \\ 0 \end{bmatrix} + \begin{bmatrix} \dot{V} \\ 0 \\ 0 \end{bmatrix} + \mathbf{R}_{WG} \begin{bmatrix} \dot{W}_x \\ \dot{W}_y \\ \dot{W}_z \end{bmatrix} \tag{6.33}$$

which, along with Eqs. (6.22), (6.23) and (6.32), implies

$$a_{cw} = \begin{bmatrix} \dot{V} \\ V r_w \\ -V q_w \end{bmatrix} + \mathbf{R}_{WG} \begin{bmatrix} \dot{W}_x \\ \dot{W}_y \\ \dot{W}_z \end{bmatrix} \tag{6.34}$$

Implementation of rotational kinematics in terms of the 3-2-1 Euler's angles, formulated in Eqs. (3.12)-(3.14), for the rotational motion of wind frame yields

$$\begin{bmatrix} p_w \\ q_w \\ r_w \end{bmatrix} = \begin{bmatrix} 1 & 0 & -\sin\gamma \\ 0 & \cos\xi & \sin\xi\cos\gamma \\ 0 & -\sin\xi & \cos\xi\sin\gamma \end{bmatrix} \begin{bmatrix} \dot{\xi} \\ \dot{\gamma} \\ \dot{\mu} \end{bmatrix} \tag{6.35}$$

which gives the angular velocities components of wind frame relative to local frame expressed in wind frame, especially $q_w,\ r_w$ components, as

$$r_w = -\dot{\gamma}\sin\xi + \dot{\mu}\cos\gamma\cos\xi \tag{6.36}$$

$$q_w = \dot{\gamma}\cos\xi + \dot{\mu}\cos\gamma\sin\xi \tag{6.37}$$

where μ and γ are already computed in the previous steps. Differentiating Eqs. (6.17)-(6.19), leads to

$$\dot{\mu} = \frac{[(\ddot{y} - \dot{W}_y)\cos\mu - (\ddot{x} - \dot{W}_x)\sin\mu]}{V\cos\gamma} \tag{6.38}$$

$$\dot{\gamma} = -\frac{(\ddot{z} - \dot{W}_z + \dot{V}\sin\gamma)}{V\cos\gamma} \tag{6.39}$$

$$\begin{aligned}\dot{V} &= [(\ddot{x} - \dot{W}_x)\cos\mu + (\ddot{y} - \dot{W}_y)\sin\mu]\cos\gamma \\ &- (\ddot{z} - \dot{W}_z)\sin\gamma\end{aligned} \tag{6.40}$$

Substituting Eq. (6.39) in Eq. (6.36) and (6.37), yields

$$r_w = \frac{(\ddot{z} - \dot{W}_z + \dot{V}\sin\gamma)}{V\cos\gamma}\sin\xi + \dot{\mu}\cos\gamma\cos\xi \tag{6.41}$$

$$q_w = -\frac{(\ddot{z} - \dot{W}_z + \dot{V}\sin\gamma)}{V\cos\gamma}\cos\xi + \dot{\mu}\cos\gamma\sin\xi \tag{6.42}$$

From Eq. (6.21) and (6.25), implies

$$a_{cw} = \frac{1}{m}\begin{bmatrix} A_x \\ A_y \\ A_z \end{bmatrix} + \mathbf{R}_{WG}\begin{bmatrix} 0 \\ 0 \\ g \end{bmatrix} \tag{6.43}$$

where the rotation matrix is written as the product of three elementary rotation matrices as

$$\mathbf{R}_{WG} = \mathbf{R}_x(\xi)\mathbf{R}_y(\gamma)\mathbf{R}_z(\mu) \tag{6.44}$$

such that

$$a_{cw} = \frac{1}{m}\begin{bmatrix} A_x \\ A_y \\ A_z \end{bmatrix} + \mathbf{R}_x(\xi)\mathbf{R}_y(\gamma)\mathbf{R}_z(\mu)\begin{bmatrix} 0 \\ 0 \\ g \end{bmatrix} \tag{6.45}$$

Multiplying both sides with $\mathbf{R}_x^T(\xi)$ gives

$$\mathbf{R}_x^T(\xi)a_{cw} = \frac{1}{m}\mathbf{R}_x^T(\xi)\begin{bmatrix} A_x \\ A_y \\ A_z \end{bmatrix} + \mathbf{R}_y(\gamma)\mathbf{R}_z(\mu)\begin{bmatrix} 0 \\ 0 \\ g \end{bmatrix} \tag{6.46}$$

where

$$\mathbf{R}_x(\xi) = \begin{bmatrix} 1 & 0 & 0 \\ 0 & \cos\xi & \sin\xi \\ 0 & -\sin\xi & \cos\xi \end{bmatrix} \tag{6.47}$$

$$\mathbf{R}_y(\gamma) = \begin{bmatrix} \cos\gamma & 0 & -\sin\gamma \\ 0 & 1 & 0 \\ \sin\gamma & 0 & \cos\gamma \end{bmatrix} \tag{6.48}$$

$$\mathbf{R}_z(\mu) = \begin{bmatrix} \cos\mu & \sin\mu & 0 \\ -\sin\mu & \cos\mu & 0 \\ 0 & 0 & 1 \end{bmatrix} \tag{6.49}$$

Substituting a_{cw} from Eqs. (6.34), and elementary rotation matrices from (6.47)-(6.49) in (6.46) leads to

$$\begin{aligned} A_x - g\sin\gamma &= \dot{V} + \dot{W}_x\cos\gamma\cos\mu \\ &+ \dot{W}_y\cos\gamma\sin\mu - \dot{W}_z\sin\gamma \end{aligned} \tag{6.50}$$

$$\begin{aligned} A_y\cos\xi - A_z\sin\xi &= Vr_w\cos\xi + Vq_w\sin\xi \\ &- \dot{W}_x\sin\mu + \dot{W}_y\cos\mu \end{aligned} \tag{6.51}$$

$$\begin{aligned} A_y\sin\xi + A_z\cos\xi &= Vr_w\sin\xi - Vq_w\cos\xi + \dot{W}_x\sin\gamma\cos\mu \\ &+ \dot{W}_y\sin\gamma\sin\mu + \dot{W}_z\cos\gamma - g\cos\gamma \end{aligned} \tag{6.52}$$

Rearranging Eqs. (6.50) gives

$$\begin{aligned} A_x &= \dot{V} + (g - \dot{W}_z)\sin\gamma \\ &+ (\dot{W}_x\cos\mu + \dot{W}_y\sin\mu)\cos\gamma \end{aligned} \tag{6.53}$$

Substituting Eq. (6.41) and (6.42) in Eq. (6.51) and (6.52), yields

$$-A_z\sin\xi + A_y\cos\xi = K_1 \tag{6.54}$$

$$A_y\sin\xi + A_z\cos\xi = K_2 \tag{6.55}$$

where

$$K_1 = \dot{\mu} V \cos\gamma + (\dot{W}_y \cos\mu - \dot{W}_x \sin\mu) \tag{6.56}$$

$$K_2 = \frac{\ddot{z} - g + A_x \sin\gamma}{\cos\gamma} \tag{6.57}$$

Where μ, γ, and V are computed in Eqs. (6.17), (6.18), and (6.19), respectively, and $(\dot{W}_x, \dot{W}_y, \dot{W}_z)$ are computed from the approximation of the wind velocity vector field in Eq. (2.2). This means, there are three unknowns in Eqs. (6.54) and (6.55): A_y, A_z, and ξ. Recall that the goal is to compute ξ. Eqs. (6.54) and (6.55) are solved to obtain

$$\sin\xi = \frac{K_2 A_y - K_1 A_z}{A_y^2 + A_z^2} \tag{6.58}$$

$$\cos\xi = \frac{K_1 A_y + K_2 A_z}{A_y^2 + A_z^2} \tag{6.59}$$

which leads to

$$\tan\xi = \frac{K_2 \frac{A_y}{A_z} - K_1}{K_1 \frac{A_y}{A_z} + K_2} \tag{6.60}$$

where $\frac{A_y}{A_z}$ is assumed to be negligible since A_y is usually much smaller than A_z, which leads to

$$\tan\xi = -\frac{K_1}{K_2} \tag{6.61}$$

If A_z is desired to be computed, Eqs. (6.54) and (6.55) can be solved for A_z as

$$A_z = K_2 \cos\xi - K_1 \sin\xi \tag{6.62}$$

6) The Euler's angles and theirs time derivatives, which describe the orientation of body frame with respect to the [$\hat{I}$] or [$\hat{G}$] frame, need to be formulated in terms of variables computed in the previous steps and the six variables that Eqs. (3.61)-(3.63) and (3.67)-(3.69) are solved for. To do this, the matrix relation between the three rotation matrices is written as

$$\mathbf{R}_{GB} = \mathbf{R}_{WG}^T \mathbf{R}_{WB} \tag{6.63}$$

By using trigonometric identity and algebra to manipulate Eq. (6.63), the Euler's angles are expressed in terms of μ, γ, ξ, α, and β as

$$\tan\phi = \frac{\cos\beta\sin\xi\cos\gamma - \sin\beta\sin\gamma}{(\cos\alpha\cos\xi - \sin\alpha\sin\beta\sin\xi)\cos\gamma - \sin\alpha\cos\beta\sin\gamma} \tag{6.64}$$

$$\sin\theta = \cos\alpha\cos\beta\sin\gamma + (\sin\alpha\cos\xi + \cos\alpha\sin\beta\sin\xi)\cos\gamma \tag{6.65}$$

$$\tan(\psi - \mu) = \frac{\sin\alpha\sin\xi - \cos\alpha\sin\beta\cos\xi}{\cos\alpha\cos\beta\cos\gamma - (\sin\alpha\cos\xi + \cos\alpha\sin\beta\sin\xi)\sin\gamma} \tag{6.66}$$

where note that Euler angles ψ, θ and ϕ depend on α and β, which are to be computed from the solution of Eqs. (3.61)-(3.63) and (3.67)-(3.69). However, in this research, Eqs. (6.64)-(6.66) are simplified by setting $\beta = 0$ and calculating α independently by

$$\alpha = \alpha_0 - m\frac{A_z}{QSC_{L_\alpha}} \tag{6.67}$$

where α_0 is the current value of angle of attack, S is the wing reference area, Q is the dynamic pressure, and C_{L_α} is the derivative of life coefficient with respect to angle of attack. With these simplifications, Eqs. (6.64)-(6.66) becomes

$$\psi = \mu + \tan^{-1}\left(\frac{\sin\alpha\sin\xi}{\cos\alpha\cos\gamma - \sin\alpha\cos\xi\sin\gamma}\right) \tag{6.68}$$

$$\theta = \sin^{-1}(\cos\alpha\sin\gamma + \sin\alpha\cos\xi\cos\gamma) \tag{6.69}$$

$$\phi = \tan^{-1}\left(\frac{\cos\gamma\cos\xi}{\cos\alpha\cos\gamma\cos\xi - \sin\alpha\sin\gamma}\right) \tag{6.70}$$

which can calculate values of the Euler angles to be used in the solution of Eqs. (3.61)-(3.63) and (3.67)-(3.69).

7) The angular accelerations components can be obtained by differentiation of Eqs. (3.12)-(3.14) as

$$\dot{p} = \ddot{\phi} - \ddot{\psi}\sin\theta - \dot{\psi}\dot{\theta}\cos\theta \tag{6.71}$$

$$\begin{aligned}\dot{q} &= \ddot{\theta}\cos\phi - \dot{\phi}\dot{\theta}\sin\phi - \dot{\psi}\dot{\theta}\sin\theta\sin\phi \\ &+ \dot{\psi}\dot{\phi}\cos\phi\cos\theta + \ddot{\psi}\sin\phi\cos\theta\end{aligned} \tag{6.72}$$

$$\begin{aligned}\dot{r} &= \ddot{\psi}\cos\theta\cos\phi - \dot{\psi}\dot{\theta}\sin\theta\cos\phi - \dot{\psi}\dot{\phi}\cos\theta\sin\phi \\ &- \dot{\theta}\dot{\phi}\cos\phi - \ddot{\theta}\sin\phi\end{aligned} \tag{6.73}$$

8) Using all the variables specified or formulated in the earlier steps in solving the six nonlinear algebraic equations given in Eqs. (3.61)-(3.63) and (3.67)-(3.69) yields the angle of attack α, side slip angle β, and more importantly the control/input variables (δ_e, δ_a, δ_r, δ_T). Solution to the nonlinear algebraic equations are obtained using MATLAB's command *fsolve*. The wind components and their derivatives needed for the solution of the algebraic equations are obtained from the estimated wind field. Note that Eqs. (6.68)-(6.70) are simplified equations with the approximation of $\beta = 0$ and α calculated by Eq. (6.67). However, the solution of Eqs. (3.61)-(3.63) and (3.67)-(3.69) will yield different values of β and α, which means Euler angles will also be different along the prescribed trajectory as they are determined by Eqs. (6.64)-(6.66).

6.3.4 Input Prediction Procedure

The algorithm of input prediction process through inverse simulation (differential-based technique) is summarized as follows.

Algorithm : Input Prediction with Incorporated Estimated Wind Field

1: **Initialization.**

Read Initial States :

$x_0,\ y_0,\ z_0,\ V_0,\ \gamma_0,\ \mu_0$

Read Initial Input/Control Variables : set them as the initial guess values

$\delta_{T_0},\ \delta_{e_0},\ \delta_{a_0},\ \delta_{r_0},\ \alpha_0,\ \beta_0$

2: **Trajectory Determination.**

Generate prescribed trajectory for specify time horizon :

Prescribe V_I, γ_I, μ_I and $\dot{\mu}_I$ then calculate

$x(t),\ y(t),\ z(t)$

Calculated the velocity and acceleration components:

$\dot{x}(t),\ \dot{y}(t),\ \dot{z}(t)$

$\ddot{x}(t),\ \ddot{y}(t),\ \ddot{z}(t)$

3: **Local Wind Determination.**

Calculate Estimated Local Wind :

$\widehat{W}_x,\ \widehat{W}_y,\ \widehat{W}_z$

$\widehat{\dot{W}}_x,\ \widehat{\dot{W}}_y,\ \widehat{\dot{W}}_z$

4: **Euler's Angles Determination.**

Calculate Euler's angles from V, μ, γ, ξ, β and α

$\psi(t),\ \theta(t),\ \phi(t)$

5: **Angular Velocity and Acceleration Determination.**

Calculate angular velocity and acceleration

$p(t),\ q(t),\ r(t)$

$\dot{p}(t),\ \dot{q}(t),\ \dot{r}(t)$

6: **Aerodynamics Forces and moments Determination.**

Calculate aerodynamic forces and moments.

7: **Input Prediction.**

Solve nonlinear algebraic equation

$F(x) = 0$

8: **End Prediction.**

Output the predicted control inputs

6.3.5 Simulation Results

Various simulation cases are run to predict the required control input variation (aerodynamic control surface deflections and thrust setting) for a KC-135 aircraft to fly though the desired trajectory within the spatially and temporally varying wind fields. Through this process, feasibility of the prescribed trajectory is determined. The predicted input variations are compared against the saturation and rate limits of the corresponding control variable. This reveals the feasibility if all control predictions are within saturation and rate limits. If a control variable is predicted to violate saturation or rate limits, this can lead to the conclusion of infeasibility of the prescribed trajectory. That is, the aircraft can not fly the desired trajectory.

In the following subsections, two different sets of simulation runs are presented. The first set includes input predictions for the aircraft to fly though accelerating/decelerating straight line flight path. The second set includes input predictions of the aircraft to fly though a racetrack maneuver with a specified speed and turn rate. In each set, three cases of the input prediction are carried out: (1) no wind assumption in prediction, (2) actual wind field used in prediction, and (3) estimated wind field used in the prediction. The second case is not realistic since the actual wind cannot be known. It is conducted nevertheless to understand how much of a prediction error can occur due to the difference between the actual wind and the predicted wind from the estimated wind field. The comparison between the first and the third cases will show the benefit of incorporating wind field estimation into the input prediction process.

6.3.5.1 Accelerating Straight Flight Trajectory

The first simulation experiment is to investigate the feasibility of the KC-135 aircraft to follow an accelerating/decelerating rectilinear trajectory, calculated from

Eq. (6.3). There are 10 aircraft flying at the same altitude of 7010 m with the same speed of 190 m/s within a spatially and temporally varying wind field generated by Wind Model-1. The feasibility of Aircraft-1 to follow the accelerating/decelerating rectilinear trajectory is evaluated at $t = 1100$ s. The roles of the other aircraft are to provide estimated or measured local wind for wind field estimation, which will be utilized in the IP process.

Figures. 6.12 (a) and (b) show the ground speed variation with time, which are generated by specified total increasing and decreasing velocities of $V_d = 20$ m/s and 50 m/s at time $t = 1100$ s, when the IP process is activated. Note also that in these simulation cases, the input prediction is carried out within $t_{LH} = 120$ s. Figures. 6.12 (c) and (d) shows the prescribed paths and the wind velocity vector along the trajectory during the periods of input prediction.

The estimated local wind information i.e., estimated local wind components and their time derivatives, are obtained from the estimated wind field parameters. Figs. 6.13 (a) and (b) show the predicted and actual wind components that Aircraft-1 is exposed to during the prediction period starting at 1100 s. The wind is in the South-West direction with increasing magnitude. In average, it is about 8% of the aircraft speed. During this prediction period, the estimated wind is very close to the actual wind. As a result, no visible difference is expected between the cases with estimated wind and actual wind.

Fig. 6.14 shows the results of the input prediction with three cases in each set of simulation. Figs. 6.14 (a) and (b) show the input prediction results when the ground speed is desired to be increasing for 20 s from 190 to 210 m/s and later on decreasing back to 190 m/s while Figs. 6.14 (c) and (d) show the results for $190 - 240$ m/s cases.

As expected, the figures show that the higher acceleration and deceleration requires higher thrust setting and lower elevator upward deflections, and results in

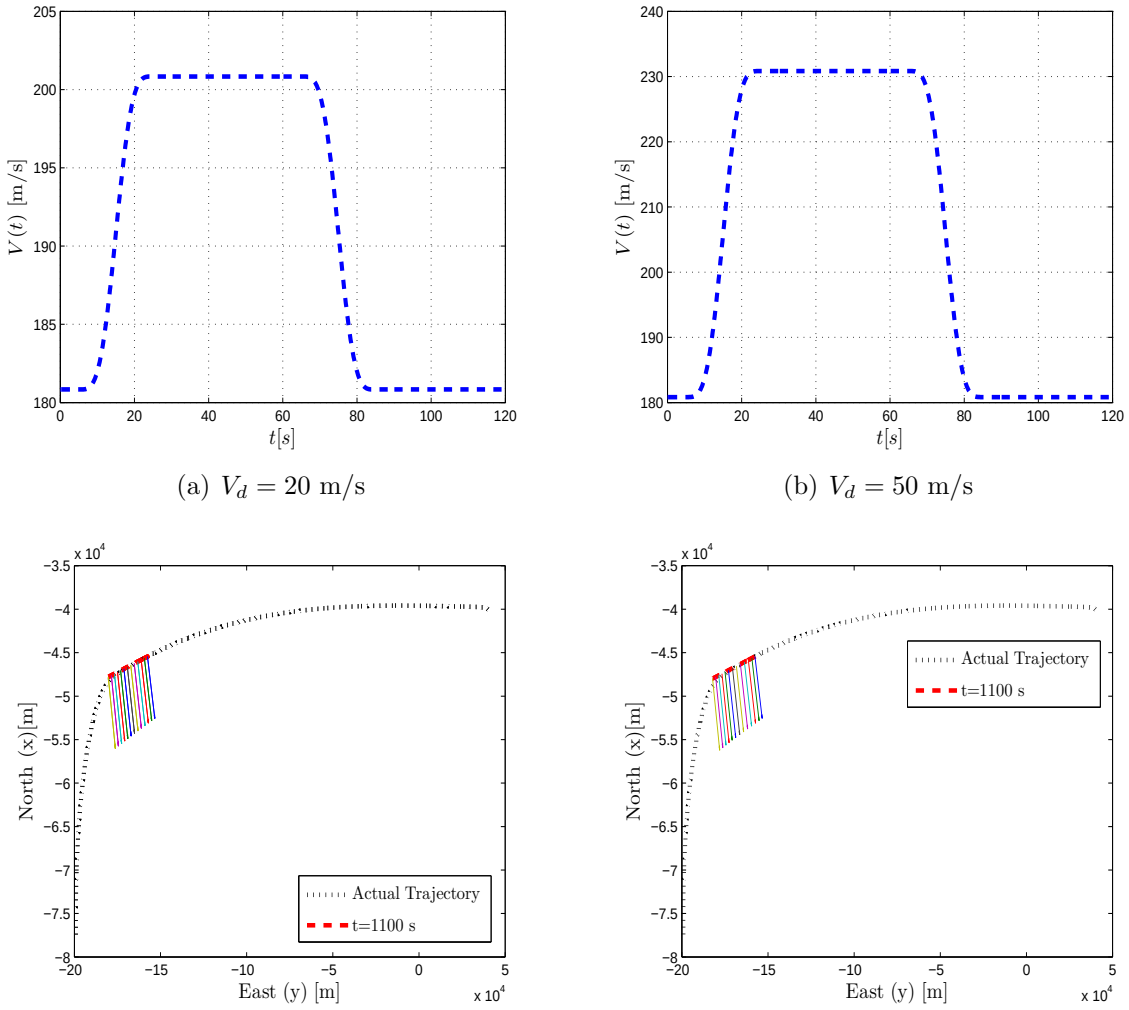

(a) $V_d = 20$ m/s

(b) $V_d = 50$ m/s

(c) $V_d = 20$ m/s

(d) $V_d = 50$ m/s

Figure 6.12. Aircraft velocity variation with time, paths in inertial frame and wind velocity vectors along the paths during the prediction period.

lower angle of attack as shown in the subfigures. Additionally, the effects of wind exposure can be clearly seen through predicted thrust setting comparison between the cases with or without wind included. As expected, When wind is not included in the input prediction procedure, the required thrust setting is lower compared to the case with wind included as shown in subfigures (a) and (c). Fig. 6.14 (c) shows that

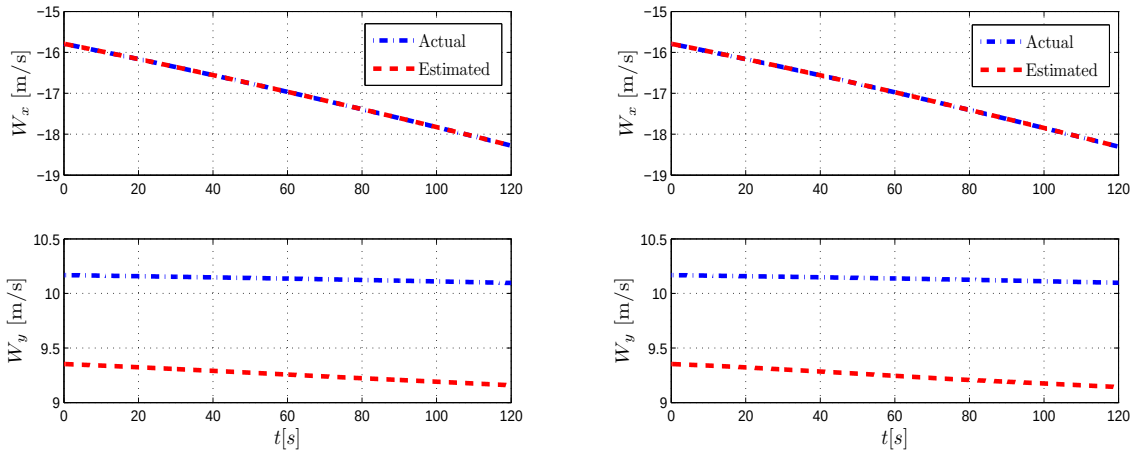

(a) $V_d = 20$ m/s (b) $V_d = 50$ m/s

Figure 6.13. Actual and estimated local wind along prescribed trajectory at $t = 1100$ s.

the required thrust setting exceed its limit. If wind field is adequately estimated and the estimated wind field is properly used in IP, this maneuver would not be initiated because the control saturation would be accurately predicted.

6.3.5.2 Racetrack Trajectory

The second simulation experiment is to investigate the feasibility of the KC-135 aircraft to follow a racetrack trajectory, with two different turn rates of 0.4 and 0.8 deg/s, calculated from Eq. (6.4). There are 10 aircraft flying at the same altitude of 7010 m with the same speed of 190 m/s within a spatially and temporally varying wind field generated by Wind Model-1. The feasibility of Aircraft-1 to follow the racetrack trajectory is evaluated at two times at $t = 500$ and 1100 s. The roles of the other aircraft are to provide estimated or measured local wind information for wind field estimation, which will be utilized in the IP process.

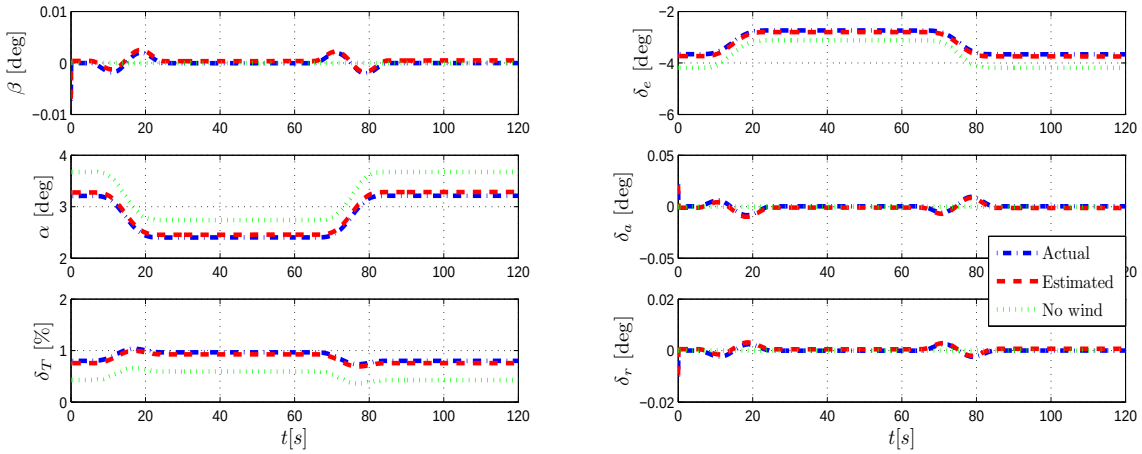

(a) $V_d = 20$ m/s : β, α, δ_T

(b) $V_d = 20$ m/s : δ_e, δ_a, δ_r

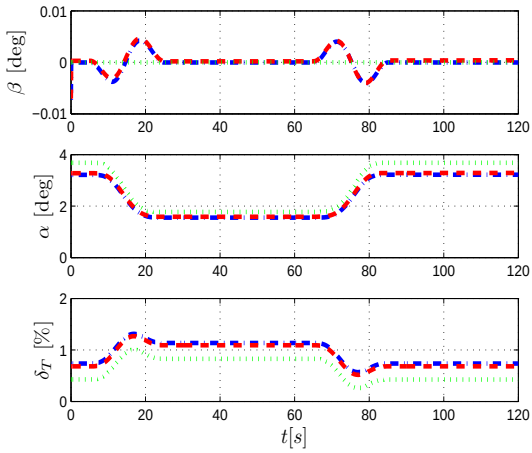

(c) $V_d = 50$ m/s : β, α, δ_T

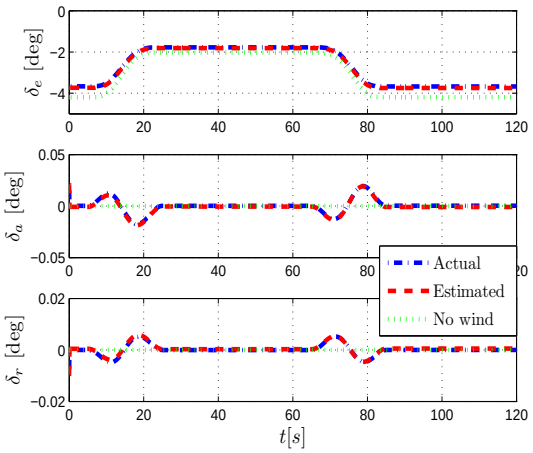

(d) $V_d = 50$ m/s : δ_e, δ_a, δ_r

Figure 6.14. Comparison of predicted input variables and aerodynamic angles of all three simulation cases.

Figures. 6.15 (a) and (b) show the turn rates variation with time, which are generated by specified $\Delta\mu = 180$ degree, $V_I = 190$ m/s and two different lateral offsets $h_{os} = 5.494 \times 10^4$ and 2.747×10^4 m at times $t = 500$ s and $t = 1100$ s, when the input prediction process is activated. Note also that in these simulation cases, the input prediction is carried out within $t_{LH} = 120$ s. Figures. 6.15 (c) and (d) show the

prescribed paths and the wind velocity vector along the trajectory during the periods of input prediction.

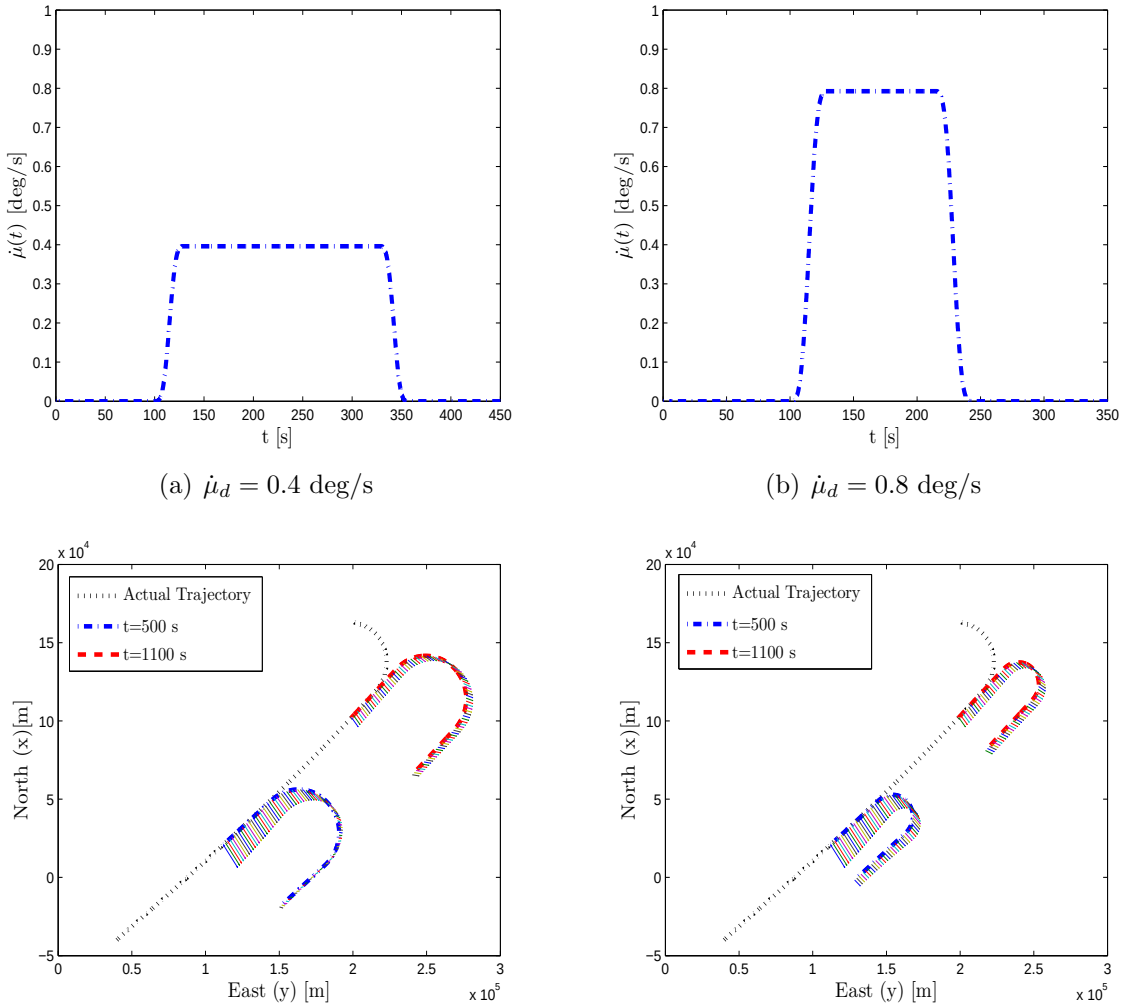

(a) $\dot{\mu}_d = 0.4$ deg/s

(b) $\dot{\mu}_d = 0.8$ deg/s

(c) Racetrack trajectory 1

(d) Racetrack trajectory 2

Figure 6.15. Heading rate variation with time and paths in inertial frame and wind velocity vectors along the paths during the prediction period.

The estimated local wind information i.e., estimated local wind components and their time derivatives, are obtained from the estimated wind field parameters.

Figs. 6.16 (a) and (b) show the predicted and actual wind components that Aircraft-1 is exposed to during the prediction period starting at 500 s. Similarly, Figs. 6.17 (a) and (b) show the same for $t = 1100$ s. The prediction period starting at $t = 500$ s, the wind is the South-West direction and in average, is about 8% of the aircraft speed. For the prediction period starting at $t = 1100$, the wind is in the same direction and in average, is about 10% of the aircraft speed.

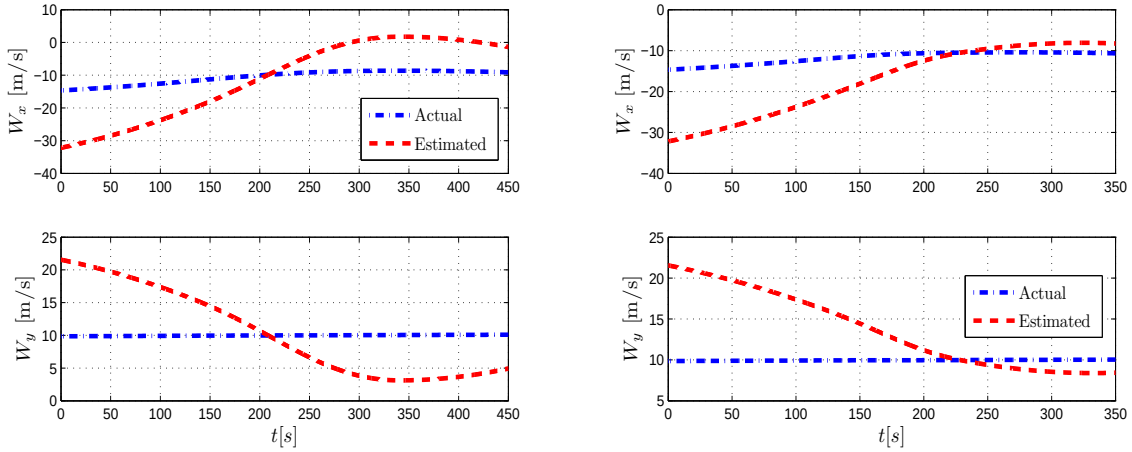

(a) $\dot{\mu}_d = 0.4$ deg/s (b) $\dot{\mu}_d = 0.8$ deg/s

Figure 6.16. Actual and estimated local wind along prescribed trajectory at $t = 500$ s.

Fig. 6.18 shows the results of the input prediction in each set of simulation. Figs. 6.18 (a) and (b) show the input prediction results when the turn is executed with 0.4 deg/s constant turn rate while Figs. 6.18 (c) and (d) show the results for 0.8 deg/s cases.

As expected, the figures clearly show the effect of the presence of wind and the structure of the wind field on the required inputs for an aircraft to fly through a desired trajectory. Further, a stronger wind requires larger input variables to complete

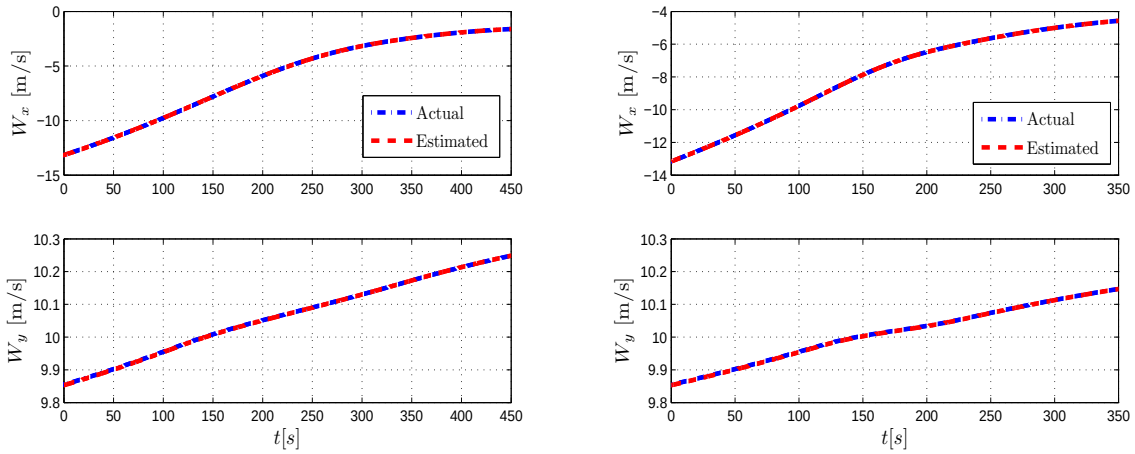

(a) $\dot{\mu}_d = 0.4$ deg/s (b) $\dot{\mu}_d = 0.8$ deg/s

Figure 6.17. Actual and estimated local wind along prescribed trajectory at $t = 1100$ s.

the turn. However, the direction of wind as much as the magnitude affects the input prediction. For example, if the aircraft happens to be flying in a tail wind region, which is to complete the right turn racetrack maneuver case, the required thrust is lower as can be seen in Fig. 6.18 (a) and (b). Additionally, as expected, sharper turn requires higher control surface deflections as can be seen in Fig. 6.18 (c) and (d). Moreover, the desired racetrack trajectories with sharper turn are not feasible for aircraft because of deflection of ailerons exceeds their limits as shown in Fig. 6.18 (d). In contrary, the aircraft would be feasible to perform racetrack maneuver in this wind field, if it flew through shallower turn or lower turn rate as shown in Fig. 6.18-(b).

As state earlier, the direction of wind as much as the magnitude affects the variation of input required for aircraft to follow the prescribed trajectory. In order to better demonstrate this, a new simulation case is run. In this case, everything is the same as the previous cases except the initial heading of the aircraft is set to be

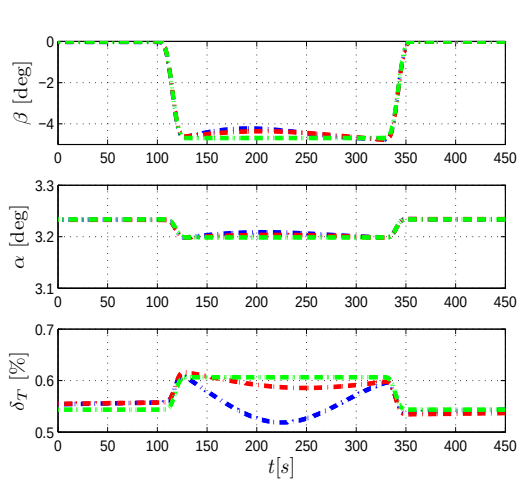

(a) $\dot{\mu}_d = 0.4$ deg/s : β, α, δ_T

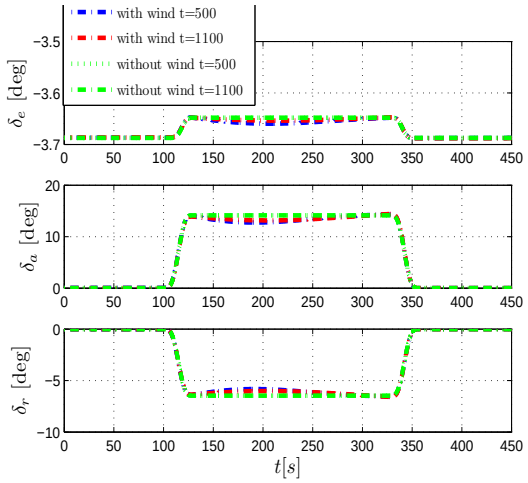

(b) $\dot{\mu}_d = 0.4$ deg/s : δ_e, δ_a, δ_r

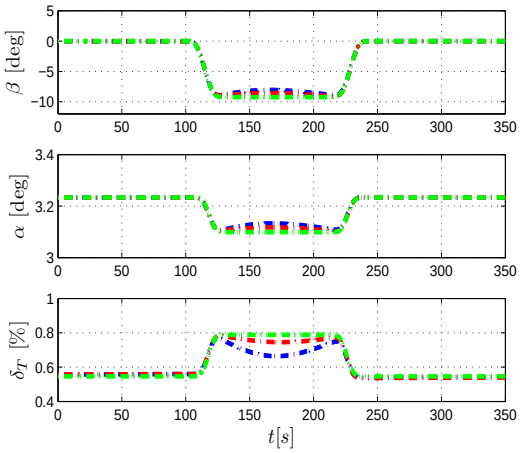

(c) $\dot{\mu}_d = 0.8$ deg/s : β, α, δ_T

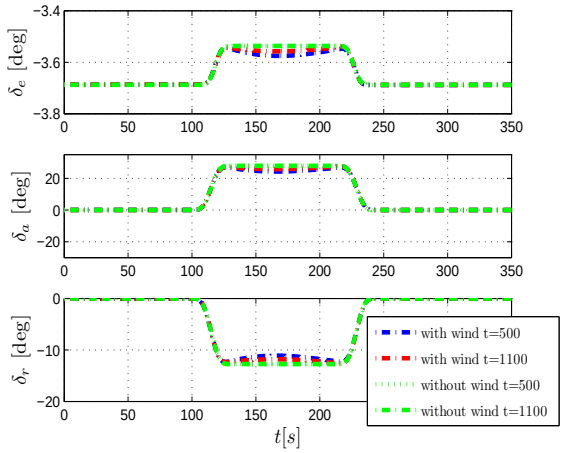

(d) $\dot{\mu}_d = 0.8$ deg/s : δ_e, δ_a, δ_r

Figure 6.18. Comparison of predicted input variables and aerodynamic angle of all simulation cases.

-85 deg. This means that the aircraft will turn in a different direction relative to the wind and be exposed to different wind variation as the wind is spatially varying.

Figures. 6.19 (a) and (b) show the turn rates variation with time. Figs. 6.19 (c) and (d) show the prescribed paths and the wind velocity vector along the trajectory during the periods of input prediction.

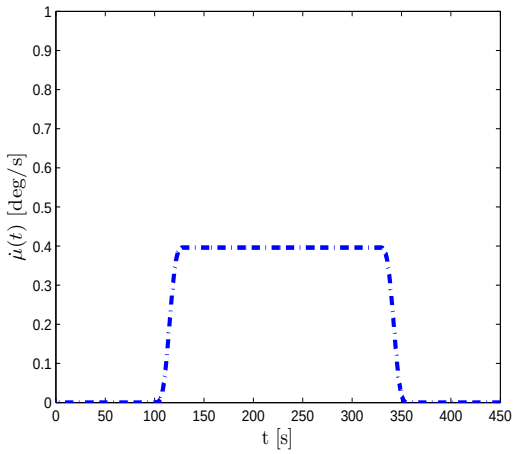

(a) $\dot{\mu}_d = 0.4$ deg/s

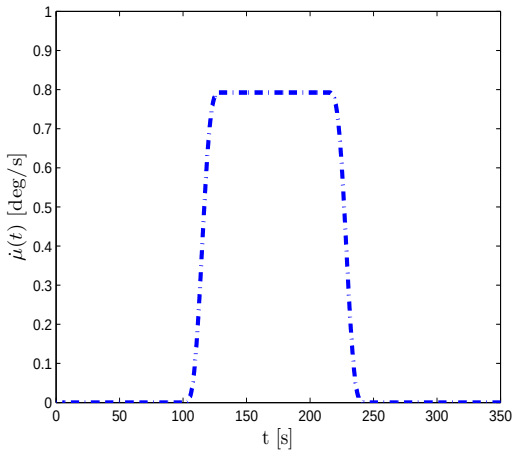

(b) $\dot{\mu}_d = 0.8$ deg/s

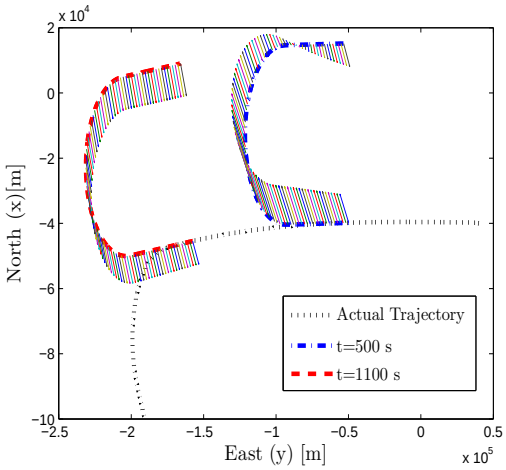

(c) Racetrack trajectory $\dot{\mu}_d = 0.4$ deg/s

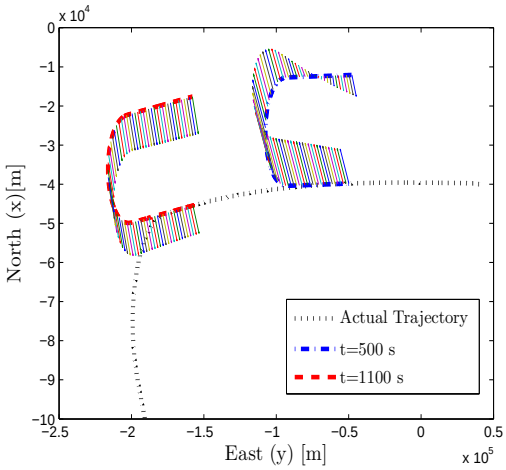

(d) Racetrack trajectory $\dot{\mu}_d = 0.8$ deg/s

Figure 6.19. Heading rate variation with time and paths in inertial frame and wind velocity vectors along the paths during the prediction period.

The estimated local wind information i.e., estimated local wind components and their time derivatives, are obtained from the estimated wind field parameters. Figs. 6.20 (a) and (b) show the predicted and actual wind components that Aircraft-1 is exposed to during the prediction period starting at 500 s. Similarly, Figs. 6.21 (a) and (b) show the same for $t = 1100$ s. The prediction period starting at $t = 500$

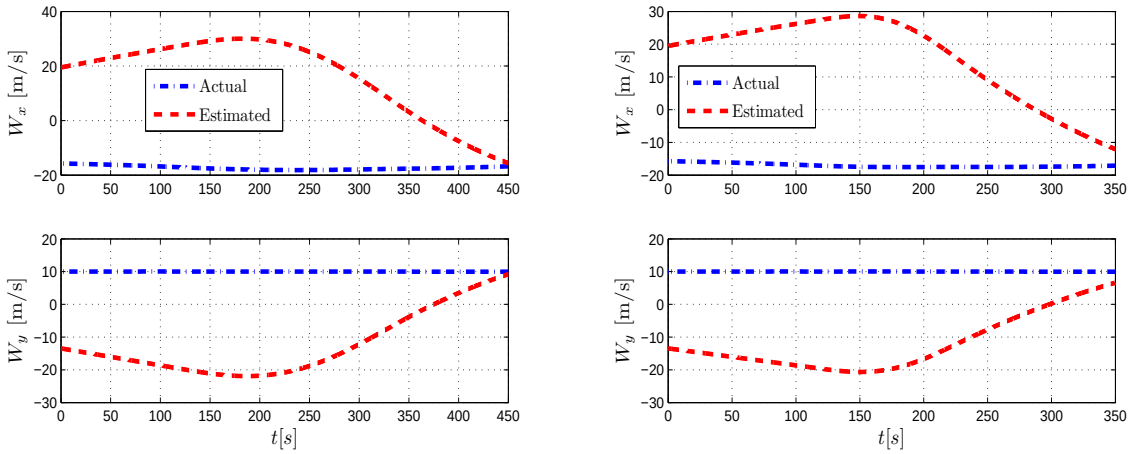

(a) $\dot{\mu}_d = 0.4$ deg/s (b) $\dot{\mu}_d = 0.8$ deg/s

Figure 6.20. Actual and estimated local wind along prescribed trajectory at $t = 500$ s.

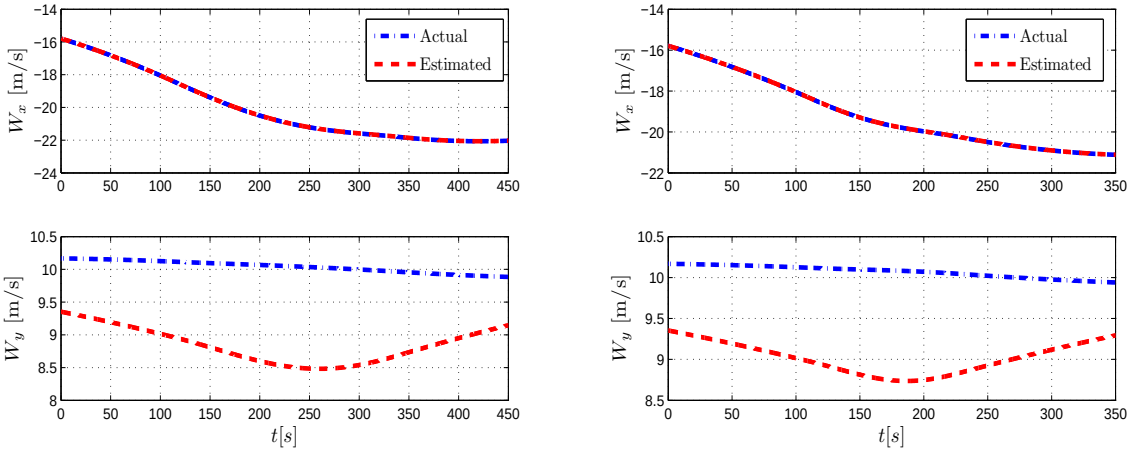

(a) $\dot{\mu}_d = 0.4$ deg/s (b) $\dot{\mu}_d = 0.8$ deg/s

Figure 6.21. Actual and estimated local wind along prescribed trajectory at $t = 1100$ s.

s, the wind is the South-West direction and in average, is about 14% of the aircraft speed. For the prediction period starting at $t = 1100$ s, the wind is in the South-West direction with increasing magnitude.

Fig. 6.22 shows the results of the input predictions with and without wind included in each set of simulation. Figs. 6.22 (a) and (b) show the input prediction results when the turn is executed with 0.4 deg/s constant turn rate while Figs. 6.22 (c) and (d) show the results for 0.8 deg/s cases.

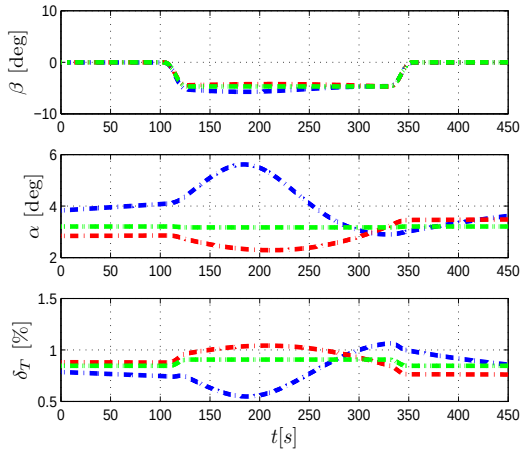

(a) $\dot{\mu}_d = 0.4$ deg/s : β, α, δ_T

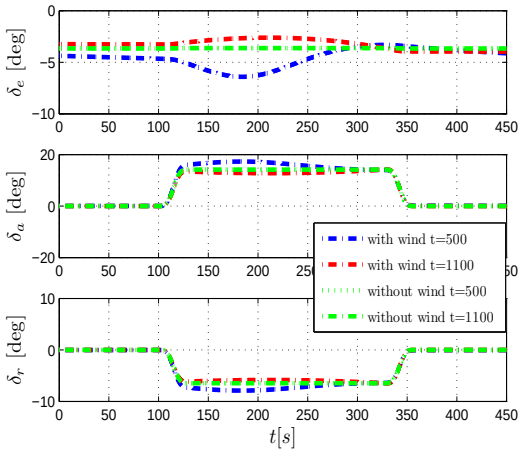

(b) $\dot{\mu}_d = 0.4$ deg/s : δ_e, δ_a, δ_r

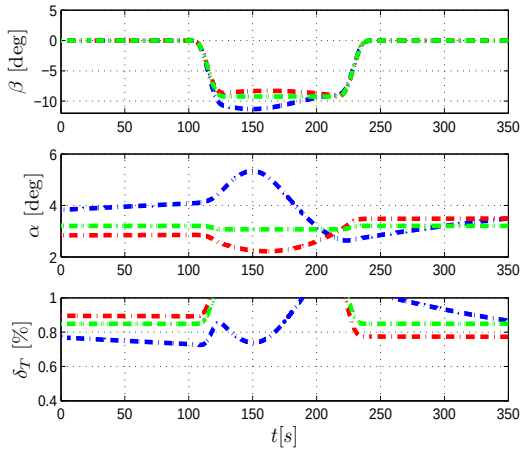

(c) $\dot{\mu}_d = 0.8$ deg/s : β, α, δ_T

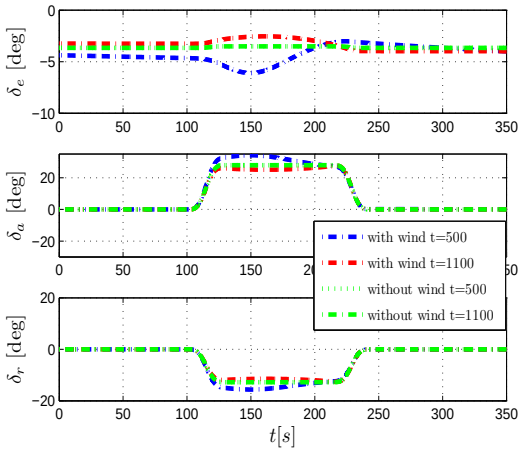

(d) $\dot{\mu}_d = 0.8$ deg/s : δ_e, δ_a, δ_r

Figure 6.22. Comparison of predicted input variables and aerodynamic angle of all simulation cases.

As expected, the figures clearly show the effect of the presence of wind and the structure of the wind field on the required inputs for an aircraft to fly through a desired trajectory. Further, a stronger wind requires larger input variables to complete the turn. However, the direction of wind as much as the magnitude affects the input prediction as well as the accurate estimated wind information. For example, if the aircraft happens to be flying in a tail wind region, which is to complete the right turn racetrack maneuver case, the required thrust is lower as can be seen in Fig. 6.22 (a) and (c). Additionally, as expected, sharper turn requires higher control surface deflections as can be seen in Fig. 6.22 (b) and (d). Moreover, the desired racetrack trajectories with sharper turn are not feasible for aircraft because the deflection of ailerons exceed the saturation limits as shown in Fig. 6.22 (d). On the contrary, the aircraft would be able to perform racetrack maneuver in this wind field, if it flew through shallower turn or lower turn rate as shown in Fig. 6.22 (b).

More importantly, Fig. 6.22 (a) shows that without wind information included, the engine thrust would be predicted to stay within its saturation limits. However, when wind information included, it is predicted that the engine thrust saturation will occur at about $t = 130$ sec. Thus, the aircraft should not execute the maneuver to follow the prescribed racetrack trajectory. The fact that prediction is never perfect, for example, at time $t = 500$ s where the input prediction start, the inaccurate estimated wind information is utilized in the input prediction process this results in inaccurate and unreliable prediction. Thus, the accurate wind information is important to know.

Chapter 7

CONCLUSIONS AND FUTURE WORK

This chapter sums up the research work, presents the conclusions and suggests directions for future work.

7.1 Conclusions

The influence of wind on aircraft can be detrimental or beneficial. Whether detrimental or beneficial, information about the wind aircraft is exposed to is important to know. This will help avoid or reduce risk associated with wind exposure or increase the benefit obtained from wind exposure. Various methods have been developed to estimate the local wind vector or some properties of it. Additionally, many applications may further benefit from the knowledge of spacial and temporal variation of wind within the airspace of operation. This information is referred to as wind field, which consists of wind velocity vector representation as a function of position and time.

This research has successfully developed on board wind field estimation method. A Weighted Least Square Estimation (WLSE) technique is developed to determine, based on local wind vector "measurements", the best functional approximation to represent the variation of wind vector over an airspace of interest, from a list of candidate models that are mathematical representations of spatial and/or temporal variations of different types of wind velocity vector field structures. The "measurements" for the estimation are obtained by multiple aircraft flying in the same airspace of operation considering as mobile sensors measuring wind vectors. The local wind

velocity vectors that each aircraft exposed to are computed using various local wind estimation methods and are shared among the aircraft through a common communication protocol like the ADS-B system. This enables each aircraft to have access to local wind information from other aircraft as well as its own for onboard wind field estimation. The weighting of the measurements in the WLSE are done based on the predicted or intended point of interest where each aircraft will be. That is, measurements coming from other aircraft flying closer the point of interest are given more weighting than the measurements from its own aircraft.

Simulation experiments have shown that, as compared to the LSE, the WLSE produces better estimations in the sense that error between the estimated wind and the actual wind along a trajectory is usually smaller. However, the WLSE methods result in more frequent switching between the estimation models, which causes discontinuity in the estimated local wind components.

Further, this research has successfully employed this wind field estimation method in aircraft trajectory prediction. The trajectory prediction is achieved by initializing aircraft point-mass-model with the current states of the aircraft and the propagating the model using aircraft intent information as well as the wind field approximation computed by the wind field estimation system. Simulation experiments have demonstrated that, when the trajectory prediction includes wind field and intent information, the prediction accuracy as well as its robustness against wind disturbance are improved. Finally, the wind estimation method is also successfully used to improve the prediction of input variables required for the aircraft to fly through a prescribed trajectory in the presence of spatially and/or temporally varying wind field. An inverse simulation method based on nonlinear 6-DOF equations of motion is employed that uses the estimated spatially and/or temporally varying wind field in solving nonlinear algebraic equations. The simulation experiments have shown that inclusion of

estimated spatially and/or temporally varying wind information in inverse simulation improves the accuracy and reliability of input prediction. For example, magnitude and rate saturations of control variables can be predicted for prescribed maneuvers in spatially varying wind when the wind information is included in inverse simulation. Such accurate predictions are crucial for determining feasibility of a prescribed trajectory before initiating the maneuver, which in turn enables aircraft not to go into an infeasible maneuver due to the presence of spatially temporally varying wind.

7.2 Future Work

The wind field estimation uses multiple aircraft flying in the same airspace as local wind vector sensors to collect data for the least squares estimation method to compute the parameters of various wind field estimation models. The trajectories that the aircraft fly along are not set for improving wind field estimation performance. There has been no effort made to determine the "optimal" number of aircraft or the optimal trajectories for purpose of wind field estimation. The future work may consider a situation where the sole purpose of multiple aircraft is to improve the wind field estimation. Thus, an optimal trajectory (speed, heading and flight path angles) planning algorithm can be carried out to determine the trajectories of a given number of aircraft to minimize the estimation error.

The spatially and temporally varying wind fields considered in this study are assumed to have only horizontal wind components. Also, the multiple aircraft are assumed to be flying at the same altitude. An extension of this work should be considered to estimate a 3-dimensional wind field from aircraft flying different altitudes.

The wind field estimation method developed in this research relies on local wind vector information coming from multiple aircraft. The local wind vector information received from other aircraft is assumed to be completed, i.e., all three components

available, and time-stamped. Further, no measurement noise or communication delay is considered in the local wind vector information. Future work should include investigation of incomplete and noisy local wind data and investigation of the effect of such wind data on wind field estimation.

It has been shown that the WLSE (Weighted Least Squares Estimation) improved wind field estimation accuracy but results in more frequent switching between wind estimation models based on the least residual errors. The switching causes discontinuity in local wind prediction along the predicted trajectory or along the prescribed trajectory for input prediction. It has been observed that some of the switching occur when the residual errors are very small and thus does not leads to any improvement. As a future work, a better switching algorithm should be investigated to prevent unnecessary switching. An example of such a modification could be to add a threshold to determine whether a switching between estimation models should be carried out.

For trajectory prediction, in this study assumed only intended trajectory of aircraft at constant altitude. An extension of this work should be considered to predict a 3-dimensional flight trajectory.

In the input prediction procedure, the prescribed trajectory is defined in terms of time variation of ground speed, heading and flight path angles. The prediction of the inputs required to fly the aircraft through the prescribed trajectory in terms of ground speed, heading and flight path angles is computed by the solution of six nonlinear algebraic equations obtained from 6-DOF translational and rotational dynamics. The number of state variables and control variables is larger than six, the number of equations. That is, some of the state variables should be determined from the prescribed trajectory and some are computed from the solution of the algebraic equations. Which state variables are determined from the prescribed trajectory and

which ones from the solution of the algebraic equations is a matter of choice. In this study, airspeed and three Euler angles are computed from the prescribed trajectory while angle of attack and sideslip angle along with the control variables are computed by the solution of the algebraic equations. This led to prescribed trajectories with nonzero slide slip angles, especially during turns. These two sets state variable can be chosen differently in a future work. For example, sideslip angle can be specified as zero, which would led to a different set of state variables to be included along with the control variables to be solved from the nonlinear algebraic equations. Another item of future work is about the solution of the nonlinear algebraic equations.

Another item of future work is about the solution of the nonlinear algebraic equations. The nonlinear algebraic equations are solved using a MATLAB-provided solver. The performance of the solver heavily depends on the initial guesses, there is no guarantee that the solver will converge to a solution and there might be multiple solutions, of which the solver can only find one depending on the initial guesses. A more robust method for solving the nonlinear algebraic equations should be investigated for realtime implementation of the input prediction algorithm. Lastly, a verification method for predicted input variables should be developed and implemented to investigate the feasibility and robustness of the procedure developed herein.

Appendix A

Reference Frames

In this appendix, the reference frames, which are required for the derivation of aircraft equation of motion, are presented.

A.1 Reference Frames

Fig. A.1 illustrated the relations between the reference frames and variables quantifying these relations. [$\hat{I}$], [$\hat{G}$], [$\hat{B}$], and [$\hat{W}$] refer to inertial, local, body and wind frames, respectively, and also shows the aircraft trajectory or flight path, and velocity vector, which are relevant to the definition of these frames. These frames play an important role in calculation of forces and moments acting on the aircraft. Additionally, the aircraft orientation with respect to the inertial frame is described by using these frames.

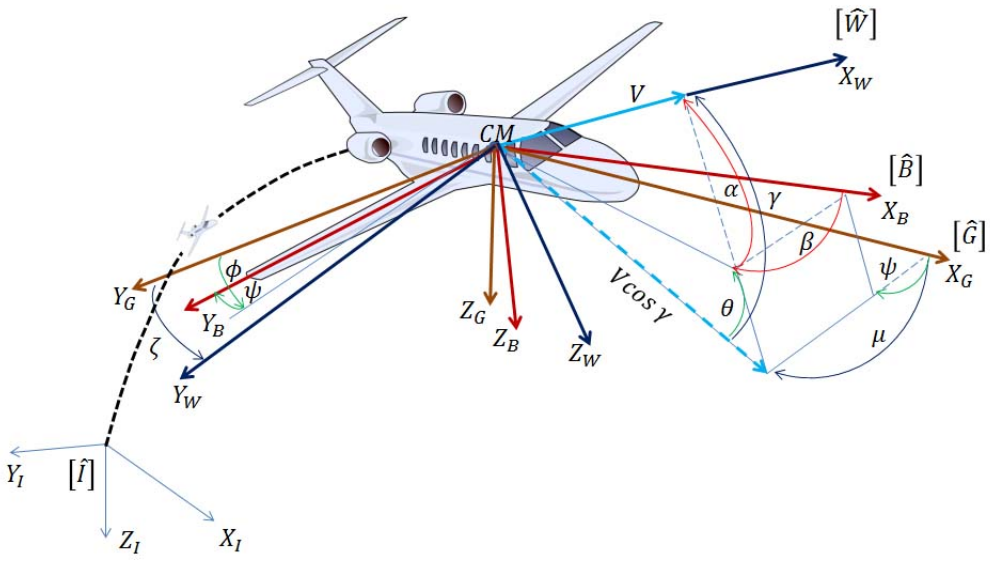

Figure A.1. Reference frames and theirs transformation angles.

A.1.1 Inertial Reference Frame

An Earth-fixed frame is considered as the inertial reference frame, with the origin located at an arbitrary point on the surface, $O_I Z_I$ is directed vertically downward. $O_I X_I Y_I$ is the local horizontal plane, $O_I X_I$ is directed local north, and $O_I Y_I$ is directed to the local east. This frame is denoted as [$\hat{I}$].

A.1.2 Local Frame

The local frame is defined such that it is always aligned with the inertial frame while its origin moves with the CM of the aircraft. This frame is denoted by [$\hat{G}$].

A.1.3 Body Fixed Frame

The Body fixed frame, which is fixed to the aircraft, is translating and rotating with it. The origin of this frame is located at CM of aircraft, with $O_B X_B$ pointing forward along the longitudinal axis. Axis $O_B Y_B$ points to the right, and axis $O_B Z_B$ is directed downward. This frame is denoted by [$\hat{B}$].

A.1.4 Wind Frame

The wind frame, moves with the aircraft, but rotates based on the velocity vector. The origin of this frame is located at CM, with $O_W X_W$ coincide with the velocity vector of the aircraft relative to the atmospheric wind, $O_W Z_W$ lies in the plane of symmetry of the aircraft, and $O_W Y_W$ points to the direction that is orthogonal to the $O_W X_W Z_W$ so as to complete the orthogonal triad. This frame is denoted by [$\hat{W}$].

Appendix B

Derivation of Wind Estimation Model-2

In this appendix, the details of the derivation of the introduced wind field model-1 in order to obtain the appropriated from, i.e., wind estimation model-2 or EM-2, for implementing in LSE method are presented.

B.1 Derivation of Wind Estimation Model-2

Wind Estimation Model-2 : This model has the same structure as Wind Model-1 in Section 2.1.

$$\begin{aligned} W_x(x,y,z,t) &= W_{x0}(z,t) + \frac{1}{2}\Big\{\Big[D(z,t)+F_1(z,t)\Big](x-x_0) \\ &\quad +\Big[-\zeta(z,t)+F_2(z,t)\Big](y-y_0)\Big\} \end{aligned} \tag{B.1}$$

$$\begin{aligned} W_y(x,y,z,t) &= W_{y0}(z,t) + \frac{1}{2}\Big\{\Big[\zeta(z,t)+F_2(z,t)\Big](x-x_0) \\ &\quad +\Big[D(z,t)-F_1(z,t)\Big](y-y_0)\Big\} \end{aligned} \tag{B.2}$$

The model can be further simplified as

$$W_x(x,y,z,t) = W_{x0}(z,t) + A(z,t)(x-x_0) + B(z,t)(y-y_0) \tag{B.3}$$

$$W_y(x,y,z,t) = W_{y0}(z,t) + C(z,t)(x-x_0) + E(z,t)(y-y_0) \tag{B.4}$$

where $A(z,t) = [D(z,t) + F_1(z,t)]$, $B(z,t) = [-\zeta(z,t) + F_2(z,t)]$, $C(z,t) = [\zeta(z,t) + F_2(z,t)]$, and $E(z,t) = [D(z,t) - F_1(z,t)]$, respectively.

Rearrange, Eq. (B.3) - (B.4) as

$$W_x(x,y,z,t) = \overline{W}_{x0}(z,t) + A(z,t)x + B(z,t)y \tag{B.5}$$

$$W_y(x,y,z,t) = \overline{W}_{y0}(z,t) + C(z,t)x + E(z,t)y \tag{B.6}$$

where

$$\overline{W}_{x0}(z,t) = W_{x0}(z,t) - A(z,t)x_0 - B(z,t)y_0 \tag{B.7}$$

$$\overline{W}_{y0}(z,t) = W_{y0}(z,t) - C(z,t)x_0 - E(z,t)y_0 \tag{B.8}$$

Let's consider the horizontal wind field model, which represent the spatially and temporally varying wind at z m altitude and all the temporal variation model as

$$A(z,t) = a_0 + a_1 t \tag{B.9}$$

$$B(z,t) = b_0 + b_1 t \tag{B.10}$$

$$C(z,t) = c_0 + c_1 t \tag{B.11}$$

$$E(z,t) = e_0 + e_1 t \tag{B.12}$$

Substitute all the parameters in Eq. (B.9)-(B.12) into Eq. (B.5)-(B.8), such that

$$\begin{aligned} W_x(x,y,z,t) &= W_{x0}(z,t) - (a_0 + a_1 t)x_0 - (b_0 + b_1 t)y_0 \\ &\quad +(a_0 + a_1 t)x + (b_0 + b_1 t)y \end{aligned} \tag{B.13}$$

$$\begin{aligned} W_y(x,y,z,t) &= W_{y0}(z,t) - (c_0 + c_1 t)x_0 - (e_0 + e_1 t)y_0 \\ &\quad +(c_0 + c_1 t)x + (e_0 + e_1 t)y \end{aligned} \tag{B.14}$$

Further simplify, so we can obtains

$$\begin{aligned} W_x(x,y,z,t) &= W_{x0}(z,t) - a_0 x_0 - b_0 y_0 - (a_1 x_0 + b_1 y_0)t \\ &\quad +a_0 x + b_0 y + a_1 t x + b_1 t y \end{aligned} \tag{B.15}$$

$$\begin{aligned} W_y(x,y,z,t) &= W_{y0}(z,t) - c_0 x_0 - e_0 y_0 - (c_1 x_0 + e_1 y_0)t \\ &\quad +c_0 x + e_0 y + c_1 t x + e_1 t y \end{aligned} \tag{B.16}$$

Consider changing of variable by define

$$X_0 = W_{x0}(z,t) - a_0 x_0 - b_0 y_0 \tag{B.17}$$

$$X_1 = -a_1 x_0 - b_1 y_0 \tag{B.18}$$

$$X_2 = a_0 \tag{B.19}$$

$$X_3 = b_0 \tag{B.20}$$

$$X_4 = a_1 \tag{B.21}$$

$$X_5 = b_1 \tag{B.22}$$

and

$$Y_0 = W_{y0}(z,t) - c_0 x_0 - e_0 y_0 \tag{B.23}$$

$$Y_1 = -c_1 x_0 - e_1 y_0 \tag{B.24}$$

$$Y_2 = c_0 \tag{B.25}$$

$$Y_3 = e_0 \tag{B.26}$$

$$Y_4 = c_1 \tag{B.27}$$

$$Y_5 = e_1 \tag{B.28}$$

Finally, the EM-1 can be expressed as

$$\widehat{W}_x(x,y,z,t) = \widehat{X}_0 + \widehat{X}_1 t + \widehat{X}_2 x + \widehat{X}_3 y + \widehat{X}_4 tx + \widehat{X}_5 ty \tag{B.29}$$

$$\widehat{W}_y(x,y,z,t) = \widehat{Y}_0 + \widehat{Y}_1 t + \widehat{Y}_2 x + \widehat{Y}_3 y + \widehat{Y}_4 tx + \widehat{Y}_5 ty \tag{B.30}$$

The EM-1 has the basis function of the form

$$h_1(x, y, z, t) = 1 \tag{B.31}$$

$$h_2(x, y, z, t) = t \tag{B.32}$$

$$h_3(x, y, z, t) = x \tag{B.33}$$

$$h_4(x, y, z, t) = y \tag{B.34}$$

$$h_5(x, y, z, t) = tx \tag{B.35}$$

$$h_6(x, y, z, t) = ty \tag{B.36}$$

References

[1] Timothy A. Lewis, "Flight data analysis and simulation of wind effects during aerial refueling," Master's thesis, The University of Texas at Arlington, May 2008.

[2] Atilla Dogan and Timothy A. Lewis and William Blake, "Flight data analysis and simulation of wind effects during aerial refueling," *AIAA Journal of Aircraft*, vol. 45, no. 6, pp. 2036–2048.
doi:10.2514/1.36 797, November-December 2008.

[3] NASA, "Nasa aviation safety program: Fact sheet," http://www.nasa.gov/centers/langley/news/factsheets/AvSP-factsheet.html, 2008, [Online; accessed 19-July-2013].

[4] B. Sridhar, H. K. Ng, and N. Y. Chen, "Aircraft trajectory optimization and contrails avoidance in the presence of winds," in *Proc. of 10th AIAA Aviation Technology,Integration,and Operations (ATIO) Conference*, Forth Worth, Texas, 13-15 September 2010, aIAA 2010-9139.
doi:10.2514/6.2010-9139.

[5] N. R.J.Lawrace and S. Sukkarieh, "Path planning for autonomous soaring flight in dynamic wind fields," in *Proc. of Robotics and Automation (ICRA), 2011 IEEE International Conference*, Shanghai, China, 9-13 May 2011, pp. 2499 – 2505.
doi:10.1109/ICRA.2011.5 979 966.

[6] J. Petrich and K. Subbarao, "On-board wind speed estimation for uavs," in *Proc. of AIAA Guidance,Navigation and Control conference*, Portland, Oregon,

8-11 August 2011, aIAA 2011-6223.
doi:10.2514/6.2011-6223.

[7] H. J. Palanthandalam-Madapusi, A. Girard, and D. S. Bernstein, "Wind-field reconstruction using flight data," in *Proc. of IEEE, 2008 American Control Conference*, Seattle, Washington, 11-13 June 2008, pp. 1863 – 1868.
doi:10.1109/ACC.2008.4 586 763.

[8] C. R. Daniel Delahaye and S. Puechmorel, "Wind field evaluation by using radar data and vector spline interpolation," in *Proc. of IEEE, 9th International Conference on Control and Automation (ICCA)*, Santiago, Chile, 19-21 December 2011, pp. 1863 – 1868.
doi:10.1109/ICCA.2011.6 138 091.

[9] A. Cho, J. Kim, S. Lee, and C. Kee, "Wind estimation and airspeed calibration using an uav with a single-antenna gps receiver and pitot tube," *IEEE transanctions on aerospace and electronic systmes*, vol. 47, no. 1, pp. 109 – 117.
doi:10.1109/TAES.2011.5 705 663, January 2011.

[10] M. Kumon, I. Mizumoto, Z. Iwai, and M. Nagata, "Wind estimation by unmanned air vehicle with delta wing," in *Proc. of the 2005 IEEE International Conference on Robotics and Automation*, Barcelona, Spain, April 2005, pp. 1896 – 1901.
doi:10.1109/ROBOT.2005.1 570 390.

[11] J. W. Langelaan, N. Alley, and J. Neidhoefer, "Wind field estimation for small unmanned aerial vehicles," in *Proc. of AIAA Guidance,Navigation and Control conference*, Toronto, Ontario Canada, 2-5 August 2010, aIAA 2010-8177.
doi:10.2514/6.2010-8177.

[12] S. Myschik and G. Sachs, "Flight testing an integrated wind/airdata and navigation system for general aviation aircraft," in *Proc. of AIAA Guid-*

ance,Navigation and Control Conference and Exhibit, Hilton Head, South Carolina, 20-23 August 2007, aIAA 2007-6796.
doi:10.2514/6.2007-6796.

[13] Lee J.,Dogan A. and Hullender D., "Estimation of aircraft states and wind exposure," in *Proc. of AIAA Atmospheric Flight Mechanics Conference*, Protland, Oregon, 8-11 August 2011, aIAA 2011-6318.
doi:10.2514/6.2011-6318.

[14] Lee J.,Sevil H.,Dogan A. and Hullender D., "Estimation of maneuvering aircraft states and time-varying wind with turbulence," in *Proc. of AIAA Guidance,Navigation and Control Conference*, Minneapolis, Minnesota, 13-16 August 2012, aIAA 2012-4532.
doi:10.2514/6.2012-4532.

[15] ——, "Estimation of receiver aircraft states and wind vector in aerial refueling," in *Proc. of AIAA Guidance,Navigation and Control Conference*, Minneapolis, Minnesota, 13-16 August 2012, aIAA 2012-4533.
doi:10.2514/6.2012-4533.

[16] J. W. Langelaan, J. Spletzer, C. Montella, and J. Grenestedt, "Wind field estiamtion for autonomous dynamic soaring," in *Proc. of 2012 IEEE International Conference on Robotics and Automation (ICRA)*, vol. 3, RiverCentre, Saint Paul, Minnesota, 14-18 May 2012, pp. 16 – 22.
doi:10.1109/ICRA.2012.6 224 954.

[17] I. Lymperopoulos and J. Lygeros, "Improved multi-aircraft ground trajectory prediction for air traffic control," *Journal of Guidance,Control, and Dynamics*, vol. 33, no. 2, pp. 347–362.
doi:10.2514/1.46 190, March-April 2010.

[18] A.C. Veld and P.M.A de Jong and M.M. van Paassen and M. Mulder, "Real time wind profile estimation using airborne sensors," in *Proc. of AIAA Guidance,Navigation,and Control Conference*, Portland, Oregon, 8-11 August 2011, aIAA 2011-6662.
doi:10.2514/6.2011-6662.

[19] A. Dogan and P. T. Kabamba, "Modified guidance laws for escaping a microburst with turbulence," *Mathematical Problems in Engineering*, vol. 8, pp. 43–67, 2002.

[20] N. R.J. and S. Sukkarieh, "Autonomous exploration of a wind field with a gliding aircraft," *AIAA, Journal of Guidance, Control and Dynamics*, vol. 34, pp. 719–733.
doi:10.2514/1.52 236, May-June 2011.

[21] G. Chalouslos and J. Lygeros, "Effect of wind correlation on aircraft conflict probability," *AIAA, Journal of Guidance,Control, and Dynamics*, vol. 30, no. 6, pp. 1742–1752.
doi:10.2514/1.28 858, November-December 2007.

[22] J. Hu, M. Prandini, and S. Sastry, "Aircraft conflict detection in presence of spatially correlated wind perturbations," in *Proc. of AIAA Guidance,Navigation,and Control Conference and Exhibit*, Austin, Texas, 11-14 August 2003, aIAA 2003-5339.
doi:10.2514/6.2003-5339.

[23] S. Mondoloni, "Aircraft trajectory prediction errors:including a summary of error sources and data,v0.2," Tech. Rep., July 2006.

[24] B. Musialek, C. F. Munafo, H. Ryan, and M. Paglione, "Literature survey of trajectory predictor technology," Tech. Rep., November 2010.

[25] J. M. Rodrigues, L. G. Deniz, and J. G. Herrero, "A model to 4d desent trajectory guidance," in *Proc. of IEEE 26th Digital Avionics Systems Conference*, 21 October 2007, pp. 1.C.2–1 – 1.C.2–12.
doi:10.1109/DASC.2007.4 391 828.

[26] M. A. Feldman, "Efficient low-speed flight in a wind field," Master's thesis, Virginia Polytechnic Institute and State University, July 1996.

[27] I. Lymperopoulos, J. Lygeros, and A. Lecchini, "Model based aircraft trajectory prediction during takeoff," in *Proc. of AIAA Guidance,Navigation and Control Conference and Exhibit*, Keystone, Colorado, 21-24 August 2006, aIAA 2006-6098.
doi:10.2514/6.2006-6098.

[28] S. M. McGovern, S. B. Cohen, and M. Truong, "Kinematics-based model for stochastic simulation of aircraft operating in the national airspace system," in *Proc. of 26th IEEE/AIAA Digital Avionics Systems Conference*, 21-25 October 2007, pp. 3.B.2–1 – 3.B.2–11.
doi:10.1109/DASC.2007.4 391 876.

[29] D. P. Boyle and G. E. Chamitoff, "Robust nonlinear lasso control: A new approach for autonomous trajectory tracking," in *Proc. of AIAA Guidance,Navigation and Control Conference and Exhibit*, Austin, Texas, 11-14 August 2003, aIAA 2003-5518.
doi:10.2514/6.2003-5518.

[30] D. McNally and J. Walton, "A holding funcition for conflict probe applications," in *Proc. of AIAA Guidance,Navigation and Control Conference*, Rhode Israng, 16-19 August 2004.

[31] Puechmorel S. and Delahaye D., "4d trajectories: A functional data perspective," in *Proc. of 26th IEEE/AIAA Digital Avionics Systems Conference*, 21-25

October 2007, pp. 1.C.6–1 – 1.C.6–12.
doi:10.1109/DASC.2007.4 391 832.

[32] Z.-H. M. Karl D. Bilimoria, Hilda Q. Lee and E. Feron, "Comparison of centralized and decentralized conflict resolution strategies for multiple-aircrft problems," in *Proc. of AIAA Guidance,Navigation and Control Conference*, Denver, Colorado, 14-17 August 2000, aIAA 2000-4268.
doi:10.2514/6.2000-4268.

[33] M. Eby and W. Kelly, "Free flight separation assurance using distributed algorithms," in *Proc. of IEEE Aerospace Conference*, vol. 2, 6-13 March 1999, pp. 429 – 441.
doi:10.1109/AERO.1999.793 186.

[34] T. Ota, M. G. Nagati, and D.-C. Lee, "Aircraft collision avoidance trajectory generation," in *Proc. of AIAA Guidance,Navigation and Control Conference*, 10-12 August 1998, aIAA 1998-4241.
doi:10.2514/6.1998-4241.

[35] L. Pallottino, A. Bicchi, and E. Feron, "Mixed interger programming for aircraft conflict resolution," in *Proc. of AIAA Guidance,Navigation,and Control Conference and Exhibit*, Montreal, Canada, 6-9 August 2001, aIAA 2001-4295.

[36] H. Versteegt and H. Visser, "Traffic complexity based conflict resolution," in *Proc. of AIAA Guidance,Navigation,and Control Conference and Exhibit*, Monteley, California, 5-8 August 2002, aIAA 2002-4443.
doi:10.2514/6.2002-4443.

[37] K. D. Bilimoria, K. Sheth, H. Lee, and S. R. Grabbe, "Performance evaluation of airborne separation assurance for free flight," in *Proc. of AIAA Guidance,Navigation,and Control Conference*, Denver, Colorado, 14-17 August 2000,

aIAA 2000-4269.

doi:10.2514/6.2000-4269.

[38] J. Krozel, T. Mueller, and G. Hunter, "Free flight conflict detection and resolution analysis," in *Proc. of AIAA Guidance,Navigation,and Control Conference*, San Diego, California, 29-31 July 1996, aIAA 1996-3763.

doi:10.2514/6.1996-3763.

[39] J. Krozel, M. Peters, and K. Bilimoria, "A decentralized control strategy for distributed air/ground traffic separation," in *Proc. of AIAA Guidance,Navigation,and Control Conference and Exhibit*, Denver, Colorado, 14-17 August 2000, aIAA 2000-4062.

doi:10.2514/6.2000-4062.

[40] S. U. Shandy and J. Valasek, "Intelligent agent for aircraft collision avoidance," in *Proc. of AIAA Guidance,Navigation,and Control Conference and Exhibit*, Montreal, Canada, 6-9 August 2001, aIAA 2001-4055.

doi:10.2514/6.2001-4055.

[41] D. McNally and C. Gong, "Concept and laboratory analysis of trajectory-based automation for separation assurance," in *Proc. of AIAA Guidance,Navigation,and Control Conference and Exhibit*, Keystone, Colorado, 21-24 August 2006, aIAA 2006-6600.

doi:10.2514/6.2006-6600.

[42] H. Chen and Y. J. Zhao, "Required action time and control effectiveness in resolving pairwise conflicts," in *Proc. of AIAA Guidance,Navigation,and Control Conference*, Chicago, Illinois, 10-13 August 2009, aIAA 2009-5749.

doi:10.2514/6.2009-5749.

[43] J. M. Shewchun, J.-H. Oh, and E. Feron, "Linear matrix inequalities for free flight conflict problems," in *Proc. of 36th IEEE Conference on Decision and*

Control, vol. 3, San diego, California, December 1997, pp. 2417 – 2422.
doi:10.1109/CDC.1997.657 518.

[44] R. Teo and C. J. Tomlin, "Provably safe evasive maneuvers against blunders in closely spaced parallel approaches," in *Proc. of AIAA Guidance,Navigation,and Control Conference and Exhibit*, Montreal, Canada, 6-9 August 2001, aIAA 2001-4293.
doi:10.2514/6.2001-4293.

[45] R. Teo and C. Tomlin, "Computing danger zones for provably safe closely spaced parallel approaches," *AIAA, Journal of Guidance, Control, and Dynamics Guidance,Control,and Dynamics*, vol. 26, no. 3, pp. 434–442.
doi:10.2514/2.5081, May-June 2003.

[46] J. P. Wangermann and R. F. Stengel, "Optimization and coordination of multi-agent systems using principled negotiation," in *Proc. of AIAA Guidance,Navigation,and Control Conference*, San diego, California, 29-31 July 1996, aIAA 1996-3853.
doi:10.2514/6.1996-3853.

[47] M. Innocenti, P. Gelosi, and L. Pollini, "Air traffic management using probability function fields," in *Proc. of AIAA Guidance,Navigation,and Control Conference*, 9-11 August 1999, aIAA 1999-4149.
doi:10.2514/6.1999-4149.

[48] B. Carpenter and J. Kuchar, "Prabability-based collision alerting logic for colsely-spaced parallel approaches," in *Proc. of 35th AIAA Aerospace Sciences Meeting and Exhibit*, Reno, Nevada, 6-10 January 1997, aIAA 1997-0222.

[49] M. Prandini, J. Lygeros, A. Nilim, and S. Sastry, "A probabilistic framework for aircraft conflict detection," in *Proc. of AIAA Guidance,Navigation,and Control*

Conference, 9-11 August 1999, aIAA 1999-4144.
doi:10.2514/6.1999-4144.

[50] L. Yang and J. Kuchar, "Using intent information in probabilistic conflict analysis," in *Proc. of AIAA Guidance,Navigation,and Control Conference*, 10-12 August 1998, aIAA 1998-4237.
doi:10.2514/6.1998-4237.

[51] H. A. P. Blom and G. J. Bakker, "Conflict probability and incrossing probability in air traffic management," in *Proc. of 41st IEEE Conference on Decision and Control*, vol. 3, Las Vegas, Nevada, December 2002, pp. 2412 – 2426.
doi:10.1109/CDC.2002.1 184 198.

[52] Z. Zhang, J. Shen, and J. Liu, "Modeling of collision risk on parallel routes based on spherical protected area," in *Proc. of IEEE Chinese Control and Dicision Conference*, China, 2010, pp. 4422 – 4425.
doi:10.1109/CCDC.2010.5 498 338.

[53] R. Paielli and H. Erzberger, "Conflict probability estimation for free flight," in *Proc. of 35th Aerospace Sciences Meeting and Exhibit*, Reno, Nevada, 6-9 January 1997, aIAA 1997-1.
doi: 10.2514/6.1997-1.

[54] R. A. Paielli, "Algorithms for tactical conflict resolution and strategic conflict probability reduction," in *Proc. of 1st AIAA Aircrat, Technology, Integration, and Operations Forum*, Los Angeles, California, 16-18 October 2001, aIAA 2001-5243.
doi:10.2514/6.2001-5243.

[55] G. Chaloulos and J. Lygeros, "Wind uncertainty correlation and aircraft conglict detection based on ruc-1 forecasts," in *Proc. of AIAA Guid-*

ance,Navigation,and Control Conference and Exhibit, Hilton Head Island, South Carolina, 20-23 August 2007.

[56] J. L.-L. Jesper Bronsvoort, Greg McDonal and H. G. Visser, "Improved trajectory prediction for air traffic management by simulation of guidance logic and inferred aircraft intent using existing data-link technology," in *Proc. of AIAA Guidance,Navigation and Control Conference*, Minneapolis, Minnesota, 13-16 August 2012, aIAA 2012-4928.
doi:10.2514/6.2012-4928.

[57] L. C. Yang and J. K. Kuchar, "Using intent information in probabilistic conflict analysis," in *Proc. of AIAA Guidance,Navigation and Control Conference and Exhibit*, 1998, aIAA 98-2437.
doi:10.2514/6.1998-4237.

[58] I. H. Javier Lovera Yepes and M. Rotea, "An intent based trajectory prediction algorithm for air traffic control," in *Proc. of AIAA Guidance,Navigation and Control Conference and Exhibit*, San Francisco, California, 15-18 August 2005, aIAA 2005-5824.
doi:10.2514/6.2005-5824.

[59] J. Krozel and D. Andrisani, "Intent inference with path prediction," *Journal of Guidance, Control, and Dynamics*, vol. 29, no. 2, pp. 225–236.
doi:10.2514/1.14 348, March-April 2006.

[60] J. L.-L. Michael A. Konyak, Dan Warburton and P. C. Parks, "A demonstration of an aircraft intent interchange specification for facilitating trajectory-based operations in the national airspace system," in *Proc. of AIAA Guidance,Navigation and Control Conference and Exhibit*, Honolulu, Hawaii, 18-21 August 2008, aIAA 2008-7145.
doi:10.2514/6.2008-7145.

[61] R. S.-B. E. G. Michael A. Konyak, Scott Doucett and P. C. Parks, "Improving ground-based trajectory prediction through communication of aircraft intent," in *Proc. of AIAA Guidance,Navigation and Control Conference*, Chicago, Illinois, 10-13 August 2009, aIAA 2009-6080.
doi:10.2514/6.2009-6080.

[62] S. Torres, "Determination and ranking of trajectory accuracy factors," in *Proc. of Digital Avionics Systems Conference (DASC), 2010 IEEE/AIAA 29th*, Salt Lake City, UT, October 3-7 2010, pp. 1.c.1–1 – 1.c.1–12, 2155-7195.
doi:10.1109/DASC.2010.5655521.

[63] D. M. Smith, "The inverse simulation approach: a focused review of methods and applications," *Elsevier,Journal of Mahtematics and Computers in Simulation*, vol. 53, no. 4-6, pp. 239–247.
doi:http://dx.doi.org/10.1016/S0378–4754(00)00 210–X, 30 October 2000.

[64] D. Thomson and R. Bradley, "The inverse simulation as a tool for flgith dynamics research principles and applications," *Elsevier,Journal of Progress in Aerospace Sciences*, vol. 42, no. 3, pp. 174–210.
doi:http://dx.doi.org/10.1016/j.paerosci.2006.07.002, 6 September 2006.

[65] Hess R.A. and Gao C. and Wang S.H., "Generalized technique for inverse simulation applied to aircraft maneuvers," *AIAA Journal of Guidance,Control,Dynamics*, vol. 14, no. 5, pp. 920–926.
doi:10.2514/3.20 732, September 1991.

[66] Gao C. and Hess R.A., "Inverse simulation of large amplitude aircraft maneuvers," *AIAA Journal of Guidance,Control,Dynamic*, vol. 16, no. 4, pp. 733–737.
doi:10.2514/3.21 074, July 1993.

[67] R.Bradley and D. Thomson, "Handling qualities and performance aspects of the simulation of helicopters flying mission task elements," *Proceedings of the 18th European Rotorcraft Forum,Avignon*, 1992.

[68] D.G. Thomson and N.Talbot and C.Taylor and R.Bradley and R.Ablett, "An investigation of piloting strategies for engine failures during take-off from off-shore platforms," *Aeronautical Journal 99*, 1995.

[69] A. Bahi and M. Abdelrahman, "Effect of atmospheric disturbances on the inverse simulation of aircraft motion," in *Proc. of 21st AIAA Atmospheric Flight Mechanics Conference*, San Diego, California, 29-31 July 1996, aIAA 1996-3414. doi:10.2514/6.1996-3414.

[70] A. Leinonen, "Application for inverse simulation of flight tracks," *Science and Technology Research Report*, August 2012.

[71] Thomson,D.G. and Coton, F.N. and Galbraith,R.A.M., "Simulation study of helicpter ship landing procedures incoporating measured flow data," *Journal of Aerospace Engineering*, vol. 219, no. 5, pp. 411–427.
doi:10.1243/095 441 005X30 351, 1 May 2005.

[72] J. E. Martin, "Mid latitude atmospheric dynamics," *John Wiley and Sons Inc.*, 2006.

[73] J. M. Wallace and P. V. Hobbs, "Atmospheric science," *New York: Academic Press*, 1997.

[74] D. G. Long, "Model-based estimation of wind fields over the ocean from wind scatterments," Ph.D. dissertation, University of Southern Califonia, January 1989.

[75] A. Pena, S.-E. Gryning, and C. B. Hasager, "Measurements and modelling of the wind speed profle in the marine atmospheric boundary layer," *Journal of*

Boundary-Layer Meteorology, vol. 129, no. 3, pp. 479–495.
doi:10.1007/s10 546–008–9323–9, December 2008.

[76] J. Reynolds, "The hidden dangers of mountain wave turbulence," *The Front*, November 2011.

[77] P. Jackson and J. Hunt, "Turbulent wind flow over a low hill," *Quart. J. R. Met.Soc.*, vol. 101, pp. 929–955, March 1975.

[78] J. H. R.E. Britter and K. Richards, "Air flow over a two-dimensional hill: studies of velocity speed-up,roughness effects and turbulence," *Quart. J. R. Met.Soc.*, vol. 107, pp. 91–110, 1981.

[79] D. R. Durran, "Mountain waves and downslope winds," *Atmospheric Processes Over Complex Terrain*, vol. 23, no. 45, June 1990.

[80] G. S. J.M. Leone and B. Bowen, "Simulating urban effects within a diagnostic wind field model," *Third International Symposium on Environmental Hydraulics with a Special Theme in Urban Fluid Dynamics*, December 2001.

[81] Liu Shi-Kuo, Fu Zun-Tao, Liu Shi-Da, Xu Huan-Bin, Xin Gua-Jun and Liang Fu-Ming, "Theory on the funnel structure of tornado," *Chinese Journal of Geophysics*, vol. 47, no. 6, pp. 1079–1084, 2004.

[82] H. Visser, "Lateral escape guidance strategies for microburst windshear encounters," in *Proc. of 35th Aerospace Sciences Meeting and Exhibit*, Reno, Nevada, 6-9 January 1997, aIAA 1997-535.
doi: 10.2514/6.1997-535.

[83] B. Gear, "Backward differentiation formulas," *Scholarpedia*, vol. 2, no. 8, p. 3162.
doi:10.4249/scholarpedia.3162, 2007.

[84] H. W. Jiang Li and N. H. Kim, "Doubly weighted moving least squares and its application to structural reliability analyis," *Journal of Structural and Multi-*

disciplinary Optimization, vol. 46, no. 1, pp. 69–82.
doi:10.1007/s00 158–001–0748–2, December 2011.

[85] I.-H. W. Won-Sang Ra and J. B. Park, "Robust weighted least squres range estimator for uav applications," in *SICE Annual Conference 2008*, The University Electro-Communications, Japan, 20-22 August 2008.

[86] G. H. Z. M. Ruohan Tang, Deyou Liu and B. de Young, "Reconstructed wind fields from multi-satellite observations," *Journal of Remote Sensing*, vol. 6, pp. 2898–2911.
doi:10.3390/rs6 042 898, March 2014.

[87] A. Nealen, "An as-short-as-possible introduction to the least squares, weighted least squares and moving least squares methods for scattered data approximation and interpolation," http://www.nealen.com/projects, year = 2004, note = "[Online; accessed 5-June-2014]".

[88] ClockBackward, "Ordinary least squares linear regression: Flaws, problems and pitfalls," http://www.clockbackward.com/2009/06/18/ordinary-least-squares-linear-regression-flaws-problems-and-pitfalls, 2009, [Online; accessed 5-June-2014].

[89] L. I. Nwankwo, "A least squares plane surface polynomial fit of two dimensional potential field geophysical data using matlab," in *Nigeria Journal of Pure and Apply Science*, vol. 2, 2006, pp. 2006–2012.

[90] D. Shepard, "A two-dimensional interpolation function for irregulary-spaced data," in *ACM 68 Proceddings of the 1968 23rd ACM national conference*, New York, USA, 1968, 517-524.
doi:10.1145/800186.810616.

[91] Alexa, M., Behr, J., Cohen-or, D., Fleishman, S., Levin, D.,and T. Silva, C., "Computing and rendering point set surfaces," in *IEEE Transactions on Visu-*

alization and Computer Graphics, vol. 9, January 2003, p. 1, 3-15.
doi:10.1145/800186.810616.

[92] H. Wendland, "Piecewise polynomial, positive definite and compactly supported radial basis functions of minimal degree," in *Advances in Computational Mathematics 4*, vol. 4, May 1995, pp. 389–396.

[93] T. A. K. A. H. T. Hamaki Inokuchi, Eiichi Endo and Y. Hirano, "Development of an airborne wind measurement system," in *Proc. of International Symposium on Photoelectronic Detection and Imaging 2009: Laser Sensing and Imaging*, Beijing, China, August 2009, sPIE7382.
doi:10.1117/12.836606.

[94] E. G. F. A. N. Javier Lopaze-Leones, Migual A. Vilaplana and C. Querejeta, "The aircraft intent description language: A key enabler for air-ground synchronization in trajectory-based operations," in *Proc. of Digital Avionics Systems Conference, 2007 IEEE/AIAA 26th*, Dallas, Texas, 21-25 October 2007, 1.D.4-1 - 1.D.4-12.
doi:10.1109/DASC.2007.4391836 .

[95] K. T. C. Robert A. Vivona, Mike M. Paglione and G. Enea, "Definition and demonstration of a methodology for validatin aircraft trajectory predictors," in *Proc. of AIAA Guidance,Navigation and Control Conference*, Toronto, Ontario Canada, 2-5 August 2010, aIAA 2010-8161.
doi:10.2514/6.2010-8161.

[96] M. M. Urban Maeder and T. I. Baumgartner, "Trajectory prediction for light aircraft," *Journal of Guidance, Control, and Dynamics*, vol. 30, no. 4, pp. 1112–1119.
doi:10.2514/1.52 124, July - August 2011.

[97] A. O. Conde, Roberto and J. A. Cobano., "Method based on a particle filter for uav trajectory prediction under uncertainties," in *Proc. of 40th International Symposium of Robotics*, Barcelona, Spain, 2009.

[98] D. T. Linghai Lu, David J. Murray-Smith, "Issues of numerical accuracy and stability in inverse simulation," *Elsevier,Simulation Modelling Practice and Theory 16*, July 2008.

[99] E.S.L.H Wiryo Hadiatmoto, "Inverse control ploblems: Mathematical preliminaries, system theoretical approaches, and their applications to aircraft dynamics," *Delft University of Technology*, October 1991.

[100] B. Etkin and D. A. Etkin, "Critical aspects of trajectory prediction: Flight in non-uniform wind," *NATO AGARD Report*, no. 301, March 1990.

[101] Jane-wit Kampoon, "Guidance of receiver aircraft to rendezvous with tanker in the presence of prevailing wind," Master's thesis, The University of Texas at Arlington, December 2009.

[102] G. Kowaleczko, "Simulations and reconstructions of aircraft flights and accidents," in *RTO Meeting Proceedings - North Atlantic Treaty Organization Research and Technology Organization RTO MP, Flight Test Symposium*, Neuilly-sur-Seine, France, 2005.

[103] B. Etkin, "Dynamics of atmospheric flight," *John Wiley and Sons Inc.*, 1972.

[104] J. Ralph E. Bach and R. C. Wingrove, "Equations for determining aircraft motions from accident data," in *NASA Technical Memorandum 78609*, June 1980.

Biographical Information

Jane-wit Kampoon was born in Bangkog, Thailand. He received his B.Eng degree in Aeronautical and Aviation Engineering (2^{nd} class honor) from the Royal Thai Air Force Academy, Thailand, in 1996. Since then, he has been working as a full time faculty at Aeronautical and Aviation Engineering Department, Royal Thai Air Force Academy, Royal Thai Air Force. He won the Royal Thai Government (RTG) scholarship for further education and received his M.Eng degree in Mechatronics from the Asian Institute of Technology (AIT), Thailand. From 1998 to 2000. After graduation, he resumed to work and research in flight mechanics until accepting scholarship from the Royal Thai Air Force for continuing his second master degree at the University of Texas at Arlington, in 2007. After graduation in 2009 with M.S. AE degree and immediately transitioned to the Ph.D. program with the financial funding from the University of Texas at Arlington. His research interests include, flight dynamics and control, trajectory prediction, input prediction, conflict detection and avoidance, autonomous navigation, guidance and control of aircraft, and wind field estimation.